THE UNIVERSITY OF MANITOBA

# *FLUORESCENCE LIFETIME ANALYSIS TO STUDY DNA CONFORMATION*

*by*

Dennis Patrick Heller

**A THESIS**

Submitted to the Faculty of Graduate Studies in partial fulfillment of the requirements of the degree of

***MASTER OF SCIENCE***

**Department of Physics**
**Winnipeg, Manitoba**
**August, 1988**

ISBN 0-315-47914-0

# FLUORESCENCE LIFETIME ANALYSIS TO STUDY DNA CONFORMATION

BY

DENNIS PATRICK HELLER

A thesis submitted to the Faculty of Graduate Studies of
the University of Manitoba in partial fulfillment of the requirements
of the degree of

MASTER OF SCIENCE

## ACKNOWLEDGEMENTS

This thesis entitled "Fluorescence Lifetime Analysis to study DNA conformation" is a result of research conducted by myself during the period from September 1986 to June 1988 at the Whiteshell Nuclear Research Establishment in Pinawa, Manitoba.

I am grateful to Atomic Energy of Canada Ltd., Research Company, for allowing me the use of their facilities.

I wish to thank Dr. Goldenburg of the Manitoba Institute of Cell Biology for the various derivatives of the P388 leukemic mice cell line.

Finally, I wish to extend my appreciation to Dr. C.L. Greenstock for his guidance, input, and support during the course of my Masters program. I also wish to thank the members of the Medical Biophysics Branch at WNRE for their assistance and support.

## TABLE OF CONTENTS



continued...

## TABLES

## FIGURES

## ABSTRACT

The sensitive spectroscopic technique of fluorescence lifetime analysis (FLA), has been applied to the study of DNA conformation. Initial experiments with ethidium bromide intercalated within calf thymus DNA have shown that the FLA is sensitive to the conditions of the analysis. Varying the region of interest over which the deconvolution analysis is performed, subtracting background noise, and fitting multi-exponential components all affect the resulting lifetime values. The severity of the effect on the resultant lifetime values, is dependent on the particular decay scheme. It was found that the difference ranged from .1% to 5%. The FLA of ethidium bromide bound within calf thymus DNA in solution, yielded a fluorescence lifetime of 23.1 nsec for Eb intercalated at the primary binding site, and a fluorescence lifetime of 1.67 nsec for unbound ethidium bromide. The bound fluorescence lifetime was found to decrease as the amount of unbound ethidium bromide present increased. A collisional quenching mechanism with unbound ethidium bromide associating with the exterior of the DNA helix, is discussed. Preliminary results with ethidium bromide stained

P388 leukemic cells, treated with adriamycin, indicate that FLA is sensitive to the amount of double stranded DNA present in the nucleus. Fluorescence lifetime analysis has proven to be highly sensitive to the conformation and local molecular environment of DNA.

## INTRODUCTION

Cancer is the result of abnormal and inappropriate growth, in which the mechanisms controlling normal growth and development are absent, damaged, suppressed, or over-ridden. This suggests interference with the genetic machinery either by changes in the DNA itself, or in the synthetic systems involved in the expression of genetic information. The transformation from a normal to a malignant state often involves a long latent period, and any insight into this pre-malignant phase, or into the development of a screening process to detect the early stages of carcinogenesis, is important to the study of cancer, its improved diagnosis and treatment, and its ultimate prevention and cure.

The sensitive technique of time-resolved fluorescence spectroscopy is being used to study conformational states of DNA, both in chemical systems, and in living mammalian cells. This single photon counting technique provides an analysis of the decay kinetics of fluorescent probes that associate within particular regions of a macromolecule. The 'deconvolution' analysis allows the experimenter to resolve, quantitatively, the fluorescence decay curve into as many as four discrete lifetime components, reflecting the many different domains or molecular interactions of the probe, within a particular target macromolecule.

The material presented in this thesis is part a project to develop and assess Fluorescence Lifetime Analysis (FLA), as a highly sensitive method for revealing possible correlations between conformational states of DNA and any anomalous changes between normal and transformed cells, and normal cells treated with mutagens, carcinogens and other toxic agents, in order to assess the feasibility of developing a method of cancer- or pre-cancer screening, based on time-resolved fluorescence spectroscopy.

Part A of this thesis provides some background information necessary to follow more clearly the principles and processes presented and discussed in the chapters that follow.

One objective of my Master's project was to develop the effective use of a Fluorescence Lifetime Instrument (FLI) to measure the decay kinetics of selected fluorescent probes bound within DNA. Part B of this thesis describes that development. Initially, each component of the FLI was optimized and its operation put on a firm physical basis. Specifically, Part B describes the optimization of the excitation light source and the data collection process in order to achieve an accurate single photon counting system, capable of high sensitivity, high resolution, high speed collection and above all good reproducibility. A computer software package is responsible for the

deconvolution of the decay data and the fitting of an exponential model to the resultant decay curve. Part B also provides a detailed appraisal of the decay analysis procedure, establishing the limitations in its ability to accurately distinguish multiple lifetime components and to separate these components from the excitation lamp profile.

An in depth study of the binding characteristics of ethidium bromide as measured by FLA and absorption spectroscopy is presented in Part C. The FLA results of Calf Thymus DNA in solution are interpreted at two distinct ionic concentrations in terms of the binding equilibria of ethidium bromide, the conformational states of DNA, and the possible fluorescence quenching mechanisms present.

The last section, Part D, describes some preliminary FLA results from P388 leukemic mouse cells of different adriamycin sensitivities, stained with ethidium bromide. A simple one-step ethidium bromide staining procedure, traditionally used for DNA analysis by flow-cytometry, was adapted to the FLA. The effects of the intracellular staining residuals on the FLA results are also analyzed.

# PART A

## BACKGROUND INFORMATION

## 1.0 Fluorescence

During the last decade, the use of intrinsic and extrinsic fluorophores has yielded much information about proteins, nucleic acids, membranes etc. in the areas of microbiology, biochemistry and biophysics. A fluorophore is a molecule capable of absorbing and emitting radiation.

Fluorescence is a form of luminescence in which the emission of photons is due to an electric dipole transition from an excited electronic state to a lower state, usually the ground state, of the same spin multiplicity (step 3, fig 1a). Such transitions are quantum mechanically "allowed" and the emissive rates are high ($\sim 10^8$ $sec^{-1}$). Phosphorescence is another form of luminescence in which the transitions are between states of different multiplicity and the emissive rates are low ($\leq 10^6$ $sec^{-1}$).

Prior to fluorescence, an incident photon must interact with a molecule in solution. The molecule absorbs energy of a particular wavelength and is excited or raised temporarily to a higher energy level (step 1, fig 1a). If the excited species is created with excess vibrational energy, this excess energy is rapidly dissipated by collisions with solvent molecules. This vibrational 'relaxation' puts the molecule at the ground level of this excited electronic state (step 2, fig 1a). From this

excited state ($S_1$) several photophysical processes compete simultaneously with fluorescence to depopulate it. These are summarized below.

1. Vibrational relaxation - of the photo-excited state.
2. Fluorescence - a radiative transition to the ground state ($S_o$ or G) with no change in spin multiplicity.
3. Internal conversion - a unimolecular transition to the $S_o$ potential surface, followed by vibrational relaxation (Fig 1b).
4. Intersystem crossing - a non-radiative transition from the singlet electronic state to an isoenergetic level in the triplet electronic state (or vice versa) followed by vibrational relaxation.
5. Energy transfer - non-radiative, to surrounding molecules.
6. Photochemical reaction - electron ejection, exciplex and excimer formation, excited state charge transfer complexes, proton transfer, etc.

The extent of each of these processes depends upon the intensity and wavelength of the light source, the characteristics of the fluorophore, other molecules in the vicinity and other general environmental factors such as solvent viscosity and temperature.

The absorption of a photon by the ground state of a molecule 'M' can be expressed in the form of a photochemical reaction

$$M(S_o) + h\nu \longrightarrow M^*(S) \qquad (1)$$

where $M^*$ is the excited state of M and $h\nu$ in the photon energy. The processes that depopulate the first excited singlet state $S_1$ can thus be expressed as

$$M^*(S_1) \xrightarrow{k_f} M(S_o) + h\nu_f \quad : \text{fluorescence} \qquad (2)$$

$$M^*(S_1) \xrightarrow{k_{nr}} \text{products} \quad : \text{non-radiative processes} \qquad (3)$$

with $k_{nr} = \Sigma\, k_i$ where $k_i$ are the rate constants for the various non-radiative processes

If the source of photons being absorbed by M to create $M^*$ is instantaneously shut off, then the change in concentration of $M^*(S_1)$ can be expressed differentially as

$$\frac{d[M^*]}{dt} = -\,(k_f + k_{nr} + \ldots)[M^*] \qquad (4)$$

or rearranging to find the concentration of $M^*$ at some later time t

$$\frac{d[M^*]}{[M^*]} = -\,k\,dt \qquad (5)$$

and integrating this becomes

$$\ln[M^*] = -\,kt \qquad (6)$$

or

$$[M^*]_t = [M^*]_{t=0}\, e^{-kt} \qquad (7)$$

$k = k_f + k_{nr} + \ldots$

$[M^*]_{t=0}$ = conc. of $M^*$ at the instant the source of photons is turned off.

The decay time constant $\tau$ is the mean lifetime of the excited species prior to returning to the ground state and is equal to the reciprocal sum of all of the emission rate constants, that is

$$\tau = \frac{1}{k} = \frac{1}{k_f + k_{nr}} \tag{8}$$

If M and $M^*$ are both singlet states then $\tau$ is equal to the fluorescence lifetime, and

$$[M^*]_t = [M^*]_{t=0}\, e^{-t/\tau} \tag{9}$$

The intensity of fluorescence $F_1$ is related to the concentration of the molecule M by

$$F_1(t) = k_f\, [M^*] \tag{10}$$

and therefore we may write

$$F_1(t) = (F_1)_{t=0}\, e^{-t/\tau} \tag{11}$$

and $\tau$ may be defined as the time necessary for the fluorescence intensity to decrease to 1/e of its intensity observed before the light source was turned off.

**FIGURE 1**

Energy level diagram

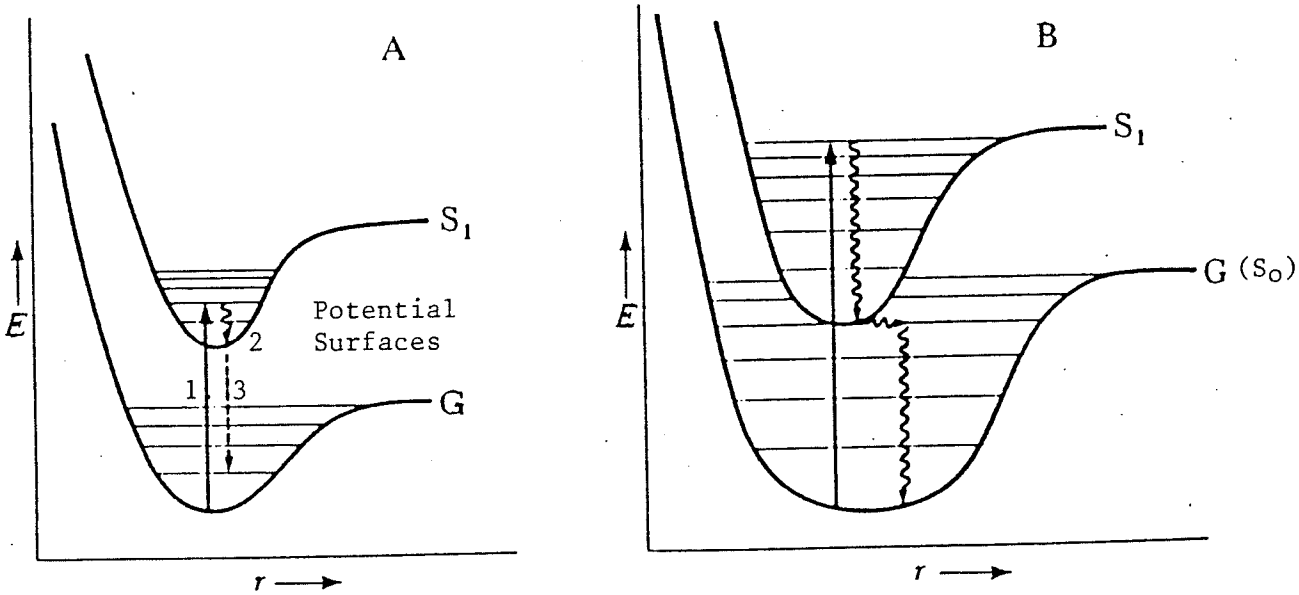


1 - absorption
2 - vibrational relaxation
3 - fluorescence

## 2.0 The fluorescence lifetime instrument: A brief description

The simultaneous competing processes which may depopulate a particular excited state can also be thought of in terms of joint probabilities. By analogy, one can also describe the time dependence of the fluorescence process itself as a probabilistic process. Experimentally, a fluorescence probability function or distribution is collected by a Fluorescence Lifetime Instrument (FLI).

There are two main techniques used to collect a fluorescence decay distribution, namely, time-resolved pulse-fluorometry and phase-modulation fluorometry. A description of the PRA[1] FLI is outlined below. It employs the pulse-fluorometry method. This method is reviewed by Ware [12], Lakowicz [13] and Badea [19].

A short pulse of light of an appropriate wavelength is used to create excited states of the molecules being studied. In our system, the sample is repeatedly excited by a low pressure thyratron gated flashlamp. An FLI employing a frequency doubled, cavity dumped, mode-locked synchronously pumped dye laser system to provide very short excitation pulses (~ 100 ps) is described by Lambert et al. [18]. A comparison of excitation sources and a

1. Photochemical Research Associates Inc

review of time-resolved fluorometry is given by Soini and Lövgren [22].

When the light source fires, a reference signal is generated by a side-on photomultiplier tube (PMT) viewing the pulse directly (refer to Fig. 2). This reference signal goes to a level crossing discriminator whose logic pulse becomes the 'START' input of the time-to-amplitude converter (TAC). The train of light pulses leaving the lamp through the front window is focussed onto the excitation monochromator. The monochromatic light then interacts with the sample, which is kept in a light tight, temperature controlled enclosure.

Fluorescence is detected at a right angle to the incident light path. Fluorescence passing through an emission monochromator set to the characteristic emission wavelength of the fluorophore is detected by a single photon detector. This constant fraction discriminator generates an anode pulse from its photocathode which is sent through a delay module to the 'STOP' input of the TAC. A delay of ~150 nsec insures that the START-STOP time interval is within the linear operating range of the TAC which, by charging a capacitor, generates an output signal whose voltage is directly proportional to the START-STOP time interval. If no fluorescence photon is detected, the device is reset to zero (see Figure 2).

This output voltage pulse then goes directly to the analog-to-digital converter (ADC) input of the multichannel analyser (MCA). The number of clock cycles generated by the ADC corresponds to a certain address location in the memory of the MCA. When a particular address is generated, one event is added to the total in that location, corresponding to the decay time of a certain fluorescence photon.

After a given period of time, a fluorescence decay curve is collected in the channels of the MCA as a histogram of fluorescence events of different lifetimes. The output voltage of the TAC may be amplified or biased (shifted) to select a portion of the fluorescence decay probability curve. The selection of an appropriate time base or sampling 'window' for a particular decay curve will be discussed in a later section.

**FIGURE 2**

Block diagram of the fluorescence lifetime instrument

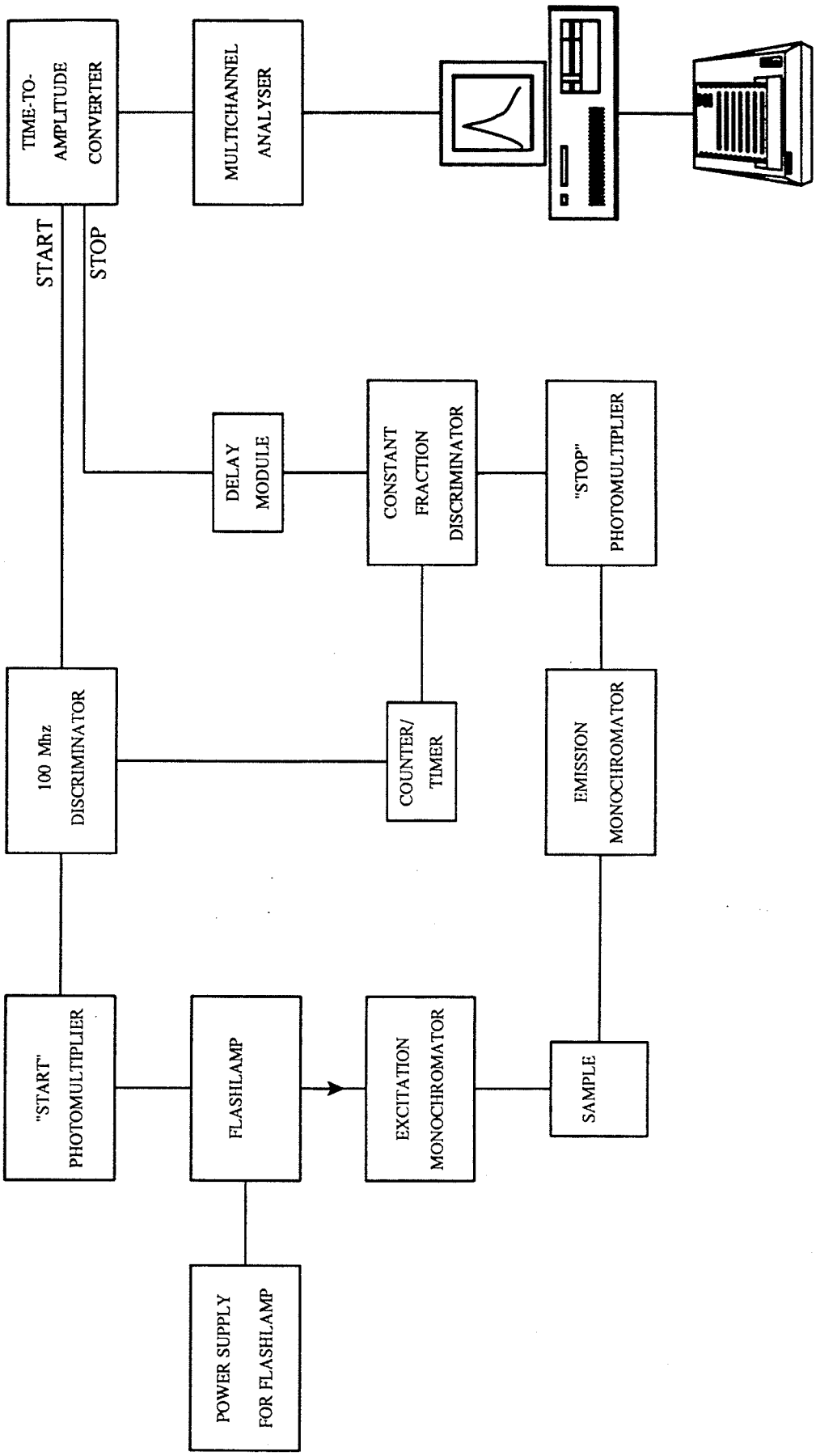
TIME-TO-
AMPLITUDE
CONVERTER
MULTICHANNEL
ANALYSER
START
STOP
DELAY
MODULE
CONSTANT
FRACTION
DISCRIMINATOR
"STOP"
PHOTOMULTIPLIER
100 Mhz
DISCRIMINATOR
COUNTER/
TIMER
EMISSION
MONOCHROMATOR
"START"
PHOTOMULTIPLIER
FLASHLAMP
EXCITATION
MONOCHROMATOR
SAMPLE
POWER SUPPLY
FOR FLASHLAMP

**FIGURE 3**

The time-to-amplitude converter
capacitor charging

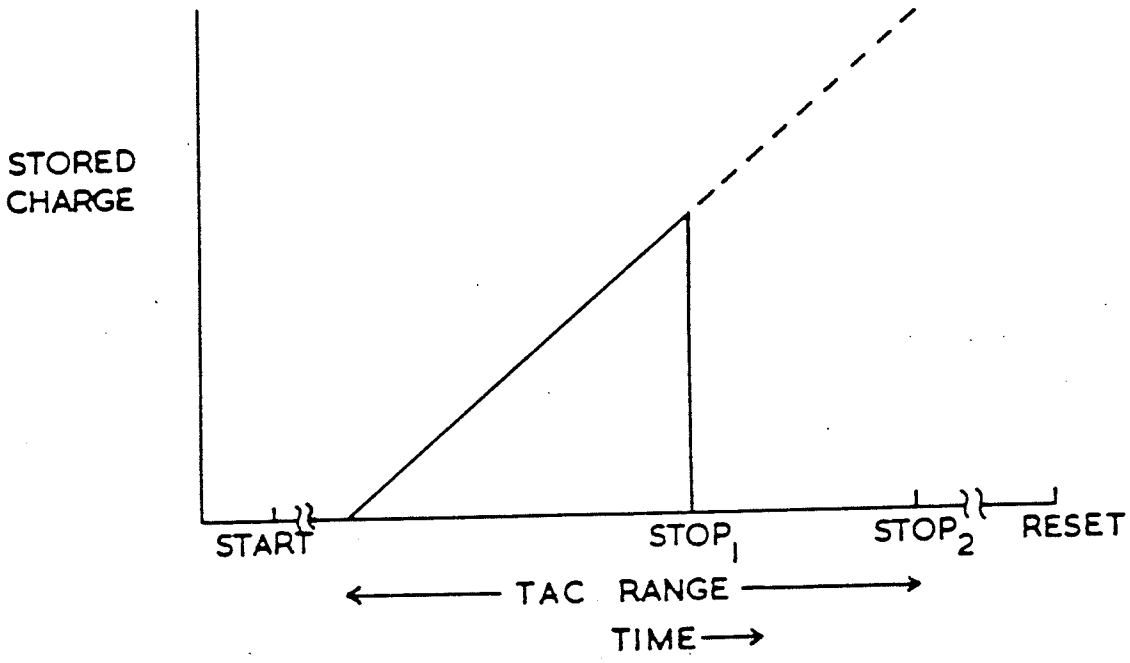
STORED
CHARGE
START
STOP1
STOP2
RESET
TAC RANGE
TIME

## 2.1 Single photon counting

A Fluorescence Lifetime Instrument utilizing the pulse-fluorometry method operates in a single photon counting (SPC) mode. A summary of time-correlated SPC is given by O'Connor [17]. In an ideal time-correlated experiment, each photon emitted by the sample as a result of an excitation flash would be timed and recorded. The response time of the detection equipment, and the mode of operation of the TAC, render it necessary to time only the first photon in a given time interval after the occurrence of the flash.

If more than one photon per excitation pulse is incident on the photocathode, the TAC will receive its 'STOP' pulse when the first photon is detected and reset itself to await another 'START' pulse. A second photon, detected by the emission PMT later in time but before the arrival of the next 'START' pulse, will not be counted since the TAC is inactive. These pulse pile-up distortions discriminate against late arriving photons and consequently the measured decay will be skewed toward lifetimes which are shorter the the actual values.

If the number of detected anode pulses is much less than the number of excitation cycles (lamp frequency), then the count in channel 'i' will be a measure of the fluorescence intensity at time 'i'. PRA recommends that the number of detected anode

pulses (count rate) be no more than 2% of the lamp frequency. Typically then, if the lamp is operating at 45 kHz, then the fluorescence count rate should not be greater than ~ 900 counts/sec.

In the single photon counting method, the resolution is quite good (~ 2 nsec). This is because the distortions normally associated with a fluorescence PMT and the recording circuitry are avoided since the PMT is used merely to time the arrival of photons at the photocathode instead of detecting the detailed shape of the entire pulse. In addition, amplitude jitter in the excitation light pulse is irrelevant provided that the pulse shape remains constant.

Thus, the SPC technique has all the advantages of digital signal processing, since it is only concerned with the occurrence time of events and not with their intensities.

## 3.0 The convolution of pulses

If the light pulses exciting the molecules in a sample were infinitely narrow (delta functions) and the response of the detection system infinitely fast, then the observed decay curve, D(t), would equal a true decay or delta-pulse response, F(t). The observed decay, with an excitation function, E(t), not a delta function, is convoluted or folded together because the molecules excited by photons from the rising edge of the flash are decaying while others are still being excited by photons from the tail of the flash.

The light pulse is assumed to be a sum of delta-pulses of amplitude E(t') at any time t'. Since the number of sample molecules excited at time t' is proportional to E(t'), the number at any later time (t - t') is proportional to E(t')F(t-t') (refer to Fig. 4). The total number of excited state molecules at time t, written as D(t), is the sum over all times t' preceding time t. For an infinite sum

$$D(t) = \int_0^t E(t')F(t-t')dt' \qquad (12)$$

where E(t') is also referred to as the time-dependent Instrument Response Function (IRF(t')).

D(t), the measured decay curve, represents the delta-function response of the sample distorted by convolution with both the excitation pulse and the detector response. The IRF(t') is also a convolution of the time-dependent optical pulse from the light source, the timing uncertainties in both the fluorescence detector and the electronics measurement system.

A mathematical process of deconvolution can solve for F(t), the true decay of the sample, if D(t) and IRF(t') are measured under the same experimental conditions. In practice, this is not quite achievable because the excitation and emission wavelengths are different, and it is the wavelength dependence of both the optical pulse profile and the PMT transit time dispersion that is one of the most serious obstacles to the accurate determination of decay times which are significantly shorter than the excitation pulse width.

Errors are also introduced by the geometric and wavelength dependence of the PMT transit-time dispersion. According to PRA, their PMT's have the lowest wavelength dependence on transit-time dispersion and their flashlamp's optical profile is virtually independent of wavelength between 300 and 500 nanometers. To reduce the PMT geometric errors, a light scattering agent, which scatters light in the same manner as the sample, should be used to collect the IRF thereby equalizing the illuminated area of the PMT photocathode in each case. LUDOX, a colloidal suspension with an optical density similar to that of a cell suspension, is used to collect the IRF data.

FIGURE 4

The convolution of pulses

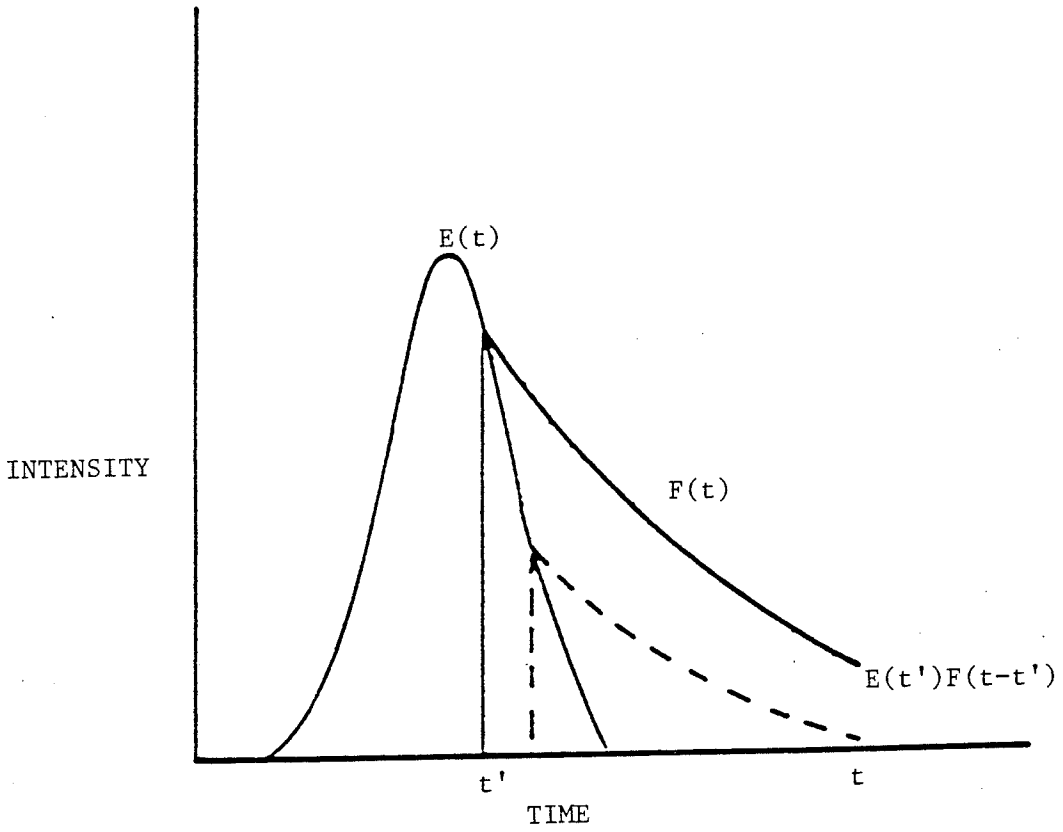
E(t)
INTENSITY
F(t)
E(t')F(t-t')
t'
t
TIME

## 4.0 Deconvolution

The task of Fluorescence Lifetime Analysis (FLA) has been approached using several mathematical algorithms to carry out the deconvolution, including least squares, method of moments, Laplace transforms, and Fourier transforms. An extensive review of least squares analysis and the other methods has been compiled by Cundall and Dale [11].

The PRA deconvolution is based in part on the least squares method of Grinvald and Steinberg [23]. The vast number of fluorescence pathways are well described by a small number of relatively simple models. The PRA deconvolution employs a least squares criterion to determine the goodness of fit of a model function to the decay data [14].

Assuming the fluorescence decay response can be described by a sum of exponentials, then

$$F(t) = \sum_i \alpha_i \, e^{-t/\tau_i} \qquad (13)$$

with $\alpha_i$ = $i^{th}$ pre-exponential factor (amplitude)
$\tau_i$ = $i^{th}$ decay time

The measured decay curve D(t) is calculated by generating a fitting function $D^c(t)$ from assumed values for $\alpha_i$ and $\tau_i$ in the model function F(t) and by using the measured IRF data. The least squares criterion for the best fit of $D^c(t)$ to D(t) is that the Poisson-weighted sum of the squares of the differences between $D^c(t)$ and D(t) be a minimum; i.e.,

$$\chi^2 = \sum_{i=m}^{n} \frac{(D_i - D_i^c)^2}{\sigma_i^2} \qquad (14)$$

with $D_i$ = # experimental events in channel i
$D_i^c$ = calc. # of counts in channel i

be minimized. 'm' and 'n' are the low and high channel numbers, respectively, and $\sigma_i^2$ is statistical weighting factor which is equal to the variance in the $i^{th}$ channel. The collection of data of this type follows a Poisson distribution, and the standard deviation $\sigma_i$ is equal to

$$\sigma_i = \sqrt{D_i} \qquad (15)$$

If, for example, a channel contains $10^4$ counts, the expected deviation would be $10^2$. Assuming the model accounts for the measured data, then the numerator and the denominator in equation (14) are both $(10^2)^2$ and this channel contributes 1.0 to the value of $\chi^2$. Hence for random errors $\chi^2$ is expected to equal the number of channels. This dependence on the number of channels makes $\chi^2$ an inconvenient value. The reduced chi-squared value $\chi_r^2$ is equal to

$$\chi_r^2 = \frac{\chi^2}{N - p} \qquad (16)$$

with N = # of channels over which the fitting is performed.
p = # of fitting parameters in the assumed decay model.

If only random errors contribute to $\chi_r^2$ then this value is expected to be 1.0 since the average $\chi^2$ per channel should be 1.0. If the model does not fit the data, then the value of $\chi_r^2$ will be much greater.

In addition to the reduced chi-squared test, PRA has included four other statistical tests to assist in the acceptance or rejection of a model; each is outlined briefly below. All of the statistical tests are written explicitly in Appendix 1. They are also described by O'Connor [17] and Lampert [18].

(a) Weighted residuals plot.

This visual indicator is scaled in terms of the number of standard deviations of the maximum residual. Non-random deviations of the residuals from the zero line indicate that the data are not adequately described by the assumed model.

(b) Auto-correlation function plot

Another visual indicator of non-random fluctuations. The auto-correlation function correlates neighboring values of residuals. The plot should fluctuate randomly about the zero line.

(c) Runs test

The runs test parameter (SGR) is much more sensitive to small deviations from the expected kinetic behavior than the $\chi_r^2$ test. If the absolute value of SGR $\leq$ 1.96, the runs test is acceptable at the 95% confidence interval.

(d) Durbin-Watson test

This parameter is more sensitive to small non-random patterns in the residuals than the $\chi_r^2$ test. For a single exponential fit the Durbin-Watson parameter should be greater than 1.65 (double > 1.75, triple > 1.85).

## 5.0 Ethidium bromide

ethidium bromide (figure 5), a phenanthridine drug, is a fluorescent cationic molecule able to interact with polynucleotides. The fluorescence properties and the binding properties of this dye have been extensively investigated and have been reviewed by Le Pecq [3,5]. These properties are summarized briefly in the following paragraphs.

ethidium bromide binds to polynucleotides primarily by an intercalation mechanism. During intercalation two base pairs of DNA break their stacking interaction and come apart. ethidium bromide, similar in size to a base pair, intercalates between the base pairs forming a sandwich complex. As each ethidium bromide molecule becomes rigidly bound, the double helical structure progressively unwinds and lengthens [6].

ethidium bromide binds specifically to double stranded polynucleotides and in the case of DNA, it has no base pair specificity. It follows the adjacent excluded site binding model. This means that each site of a nucleic acid is accessible to the dye with the same 'a priori' affinity, but a site adjacent to an already occupied one is prohibited [6]. There is evidence that ethidium bromide also binds to the outside of the DNA helix. This topic will be discussed in more detail in a later section.

Being a highly planar aromatic molecule, ethidium bromide has very useful fluorescence properties. Free dye in aqueous solution is strongly quenched by $O_2$ and is therefore only weakly fluorescent. Upon intercalation, the ethidium bromide molecule enters a hydrophobic environment. The steric protection of ethidium bromide provided by the DNA base pairs prevents collisions with $O_2$. The $O_2$ quenching rate of ethidium bromide's fluorescence decreases 30 fold upon intercalation [8].

ethidium bromide has proven to be an extremely useful fluorescent stain for the visual detection of double stranded DNA and has been used extensively for in vitro cytofluorometric studies. Using ethidium bromide's fluorescence properties to study the conformation of nucleic acids in vitro has also been summarized by Le Pecq [3]. Basically, because ethidium bromide intercalates between base pairs of DNA, it is highly sensitive to subtle changes in the conformation of the DNA helix. Its increased fluorescence intensity upon binding and its long monoexponential lifetime (~ 24ns) make it a good candidate for monitoring DNA conformation with techniques such as Fluorescence Lifetime Analysis (FLA) and rotational anisotropy analysis of the fluorescence depolarization.

The fluorescence properties of ethidium bromide bound within the DNA helix should be highly sensitive to changes in the conformation and local molecular environment of DNA both in vitro, and in vivo as indicated by Le Pecq [3].

FIGURE 5

ethidium bromide

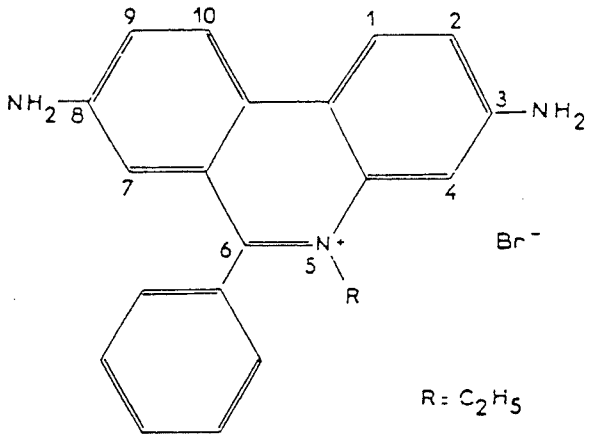
9
10
1
2
NH2
8
3
NH2
7
4
6
N+
5
R
Br-
R = C2H5

# PART B

## OPTIMIZING DATA COLLECTION AND ANALYSIS

## 6.0 Flashlamp performance and pulse stability

The reproducibility of the pulse profile is crucial in a single photon counting experiment. An unstable flashlamp pulse profile affects the time resolution of the experiment, increasing the difficulty in deconvoluting the decay curve and decreasing the reliability of the results. Maximum flashlamp output is also of primary importance. Maximizing the fluorescence intensity will reduce the overall data collection time.

The pulse stability is improved with a narrow pulse width. A narrow pulse width is also preferred for deconvolution and for resolution of very short lifetime values. The pulse stability is also improved with a stable arc configuration. 'Arc' refers to the voltage discharge across the electrodes. The conditions for optimum light intensity must not exceed those for maximum arc stability.

The variables which influence the photon intensity per pulse and the pulse width are as follows:

(a) pulse repetition rate (lamp frequency)
(b) type of gas
(c) gas pressure
(d) electrode separation
(e) applied voltage

The fluorescence intensity increases and the pulse width decreases as the lamp frequency increases.

Increasing the gas pressure reduces the pulse width and reduces the photon intensity.

Increasing the gap between the electrodes increases the pulse width and increases the photon intensity. However, as the gap is increased, it requires an increase in the applied voltage to achieve gas breakdown.

Increasing the voltage applied across the electrodes above the gas breakdown voltage increases the photon intensity per pulse.

Several gases may be used to fill the flashlamp, the most useful being nitrogen ($N_2$) and hydrogen ($H_2$)(ultra high purity). Nitrogen produces intense spectral lines in the 300 to 400 nm range with an intensity of $10^{10}$ to $10^{11}$ photons/flash at a repetition rate of 25kHz. Hydrogen has a continuous emission spectrum down to 200 nm but with only $10^8$ photons/flash, a 100-fold reduction in intensity compared to $N_2$. However, $H_2$ has a narrower and cleaner pulse than $N_2$.

Experiments in which the fluorescence count rate was

Table 1

Maximized Lamp Parameters

| Parameter | $N_2$ | $H_2$ | PRA* - $N_2$ (1) | (2) |
|---|---|---|---|---|
| Electrode gap (mm) | 2.0 | 2.0 | 2.0-4.0 | 0.25-1.5 |
| Gas pressure "Hg(kPa) | 15(-50) | 15(-50) | 20-15 (-70to-50) | 13-0 (-44to 0) |
| Voltage (kv) | 3.0 | 6.0 | 5.5-6.5 | 3.0-5.0 |
| Frequency (kHz) | ~46(max) | ~46(max) | 30-35 | <30 |

* Photochemical Research Associates recommended values

(1) For stable intensity, but pulse.

(2) For less stable intensity, but shorter.

monitored while varying the parameters mentioned above have been discussed in detail by Heller [14]. The results in table 1 show the settings for maximum fluorescence intensity with minimum pulse width for nitrogen and hydrogen. Also in table 1 are the recommended settings from the FLI manufacturer (PRA).

The main difference between using nitrogen and hydrogen is that with nitrogen, the intensity is higher (even at the lower voltage) and the arc stability is much greater than with hydrogen. Even with a voltage that is twice that of nitrogen, hydrogen is still only half as intense. The 6.0 kv was also needed to improve arc stability. A warm up time of at least 1 hour is necessary with hydrogen to achieve a reasonably stable arc, and hence a reasonably stable intensity. However, a stable intensity is not that important, unless you are using this system to measure relative fluorescence intensities. It is recommended that nitrogen be used for this purpose since it provides a much more stable intensity.

### 6.1 The instrument response function

In Figure 6 a and b are the IRF's for $N_2$ and $H_2$ respectively. These were obtained using the lamp settings in table 1. Figure 6c, taken from Lakowicz [13],page 36, shows typical IRF's for $N_2$ and $H_2$. The $N_2$ peak in fig. 6c is slightly narrower than in fig. 6a, probably due to the higher gas

pressure. Both $H_2$ curves have similar peak widths, although our's does not have the exponential tail section. As will be seen in a later chapter, this is very important for the decay analysis. The large exponential tail in the case of $N_2$ is due to an after-glow effect from the pulsed light source. Increasing the gas pressure in excess of 1 atmosphere generally reduces the intensity of the tail. However in Figure 6c, with a gas pressure of 1.5 atm., the tail section is still quite significant.

The IRF peak width decreases slightly as the lamp frequency is decreased, as seen in Figure 7. The opposite is seen with the excitation pulse width, which increases as the lamp frequency is decreased. The IRF peak width also decreases slightly as the lamp voltage is lowered. A narrow IRF is desirable for better resolution of fast lifetime components (~ 1 nsec). However, in the case of $H_2$, lowering the lamp frequency from the maximum value and lowering the voltage applied reduce both the photon intensity and the stability of the intensity. These disadvantages outweigh the benefits of a slight reduction in IRF peak width.

Note in Figure 7b, the small hump on the decay side of the IRF, as illustrated by the dots. A similar hump is also evident in the IRF for $H_2$ in Figure 6c. This secondary peak arose after the lamp had been running for approx. five hours. Once the

electrodes were cleaned with emery cloth, the peak disappeared. It was found that this peak affected the deconvolution analysis of fast decaying species, with undesirable results. Depending on the sampling time, this may pose a limitation on the number of samples that can be run before the lamp requires cleaning. This secondary peak did not occur with $N_2$.

In summary, the benefits of using $N_2$ are a high photon intensity which is reasonably stable for long periods of time. The disadvantage is the long exponential tail on the IRF. This will be discussed in more detail in a later section. With $H_2$, the disadvantages are an intensity which is 50% lower than that with $N_2$ and much less stable (stability is improved however, with a 1 hour warm-up time), and the electrodes require more frequent cleaning to prevent irregularities in the IRF profile. The advantage of $H_2$ is the lack of any tail on the IRF. The significance of this will also be discussed in a later section.

Using the lamp settings listed in table 1, the photon intensity is maximized with reasonable excitation pulse stability and good instrument response functions. This should minimize the overall sample collection time which in turn helps to reduce the effect of any long term instabilities or drift in the lamp output. Minimizing collection time is also crucial when the samples being investigated have a very low fluorescence quantum yield or are present in very low concentration.

**FIGURE 6**

The instrument response function
6a: nitrogen gas
6b: hydrogen gas
6c: IRF's from Lakowicz [13]
$H_2$ - .5 atm (-50kPa)
$N_2$ - 1.5 atm (50 kPa)

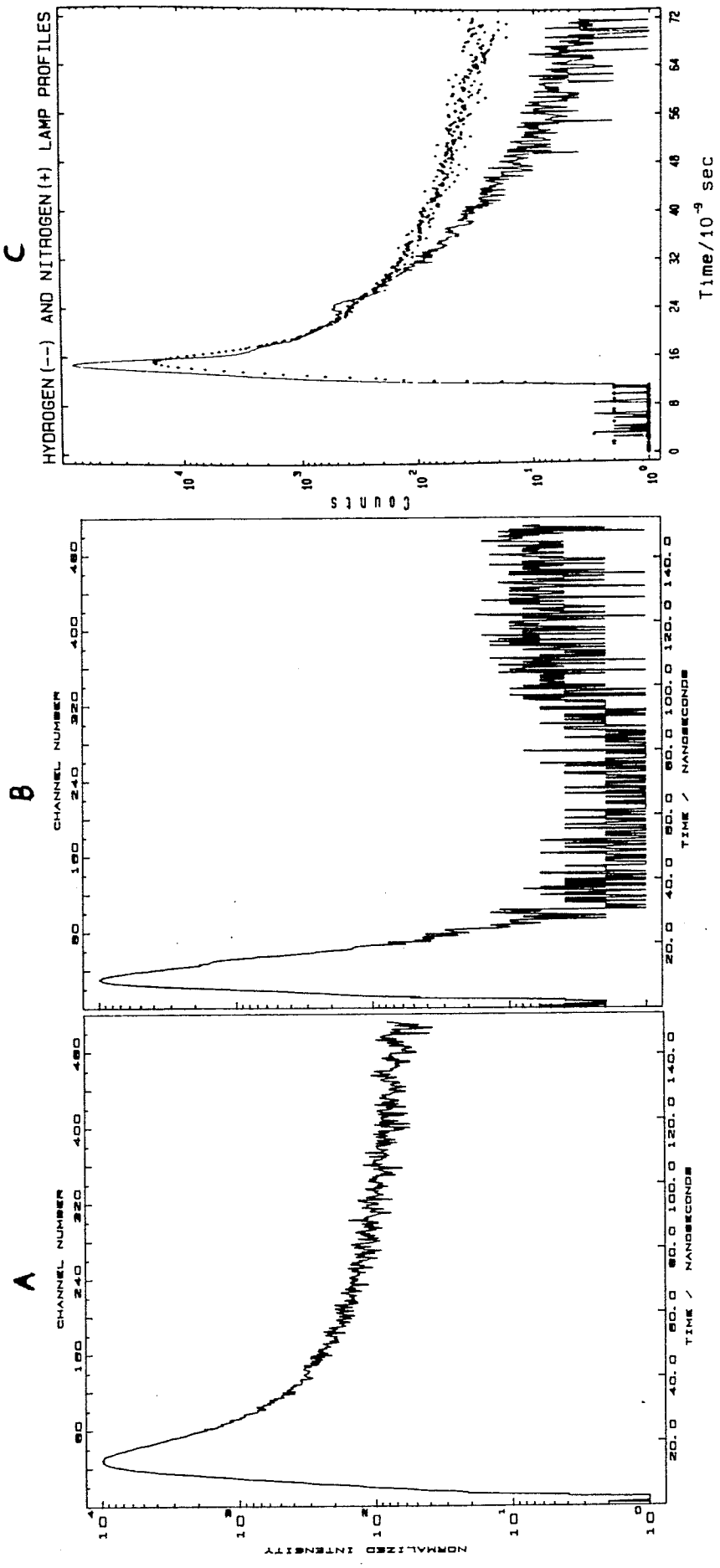
A
B
C
CHANNEL NUMBER
TIME / NANOSECONDS
NORMALIZED INTENSITY
HYDROGEN (--) AND NITROGEN (+) LAMP PROFILES
Counts
Time/10⁻⁹ sec

FIGURE 7

The IRF at two frequencies
7a: 46 kHz (····)
35 kHz (——)
7b: deterioration in the IRF profile

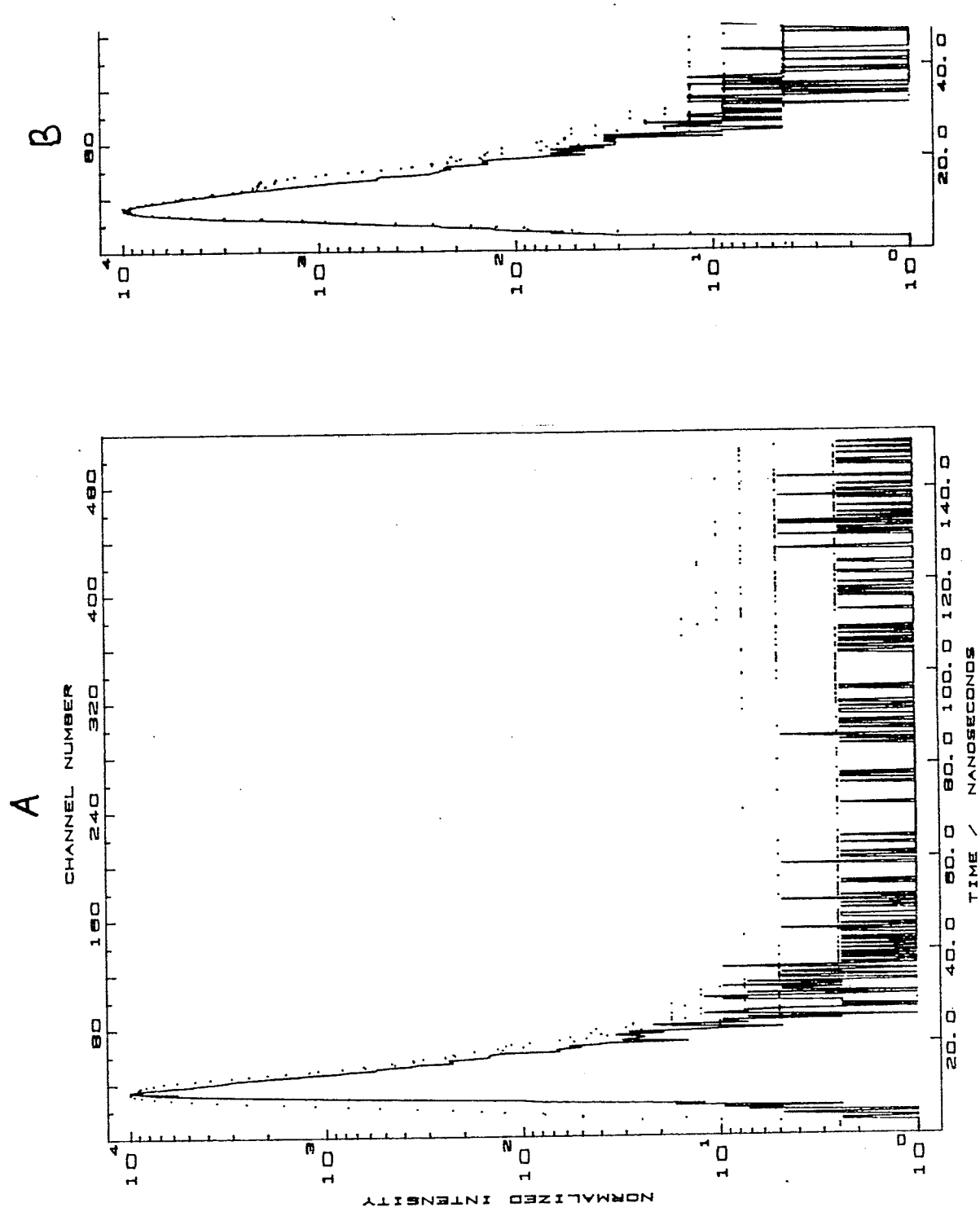
A
B
CHANNEL NUMBER
80
160
240
320
400
480
NORMALIZED INTENSITY
10^0
10^1
10^2
10^3
10^4
20.0
40.0
60.0
80.0
100.0
120.0
140.0
TIME / NANOSECONDS

## 7.0 Data sampling and precision

Once the flashlamp output has been maximized, a fluorescence decay curve is collected in the multi-channel analyzer (MCA) as a histogram of the number of counts (photon intensity) versus the time base. With the number of channels fixed (max. 512 allowed by deconvolution software), the time base is expressed in terms of the time-per-channel (T/CH).

To 'set up' a decay curve such that the region of interest (ROI) is within the 'window' of the MCA with maximum resolution requires careful and subtle adjustment of the MCA and TAC controls, particularly if an unknown sample is being studied for the first time. Choosing the correct T/CH is very important to the results of the decay experiment. In this chapter, the effects of varying the T/CH, and the number of counts collected, on the precision of the Fluorescence Lifetime Analysis (FLA), will be examined.

The criterion for choosing an ROI is not a rigid one. Initially, the entire decay curve of a sample should be displayed using a large T/CH. This facilitates the determination of the ROI and hence the T/CH required such that the curve has sufficiently decayed to the constant background level. The PRA deconvolution software package can calculate up to four separate lifetime components and therefore it is crucial that the entire portion of the curve which is significant to the analysis be recorded in

order that no information is lost. Exactly where the decay stops and the background starts can be difficult to determine, when looking at the convoluted decay curve, especially when using $N_2$ gas in the flashlamp. On a log scale, the long tail produced in the sample decay curve looks like it may be from some long lived fluorescence component, but in fact it may be just the background level of counts above the IRF. This is evident in Figures 8a and 8b.

If there are no pulse pile-up errors in the experiment, then the histogram collected in the MCA is an exponential. Depending upon the T/CH, the decay will fall slowly, moderately or steeply. A slowly decaying histogram provides a good estimate for the pre-exponential factor and a poor estimate for $\tau$ (in equation 13). A fast decaying histogram provides a poor estimate for both parameters. There should be some intermediate optimum value [16]. With the PRA system, by maximizing the ROI within the 512 channels, the decay will always fall with a moderate slope (~ 45°) which is close to optimum.

A decay curve is statistically approximated by a Poisson distribution with '$\tau$' as the mean. The variance is given by

$$\mathrm{var}(\bar{\tau}) = \frac{1}{n-1} \sum_{i=1}^{n} (\tau_i - \bar{\tau})^2 \qquad (17)$$

Since the probability of observing any specific number of counts is given by a Poisson distribution, every count in every channel represents an estimate of the mean for that channel [17]. The uncertainty in the number of counts $N_i$ in channel i is $\sigma_i$ with

$$\sigma_i = \sqrt{N_i} \tag{18}$$

This uncertainty determining the number of counts necessary to record a decay curve with a given precision. For example, to achieve 10% precision in channel i, then

$$.10 = \frac{1}{\sigma_i} = \frac{1}{\sqrt{N_i}} \quad \text{and} \quad N_i = 100 \tag{19}$$

If in channel i, the curve has decayed to 1% of its maximum, the number of counts necessary in the peak would be 10,000.

How does the number of counts in the peak channel relate to the T/CH and the data sampling time or to the total number of counts in the ROI (area under the curve)? How do these parameters affect the precision of the lifetime values?

Figure 8 shows two curves in which 10,000 counts were collected in the peak channel for 2 different T/CH's, with curve A taking twice as long to collect. This is because the T/CH, which is equal to the width of the peak channel, is only half of that in curve B and therefore collecting the same number of counts in a channel half as wide takes twice as long. With half the T/CH in curve A, the same ROI spans twice as many channels, and the total number of counts is doubled.

Note in each case the uncertainty in the channel total at end of the 2 decade decay is 10%. It would seem that for the same precision in the ROI, curve A took twice as long to collect.

However, in curve A, because the ROI is divided into twice as many channels, the resolution of the lifetime components should be better. Also with twice as many total counts, one would also predict that the resolution of the lifetime components in curve A should better.

Selinger et el. [17] conducted a simulation in which six different decay curves (six $\tau$ values) were collected for 10 different sets of total number of counts. For each combination, 200 experimental sets of data were generated and fitted. The results are shown in Figure 9. The six curves are expressed in terms of the number of channels (10,20,30 etc.) with a fixed T/CH. This corresponds to the PRA system by expressing the six curves as six different T/CH's with the same ROI. The mantissa 'R' is the relative sample standard deviation for $\tau$.

$$R = \frac{[\mathrm{var}(\bar{\tau})]^{1/2}}{\tau} \qquad (20)$$

The results show that as the T/CH decreases, the error on $\tau$ decreases in a non-linear fashion, which is dependant on the total number of counts. Also, at high total count values, the

error on $\tau$ becomes independent of T/CH. There also seems to be an optimum T/CH at which a low error can be achieved with very few counts.

How does this relate to the example above? Selinger's results would indicate that in curve A, because the T/CH is less than in B, the error should be less. Also, because the total number of counts in A is double that of B, the error should be less as well. In each case, 'how much' less depends upon the complexity of the decay curve. Selinger's results are for a simple mono-exponential decay scheme. To reach the area in Figure 9 where the errors are independent of the T/CH and the total number of counts for multi-exponential components, it is likely to require larger T/CH and total count values.

In the example illustrated in Figure 9, I would recommend that the set-up in curve A (with the lower T/CH) be selected. This maximizes the ROI within the MCA such that the angle of the decay is moderate, and the error is a minimum. The total number of counts could probably be halved with little loss in the resolution of the lifetime components. This would require only 5,000 counts to be collected in the peak channel at half the sampling time. Minimizing the sampling time is very important for the reasons outlined at the end of the previous chapter. Examples showing the effects of varying the T/CH on the lifetime components are presented in the next section.

**FIGURE 8**

A region of interest collected
at two time-per-channel settings
8a: T/CH = .365, total counts $6.6 \times 10^5$
8b: T/CH = .729, total counts $3.4 \times 10^5$

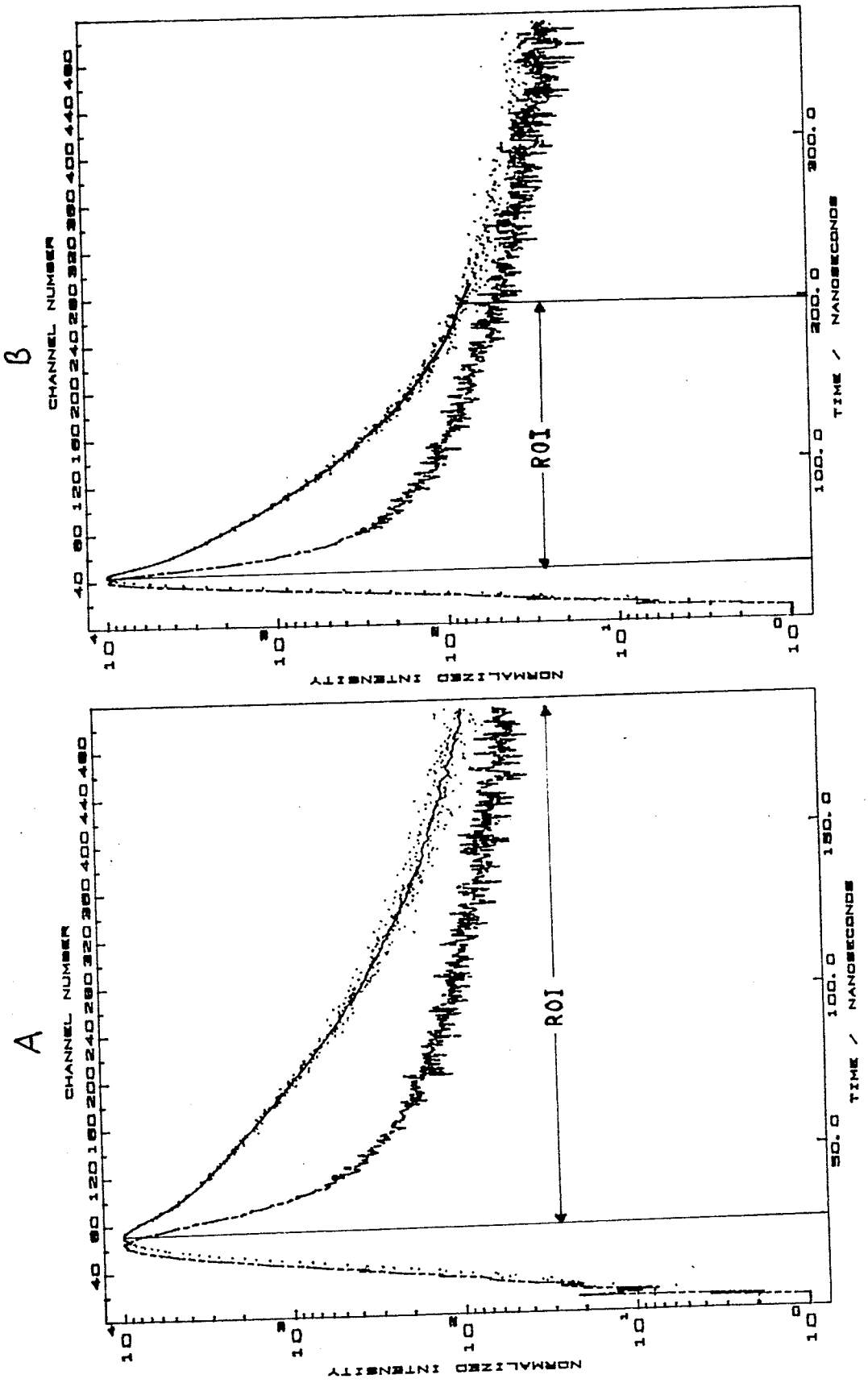
B
CHANNEL NUMBER
40 80 120 160 200 240 280 320 360 400 440 480
NORMALIZED INTENSITY
ROI
TIME / NANOSECONDS
100.0
200.0
300.0
A
CHANNEL NUMBER
40 80 120 160 200 240 280 320 360 400 440 480
NORMALIZED INTENSITY
ROI
TIME / NANOSECONDS
50.0
100.0
150.0

FIGURE 9

Precision v. T/CH v. total number of counts

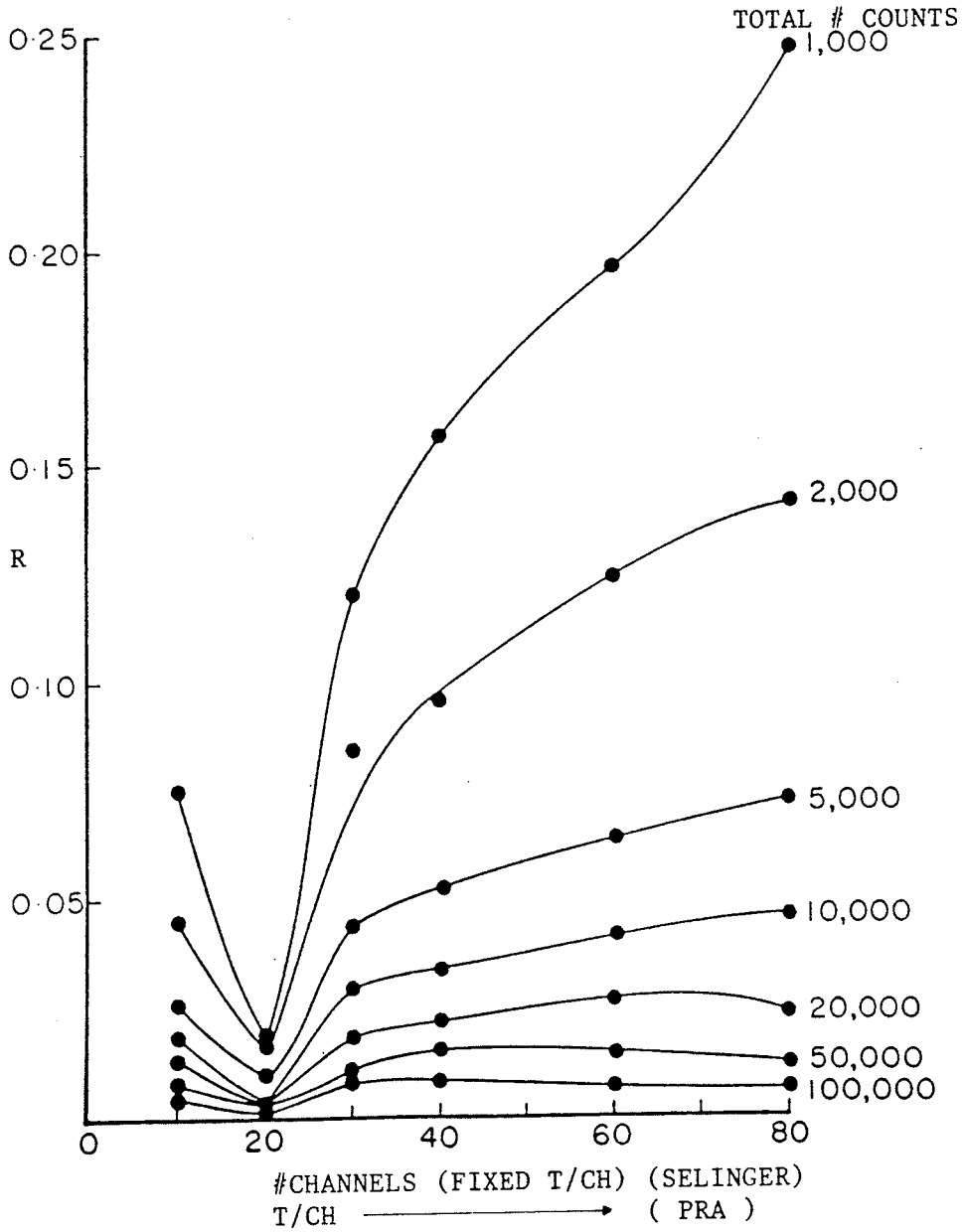
TOTAL # COUNTS
1,000
2,000
5,000
10,000
20,000
50,000
100,000
0·25
0·20
0·15
0·10
0·05
R
0
20
40
60
80
#CHANNELS (FIXED T/CH) (SELINGER)
T/CH
( PRA )

## 8.0 Choosing an exponential model

Recall from chapter 4.0 that the PRA Fluorescence Lifetime Analysis (FLA) fits a decay curve to a sum of exponentials

$$F(t) = \sum_i \alpha_i \, e^{-t/\tau_i} \qquad (21)$$

with $\alpha_i$ = $i^{th}$ pre-exponential factor (amplitude)
$\tau_i$ = $i^{th}$ decay time

If an unknown sample is being analyzed, assuming the simplest model, a single exponential, is the most logical place to start. The computer program requires initial estimates for $\alpha_i$ and $\tau_i$. An estimate for $\tau_i$ can be obtained from the value of the 1/100 decay time, that is, the time at which the curve has decayed to $1/100^{th}$ of its initial intensity.

$$\tau_{est} = \frac{t(1/100)}{\ln 100} \qquad (22)$$

An estimate of $\alpha_i$ is $1/\tau_{est}$. Once convergence has been reached, there are 5 statistical tests to indicate whether a 'good fit' has been obtained. These tests are described in chapter 4.0 and in Appendix 1. Table 2 is a summary of the conditions for an acceptable fit. These values are those suggested by PRA for their least squares analysis, and were found to be easily obtainable in virtually every experiment.

Table 2

Statistical parameters
Values for an acceptable fit

| Test | Parameter | Value |
|---|---|---|
| Reduced Chi-squared | $\chi_r^2$ | $\simeq 1.0$ , $\leq 1.2$ is acceptable |
| Runs | SGR | $-1.96 < SGR < 1.96$ , runs test accepted at 95% confidence interval |
| Durbin-Watson | DW | > 1.65 single exp.<br>> 1.75 double exp.<br>> 1.85 triple exp. |
| Residuals | plot | random fluctuations about the zero line |
| Auto-correlation | plot | random fluctuations about the zero line |

If an unacceptable fit is obtained (ie. $\chi_r^2 > 1.3$, DW < 1.65, |SGR| > 1.96, non-random residual and auto-correlation plots), then additional exponentials may be estimated until a good fit is obtained. In any case, the fit must be repeatable. Usually when too many components are included in the model the resulting error estimates for $\alpha_i$ and $\tau_i$ increase dramatically and the lifetime values are not repeatable.

It is important to realize that the exponential model is fitting a curve, and an improved fit can often be obtained by proposing a more complex model, which may not be a true reflection of the sample. An example of this was encountered when nitrogen gas was used in the flashlamp. An improved fit was often obtainable when a long lifetime component (>200 nsec) was included in the model, when in fact the sample did not contain a long lived species. The long lifetime component was actually fitting the difference in the level of background between the IRF and the sample curve which is present because the sample curve is collected for a considerably longer period of time. This example is shown in the next section.

In such cases, the resulting decay times should be interpreted in terms of discrete molecular entities within the sample. Where possible, the components should be isolated and analyzed as a single exponential to verify the lifetime for that species.

The estimates of uncertainty in the $\alpha_i$ and $\tau_i$ parameters (± values), provided by the least squares analysis method, are based on the assumption that the parameters are not correlated. This assumption is not true for multi-exponential decays. The $\alpha_i$ and $\tau_i$ values become more strongly correlated as the decay times become more closely spaced. The effect of this correlation is that a variation in one parameter will bring about a compensating change in the other parameters such that $\chi_r^2$ remains unchanged. Hence the actual uncertainties in the parameters are larger than those returned by the least squares algorithm [13].

The three figures at the end of this section are examples of various decay curves fitted with different exponential models. The resulting statistical parameters are given in table 3. In figure 10(a), it is obvious that the single exponential model does not adequately describe the decay, whereas a double exponential decay does (fig. 10(b)). Note, in figure 11(b), although a third order fit provides a better fit, the error values increase slightly over those in figure 11(a). This indicates that a third order model adequately describes the curve, but the ROI is not large enough. Figure 12 is a case where a third and fourth order model seem to provide good fits when looking at the fit parameters, although, if you look at the ± values on the lifetimes, they increase dramatically, and in one case, the error is over 50%. This component is highly questionable, and is probably not real. Also note the change in the third order lifetimes as one goes to the fourth order.

Table 3

Statistical test results
Various exponential models

| Figure | number exp | $\chi_r^2$ | DW | SGR | Randomness of plots | | |
|---|---|---|---|---|---|---|---|
| GOOD | | | | | Residual | Auto-corr | FIT |
| 10(a) | 1 | 3.52 | 0.56 | -6.39 | no | no | no |
| 10(b) | 2 | 0.99 | 2.03 | 0.53 | yes | yes | yes |
| 11(a) | 2 | 1.66 | 1.18 | 4.40 | no | no | no |
| 11(b) | 3 | 1.01 | 1.95 | 0.10 | yes | no | yes |
| 12(a) | 3 | 1.13 | 1.88 | 0.68 | yes | yes | yes |
| 12(b) | 4 | 1.11 | 1.92 | 0.74 | yes | yes | yes |

In the next section, limitations of the FLA will be examined, in terms of the variability of the lifetime components, as the parameters of the analysis are changed. With such an examination, a more realistic appraisal of the accuracy and precision of FLA results can be made. This step is crucial if very complex biological systems are being studied, in which any small perturbation would only translate into minor changes in the FLA.

FIGURE 10

A two component decay
10a: A single exponential fit
10b: A double exponential fit

A

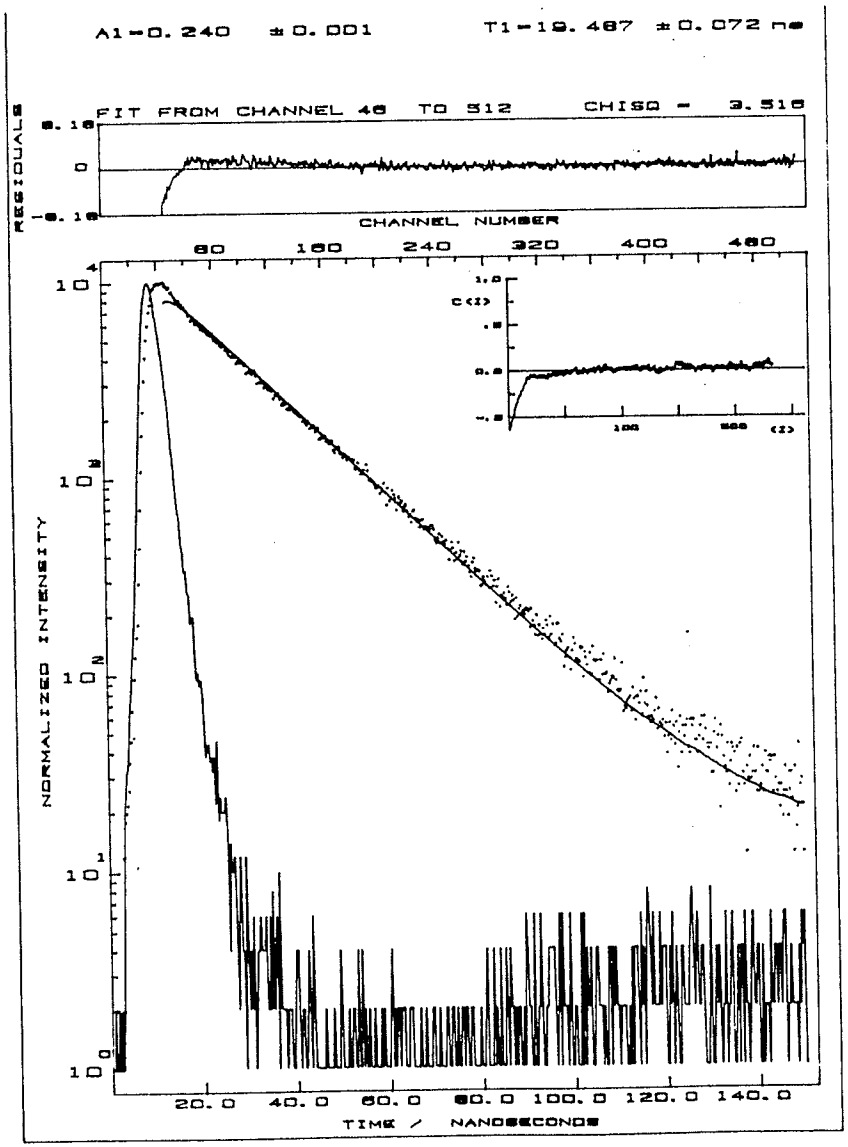
A1=0.240 ±0.001
T1=19.487 ±0.072 ns
FIT FROM CHANNEL 48 TO 512
CHISQ = 3.516
RESIDUALS
CHANNEL NUMBER
NORMALIZED INTENSITY
TIME / NANOSECONDS

B

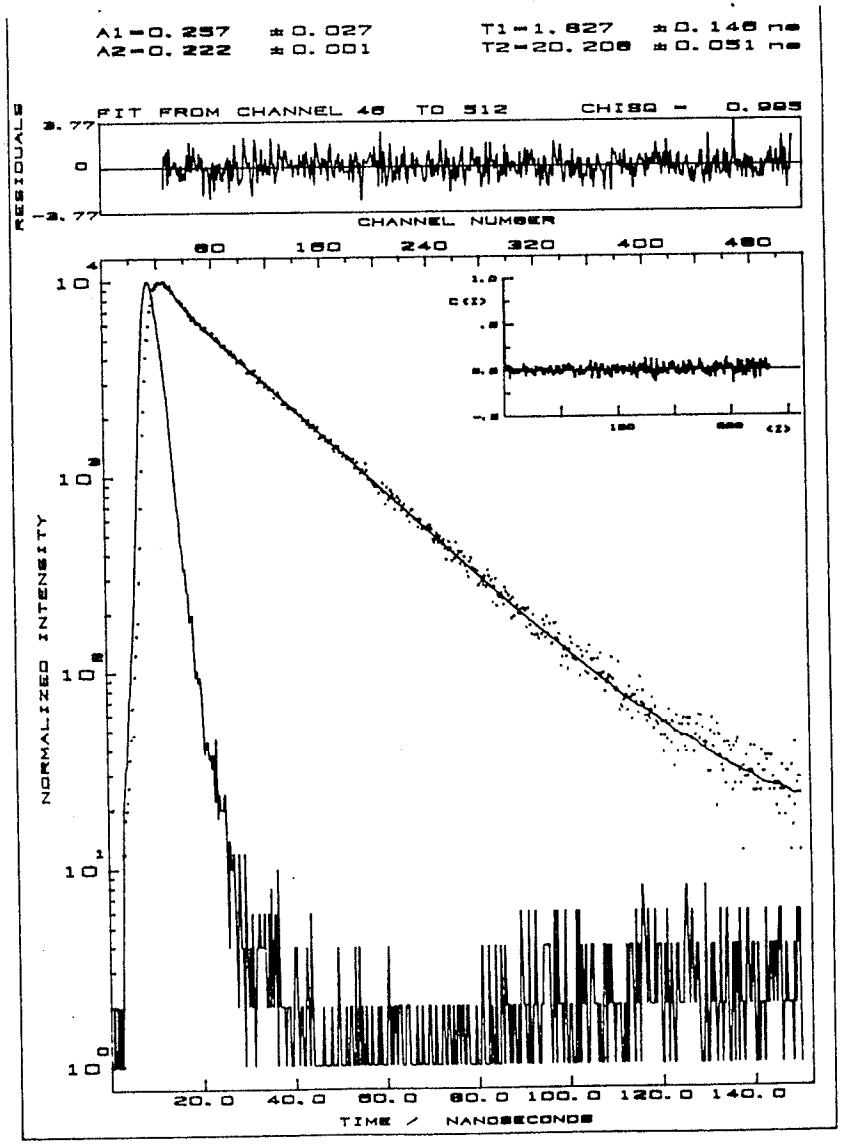
A1=0.257 ±0.027
A2=0.222 ±0.001
T1=1.827 ±0.146 ns
T2=20.208 ±0.051 ns
FIT FROM CHANNEL 48 TO 512
CHISQ = 0.985
RESIDUALS
CHANNEL NUMBER
NORMALIZED INTENSITY
TIME / NANOSECONDS

FIGURE 11

A three component decay
11A: A double exponential fit
11b: A triple exponential fit

A

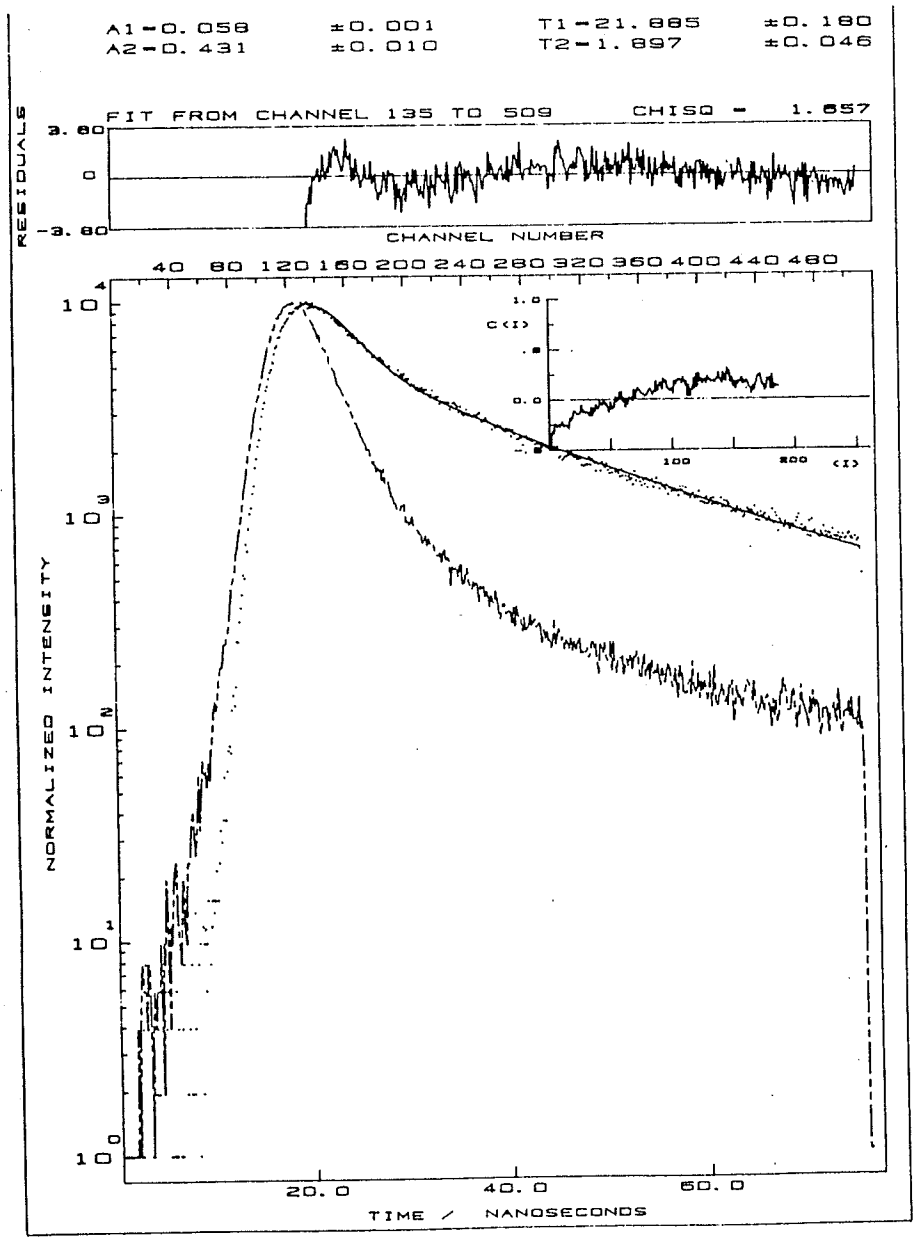
A1 = 0.058 ±0.001 T1 = 21.885 ±0.180
A2 = 0.431 ±0.010 T2 = 1.897 ±0.046
FIT FROM CHANNEL 135 TO 509 CHISQ = 1.857
RESIDUALS
3.80
0
-3.80
CHANNEL NUMBER
40 80 120 160 200 240 280 320 360 400 440 480
NORMALIZED INTENSITY
C(I)
1.0
0.0
100
200
(I)
20.0
40.0
60.0
TIME / NANOSECONDS

B

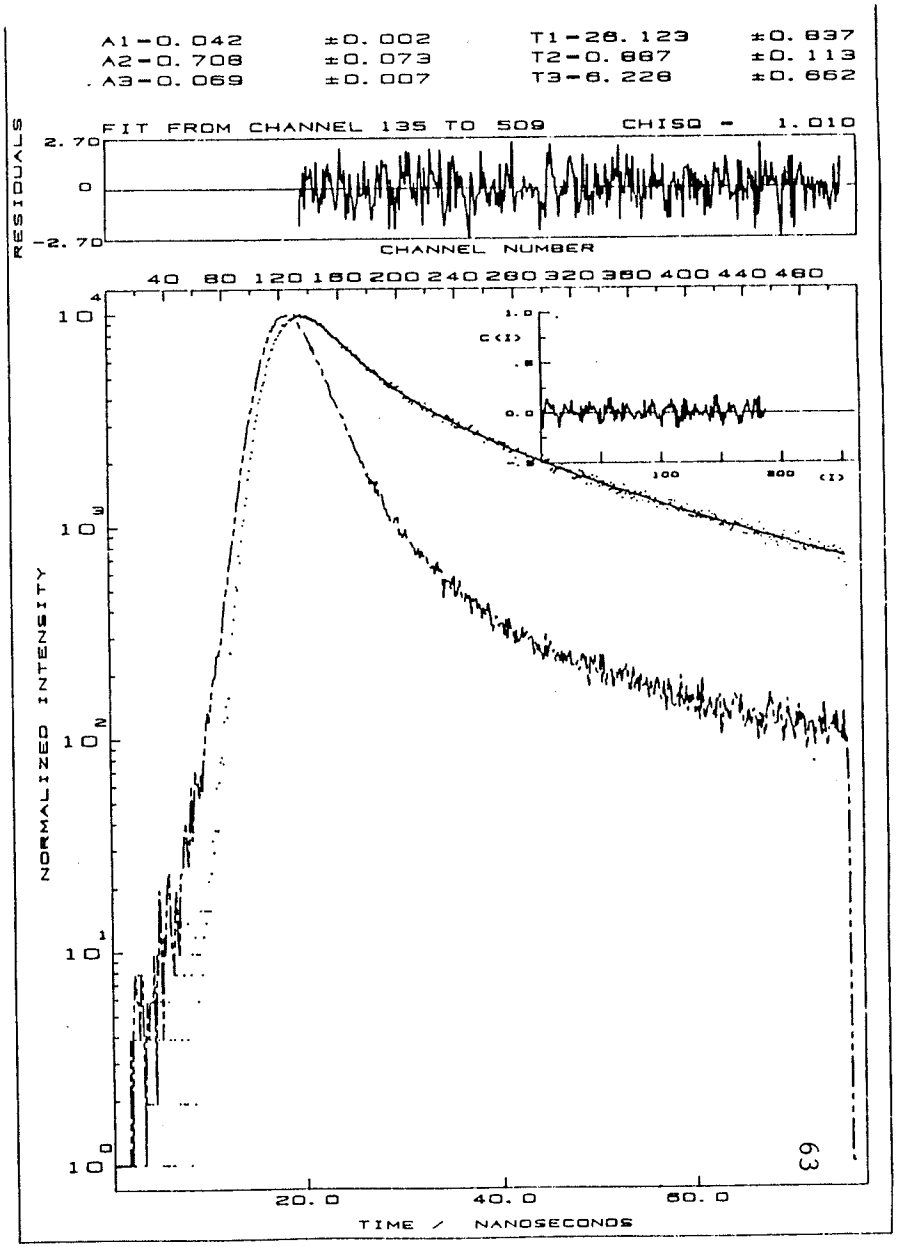
A1 = 0.042 ±0.002 T1 = 28.123 ±0.837
A2 = 0.708 ±0.073 T2 = 0.887 ±0.113
A3 = 0.069 ±0.007 T3 = 6.228 ±0.662
FIT FROM CHANNEL 135 TO 509 CHISQ = 1.010
RESIDUALS
2.70
0
-2.70
CHANNEL NUMBER
40 80 120 160 200 240 280 320 360 400 440 480
NORMALIZED INTENSITY
C(I)
1.0
0.0
100
200
(I)
20.0
40.0
60.0
TIME / NANOSECONDS
63

**FIGURE 12**

Fitting the exponential tail
12a: A triple exponential fit
12b: A quadruple exponential fit

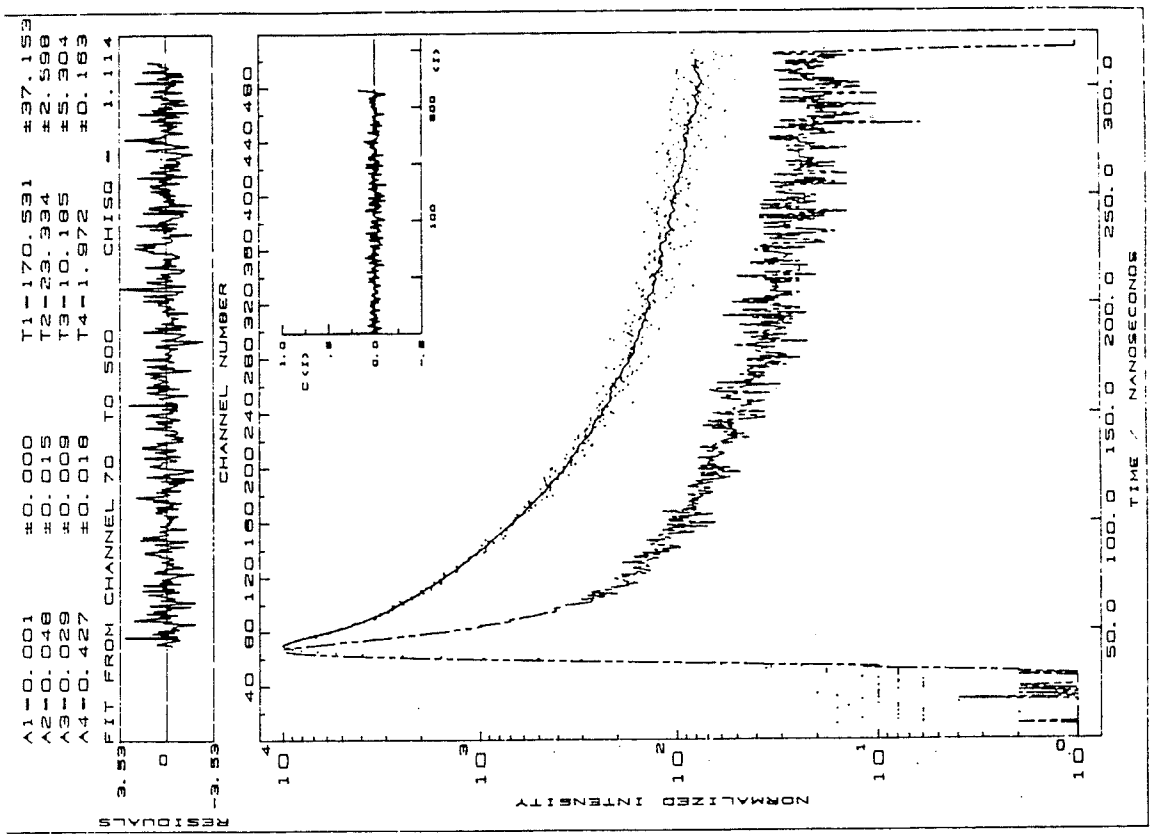
B
A1=0.001 ±0.000 T1=170.531 ±37.153
A2=0.048 ±0.015 T2=23.334 ±2.598
A3=0.029 ±0.009 T3=10.185 ±5.304
A4=0.427 ±0.018 T4=1.972 ±0.183
FIT FROM CHANNEL 70 TO 500 CHISQ = 1.114
RESIDUALS
CHANNEL NUMBER
NORMALIZED INTENSITY
TIME / NANOSECONDS

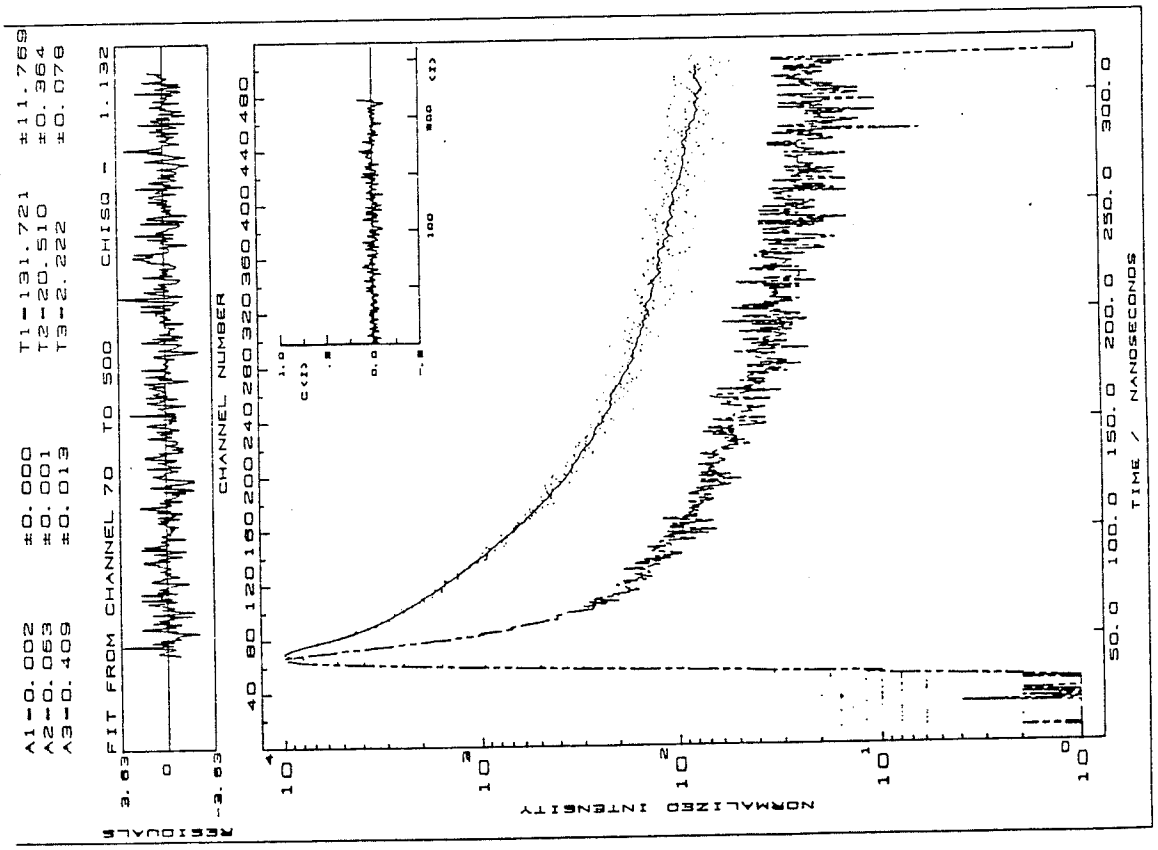
A
A1=0.002 ±0.000 T1=131.721 ±11.769
A2=0.063 ±0.001 T2=20.510 ±0.364
A3=0.409 ±0.013 T3=2.222 ±0.078
FIT FROM CHANNEL 70 TO 500 CHISQ = 1.132
RESIDUALS
CHANNEL NUMBER
NORMALIZED INTENSITY
TIME / NANOSECONDS

## 9.0 Limitations of the analysis

Data in this section come from the studies that were done with ethidium bromide in solution and in cells in vitro. One of the prime objectives of this thesis is to assess the ability of Fluorescence Lifetime Analysis to measure conformational changes in DNA. A introduction to ethidium Bromide is given in chapter 5.0. A discussion of the significance of the analysis with respect to DNA conformation is presented in part C of this thesis. In this section, only the variabilities of the results will be discussed.

It was fortuitous that ethidium bromide mixed with DNA at various DNA/Eb ratios provided various multi-exponential decay curves with one very fast component (1.7 nsec), due to unbound ethidium bromide, and one reasonably slow component, which varied from 16 to 25 nsec, due to ethidium bromide bound to the DNA. As reference experiments, several known single exponential compounds were analyzed, and the results compared to published values.

The following is a series of experiments in which the effects of varying the fitting protocol are compared and summarized.

## 9.1 Comparison 1

In this comparison, data were collected at three T/CH values (1.46,.729,.365), for the same period of time. This resulted in three corresponding number of counts collected in the peak channel (20,000, 10,000, 5,000). The FLA was done for second and third order fits. The results are shown in table 4, and the decay curves are shown in figure 13. Nitrogen gas was used to investigate the effect of fitting the tail region on the other lifetime components.

For all second order fits, the ROI was determined by optimizing the statistical indicators for the best fit, while minimizing the error values for the lifetime components. It was found that as the number of channels included in the fit decreased from the maximum value, the goodness of fit, and the $\tau_i$ error values, improved to a certain point. Decreasing the fitting area any further past this point produced worse results. This 'point of best fit' became the ROI for the second order fit. This fitting characteristic of an ideal ROI seemed to be fundamental, occurring in every decay curve. Finding this ROI is, however, a tedious process when applies to every decay curve. It is much more efficient to carry out this detailed analysis once for a particular decay scheme and then fit to the same ROI in subsequent profiles, as long as the shape of the decay does

not change. This approach was implemented and proved to be a reasonable refinement for the FLA process. For this example, the best second order fit always occurred at approx. 110 nsec., which indicates that for this system, the T/CH could have been reduced further to maximize the ROI within the MCA.

Table 4 shows that the errors of the $\tau_1$ and $\tau_2$ components are similar for both fitting models, at each of the T/CH-peak-count combination. This indicates that as the T/CH is decreased, the same resolution of the decay components in the ROI can be obtained with a corresponding decrease in the number of counts-peak. These findings are similar to the relationship between the upper two curves in figure 9, part B. This would indicate that it takes a larger number of <u>total</u> counts in the case of multi-exponential fits to achieve the maximum precision in the components, which is independent of the T/CH. If the number of counts is not decreased, and the T/CH halved, the collection time will double, but the precision in the lifetime values may not increase linearly as was found by Selinger [16] in figure 9.

By changing to a third order fit over the entire range of the data, the values of the first two lifetime components are altered. At each T/CH, the difference in $\tau_1$ and $\tau_2$ from the second to the third order fit is similar; $\tau_1$ increased by 10% and $\tau_2$ increased by 5%. Note also, that the errors in the lifetimes

did not change. The existing second order fits were good fits of the data, and fitting another component over a larger ROI, did not improve the precision of the first two components. As will be seen later this long lived component is not a fluorescence lifetime inherent to the sample, but rather an artifact of using $N_2$ gas. If this was not known, and the third order fit data used, incorrect interpretations of the biological or chemical processes taking place in the sample would be made and the corresponding lifetimes would be erroneous.

Notice how the error $\tau_3$ increases from 3% to 12% to 110% as the region included in the fit decreases. This is to be expected, since the long $\tau_3$ value represents the data in the tail section and if the tail is excluded from the fit, the error increases. This demonstrates the importance of examining the entire decay curve in order that the data contributing to any long lived species be included, and its resolution maximized.

Table 4

FLA comparsion number1
Two exp. models, various T/CH

| T/CH (ns) | numbercounts peak | MODEL (number exp., ROI) (2, ~ 110 nsec) $\tau_i$ | ± (ns) | (3, 512 channels) $\tau_i$ | ± (ns) |
|---|---|---|---|---|---|
| 1.46 | 20,000 | 1.27 | .07 | 1.40 | .06 |
| | | 18.53 | .19 | 19.44 | .15 |
| | | | | 359 | 11 |
| .729 | 10,000 | 1.79 | .08 | 1.98 | .07 |
| | | 19.08 | .15 | 20.30 | .16 |
| | | | | 382 | 41 |
| .365 | 5,000 | 1.78 | .08 | 1.90 | .08 |
| | | 19.12 | .14 | 20.01 | .30 |
| | | | | 321 | 362 |

**FIGURE 13**

Second and third order fits at two T/CH settings

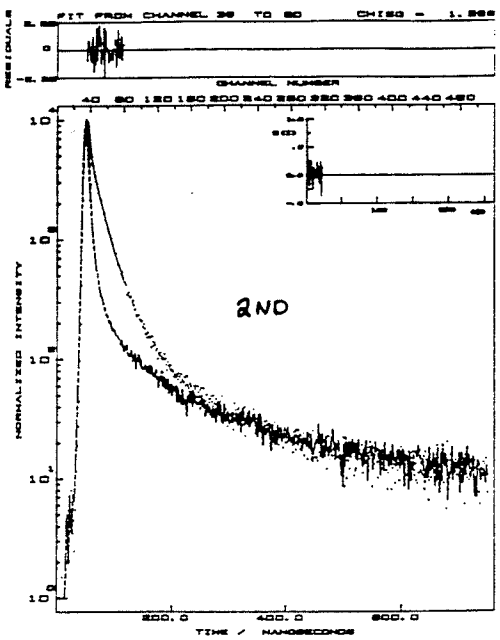


T/CH
1.46

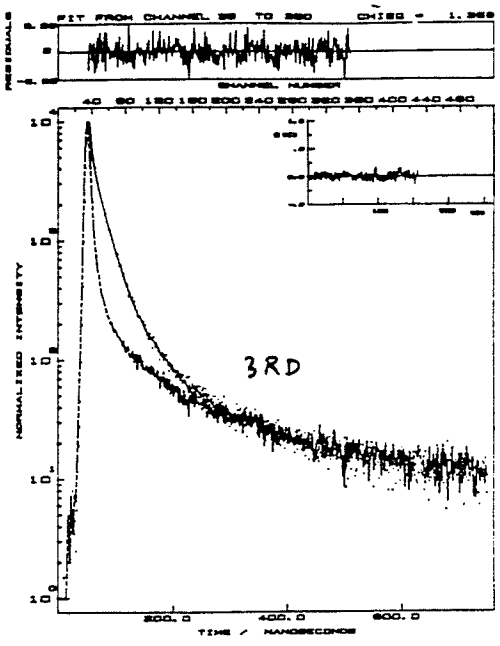


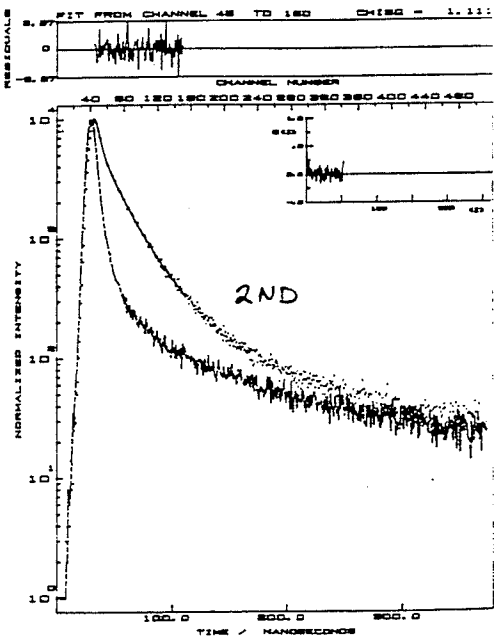


T/CH
.729

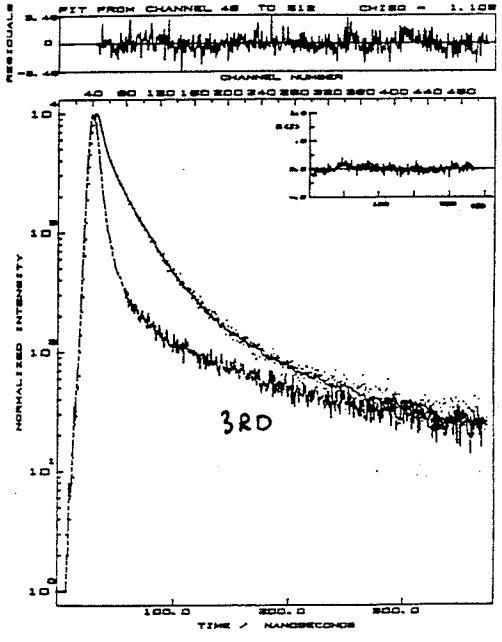


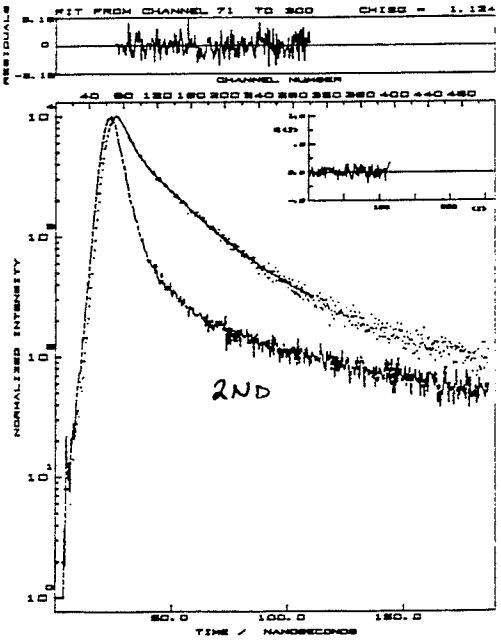


T/CH
.365

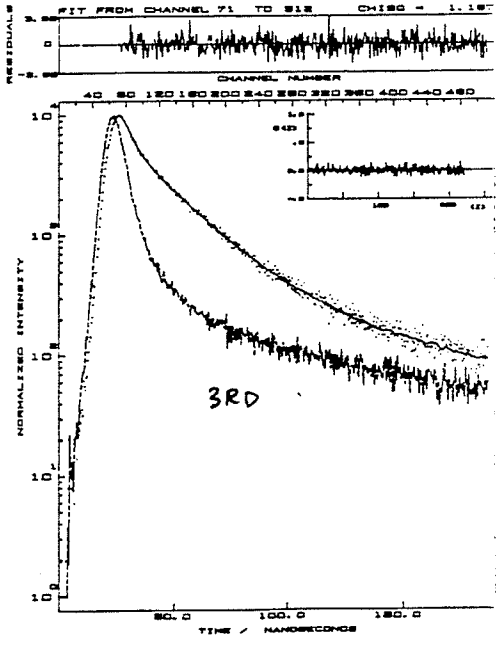

## 9.2 Comparison 2

The data in these experiments were collected from samples similar to those in the previous comparison, except here the amount of each component varies. The FLA determines the fractional intensity (int) of fluorescence due to each lifetime component in the decay curve, and reports the %int values, with

$$\%\text{int} = \frac{\tau_i \times \alpha_i}{\bar{\tau}} \times 100\% \qquad (23)$$

$\bar{\tau}$ = mean lifetime of the decay curve given by

$$\bar{\tau} = \sum_{i=1}^{n} (\tau_i \times \alpha_i) \qquad (24)$$

The %int values are a function of the concentration of each of the fluorescence species, but the % fuorescence intensity is also influenced by many other factors, some of which were outlined in the background material in part A.

Table 5 shows the results of this comparison. Four fitting protocols were used, two similar to those in comparison 1, and two with hydrogen gas in the flashlamp. As seen in chapter 7.1, when using $H_2$, the instrument response function (IRF) does not contain a tail section. It is closer to a delta function, falling off rather quickly down to the background level. Thus, in this study, the lifetime results affected by a broad IRF are compared to those having a somewhat narrower IRF.

Table 5

FLA comparsion number2
Two lifetime components, varying amounts
Various FLA protocols

| Protocol | Mixture number | $\tau_1$ (ns) | ± | %int | $\tau_2$ (ns) | ± | %int | $\tau_3$ (ns) | ± | %int |
|---|---|---|---|---|---|---|---|---|---|---|
| (a) | 1 | 1.66 | .04 | 65.4 | 16.52 | .22 | 34.6 | | | |
| | 2 | 1.39 | .05 | 51.1 | 17.46 | .16 | 48.9 | | | |
| | 3 | 1.65 | .06 | 35.0 | 19.45 | .10 | 64.9 | | | |
| | 4 | 1.55 | .09 | 19.1 | 20.40 | .08 | 80.9 | | | |
| | 5 | 1.05 | .53 | 7.6 | 21.50 | .07 | 92.4 | | | |
| (b) | 1 | | | | -- NOT OBTAINABLE -- | | | | | |
| | 2 | 1.49 | .05 | 48.0 | 18.48 | .18 | 48.8 | 459 | 78 | 6.2 |
| | 3 | 1.74 | .06 | 32.7 | 20.04 | .13 | 60.1 | 871 | 304 | 7.2 |
| | 4 | 1.68 | .09 | 18.6 | 20.86 | .10 | 77.7 | 495 | 134 | 3.8 |
| | 5 | 1.03 | .43 | 7.8 | 21.79 | .08 | 88.4 | 665 | 261 | 3.8 |
| (c) | 1 | 1.63 | .02 | 68.6 | 16.65 | .13 | 31.4 | | | |
| | 2 | 1.69 | .02 | 42.5 | 18.87 | .09 | 57.5 | | | |
| | 3 | 1.72 | .04 | 25.6 | 20.17 | .07 | 74.4 | | | |
| | 4 | 1.78 | .06 | 12.4 | 21.15 | .06 | 87.7 | | | |
| | 5 | 1.52 | .23 | 3.6 | 22.06 | .06 | 96.4 | | | |
| (d) | 1 | 1.69 | .02 | 63.6 | 17.36 | .13 | 36.4 | | | |
| | 2 | 1.70 | .02 | 45.5 | 18.91 | .09 | 54.5 | | | |
| | 3 | 1.76 | .04 | 28.9 | 19.96 | .07 | 71.1 | | | |
| | 4 | 1.77 | .10 | 13.2 | 21.04 | .06 | 86.8 | | | |
| | 5 | 1.49 | .24 | 4.8 | 21.70 | .05 | 95.2 | | | |

(a) $N_2$ gas, T/CH .729
Best 2nd order fit

(b) $N_2$ gas, T/CH .729
3rd order to 512 channels

(c) $H_2$ gas, T/CH .365
2nd order to data edge

(d) $H_2$ gas, T/CH .293

In the five mixtures, the %int of the fast component, $\tau_1$, decreases from mixture 1 to 5 while the %int of the $\tau_2$ component increases from mixture 1 to 5. The data immediately show that the error in the lifetimes increases as the %int decreases. It was found that at least 5% int was needed to resolve the fast component with $N_2$, and slightly less (~3%) with $H_2$.

The difference in $\tau_2$ between the second and third order fits with $N_2$ (protocols (a) and (b)) is dependent on either the value of the lifetime or the %int. The difference decreases as the lifetime and the %int increase.

Notice that the $\tau_3$ component in (b) is highly variable, has a large variable error, and only contributes approximately 5% to the decay intensity. In one experiment in this comparison, and actually in many other experiments, a third order fit was not obtainable either because convergence was not reached or because the results were not repeatable. The above factors support the argument against $\tau_3$ being a decay component originating in the sample.

The analyses using $H_2$ show conclusively that <u>there is no long third lifetime component</u>. Refer to figure 14. The fluorescence decay curve is not convoluted by a long tail in the IRF, and is clearly a two component system, right down to the background level.

The actual value of $\tau_1$ as measured with this FLA system is ~ 1.70 to 1.71 nsec. With $H_2$ in the flashlamp, the estimates of this component are closer to the actual value than if $N_2$ is used, as well the resolution with $H_2$ is slightly better. However for $\tau_2$, all four protocols yield similar results, the difference ranging from ~ 5% in mixture 1 to 1% in mixture 5. The significance of this difference to the results depends upon the purpose of the particular experiment and the lifetimes involved. $H_2$ gas does not produce a long tail in the IRF but, as mentioned previously, the excitation intensity is 50% lower and is less stable. The IRF profile also acquires small variations or humps after several hours of use. $N_2$ has just the opposite characteristics.

The intensity of $H_2$, with the lamp configuration described in a previous section, was adequate for our experiments. We also favoured the unambiguous resolution of only the lifetime components from the sample being tested. Monitoring the IRF profile and excitation intensity between each experiment was required, however.

FIGURE 14

Fluorescence decay curve of a two component system; with $H_2$

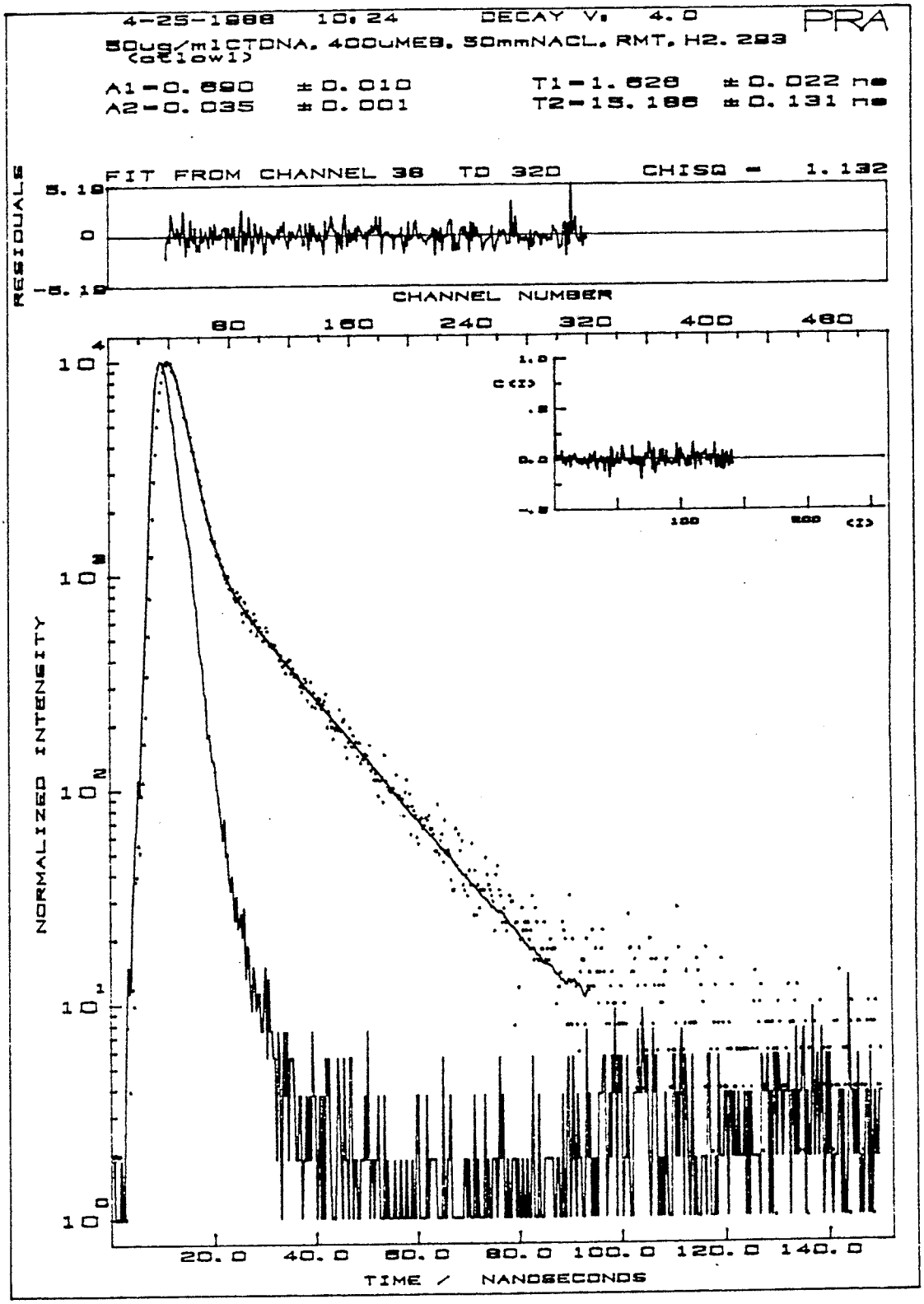
4-25-1988 10:24 DECAY V: 4.0
PRA
50ug/ml CTDNA, 400uMEB, 50mmNACL, RMT, H2, 293
<o2flow1>
A1=0.890 ±0.010 T1=1.628 ±0.022 ns
A2=0.035 ±0.001 T2=15.186 ±0.131 ns
FIT FROM CHANNEL 38 TO 320 CHISQ = 1.132
RESIDUALS
5.10
0
-5.10
CHANNEL NUMBER
80 160 240 320 400 480
NORMALIZED INTENSITY
10^4
10^3
10^2
10^1
10^0
20.0 40.0 60.0 80.0 100.0 120.0 140.0
TIME / NANOSECONDS
C<I>
1.0
.5
0.0
-.5
100
200
<I>

## 9.3 Comparison 3

This example demonstrates the limitations in FLA pertaining to the resolution of multi-exponential components in which the fluorescence lifetime values are close together. The decay curve shown in figure 15 has three known exponential components, the values of which range from 1.6 to 2.0 nsec, 6 to 7 nsec, and 23 to 24 nsec. The experiments from which these data were taken are discussed in part D of this report.

At first glance, the decay curve appears to be a double exponential similar to those in the previous examples. Figure 15 (a) shows the FLA for a 2 component fit. The lifetime values and the fit statistics are listed in table 6. As one can see from the plot of the residuals and the fit statistics, the second order fit is not acceptable even though the errors on the $\tau$ values are typical of similar 2-component systems. If one simply refers to the lifetime error values, and accepts the results of the second order FLA, the wrong interpretation of the data will be made and very important information could possibly be overlooked.

The third order fit (figure 15 (b)) yields ideal fit statistics. The shorter lifetime from the second order fit, $\tau_1$, has been resolved into two significantly different lifetimes, $\tau_1$ and $\tau_2$, in the third order fit. The errors in these two components (13% & 10% respectively) are much higher than the error in the original $\tau_1$ (2%). The %int is split between the two. The %int of the longest lifetime, $\tau_3$, does not change much, but

the value of this lifetime increases by 3.3% and the error increases by 75% from .4% to .7% in the third order fit. The errors in the third order fit increase because the same amount of information is being used to fit a more complex model. The only way the errors can be reduced is to collect for a longer period of time thus increasing the number of counts in each channel, because the ROI has already been maximized in the MCA.

The small drop at the start of the auto-correlation plot in figure 15 (a) actually represents a discrepancy at the tail end of the fit of the decay curve. The wave in the residuals plot indicating a poor fit of the information in the peak region of the decay curve is seen at the right side of the auto-correlation plot, where the plot travels slightly above the zero line.

The auto-correlation function is very sensitive to discrepancies in the lower end of the decay curve where the number of counts is quite low. This is discussed in the next section on background noise removal.

Table 6

FLA comparsion number3
Three lifetime components

| Protocol | $\tau_1$ (ns) | ± (ns) | %int | $\tau_2$ | ± | %int | $\tau_3$ | ± | %int |
|---|---|---|---|---|---|---|---|---|---|
| (a) | 3.29 | .07 | 26.0 | | - | | 22.30 | .09 | 74.0 |
| (b) | 1.75 | .23 | 14.1 | 6.33 | .68 | 17.1 | 23.03 | .16 | 68.8 |

(a) $H_2$ gas, T/CH .293
2nd order to 512

Chi-sqr = 1.26
DW = 1.72
Sgr = -2.94

(b) $H_2$ gas, T/CH .293
3rd order to 512

Chi-sqr = 1.03
DW = 2.13
Sgr = -.14

FIGURE 15

A three component decay curve, with $H_2$
15a: A second order fit
15b: A third order fit

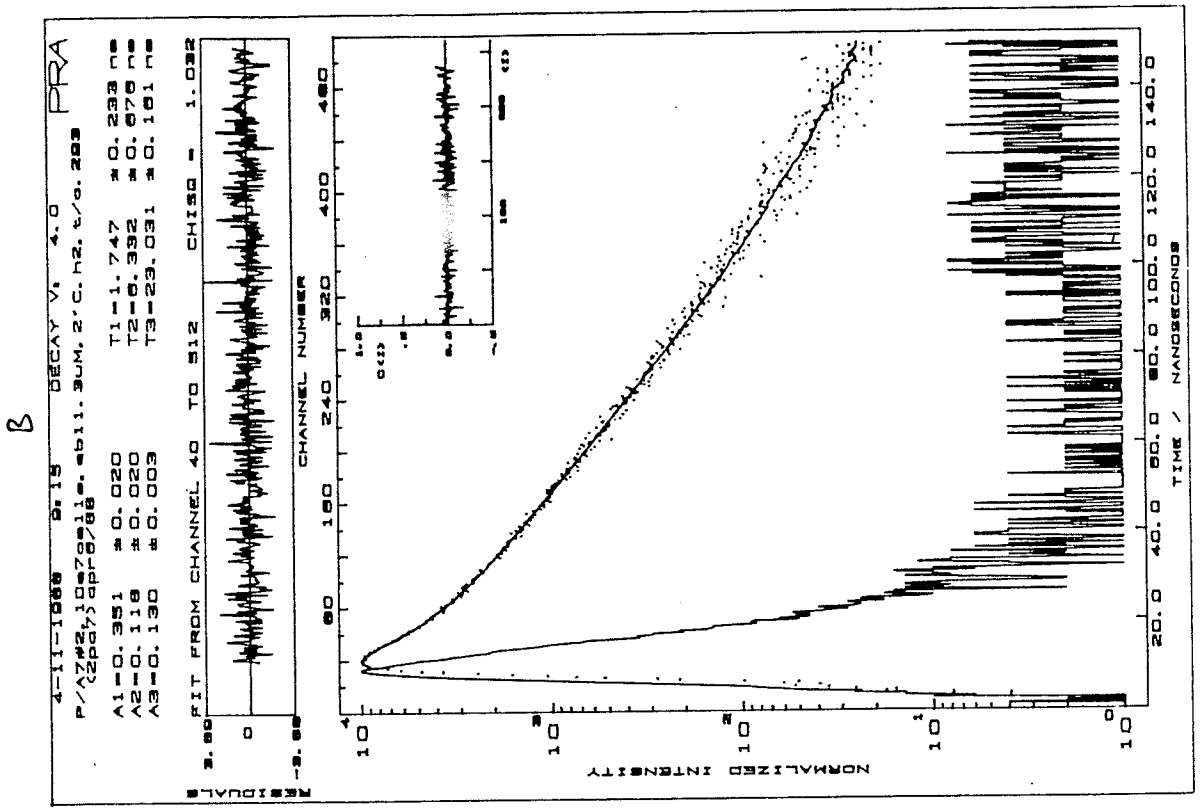
B
4-11-1988 9:15 DECAY V: 4.0 PRA
A1=0.351 ±0.020 T1=1.747 ±0.233 ns
A2=0.118 ±0.020 T2=6.332 ±0.676 ns
A3=0.130 ±0.003 T3=23.031 ±0.161 ns
FIT FROM CHANNEL 40 TO 512 CHISQ = 1.032
RESIDUALS
CHANNEL NUMBER
NORMALIZED INTENSITY
TIME / NANOSECONDS

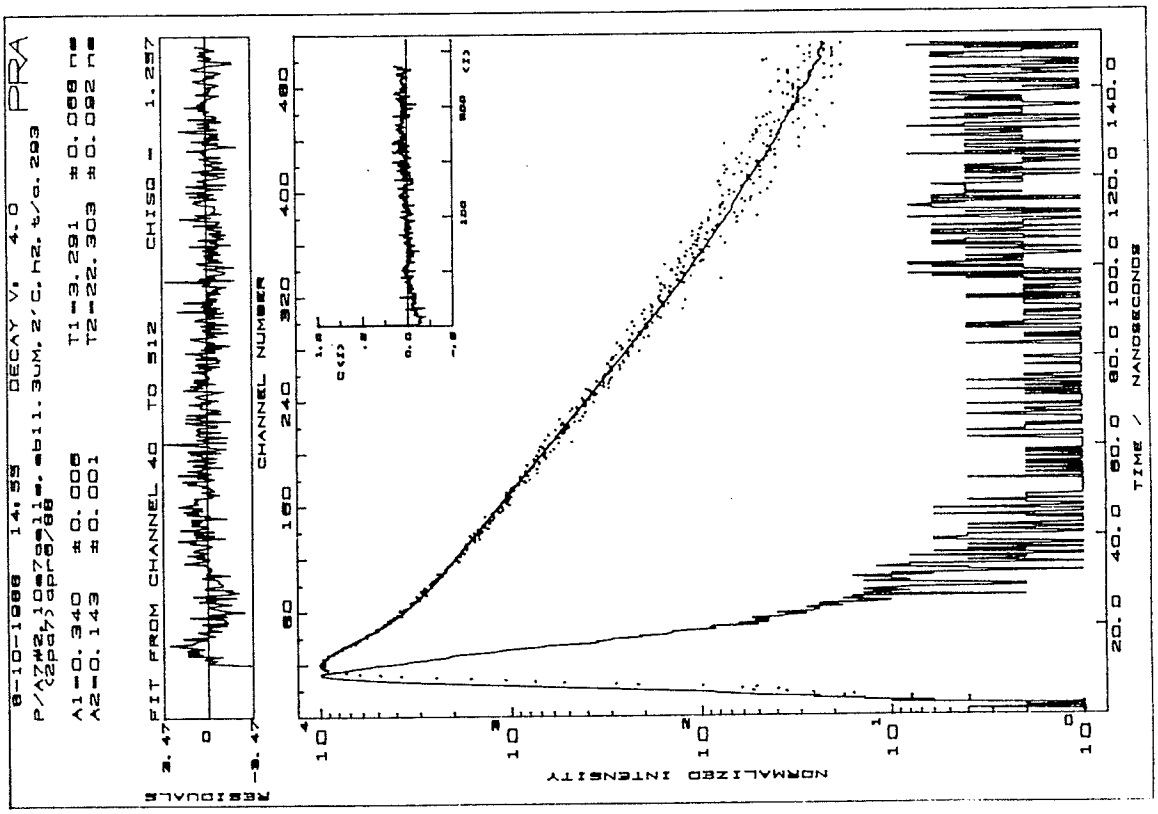
A
8-10-1988 14:55 DECAY V: 4.0 PRA
A1=0.340 ±0.006 T1=3.291 ±0.068 ns
A2=0.143 ±0.001 T2=22.303 ±0.092 ns
FIT FROM CHANNEL 40 TO 512 CHISQ = 1.257
RESIDUALS
CHANNEL NUMBER
NORMALIZED INTENSITY
TIME / NANOSECONDS

## 9.4 Comparison 4

In this study, the FLA for a known single exponential compound, quinine sulfate, is compared for different regions of interest. In the analysis of Lampert et al. [18], "the lifetime value did not depend on the section of the curve chosen for analysis". In this reference the FLI employed a synchronously pumped dye laser as an excitation source, which provided very narrow IRF's, and thus the deconvolution process was more straight forward.

Table 7 lists the results for the single exponential FLA, at two T/CH's with $N_2$ and one with $H_2$. Also listed are the fit statistics and the ROI over which the analysis was performed. One can see in protocol (a), that as the ROI is decreased, the fit statistics show a minor improvement, and the error on the lifetime increases slightly. The lifetime value progressively decreases with a maximum deviation of only .5%. By going to a smaller T/CH with the same number of counts collected in the peak channel, the fit improves and the lifetime error is decreased by 15%, but the value of the lifetime does not change significantly. This is to be expected since the ROI in (b) is in the range of ROI's used in (a).

With $H_2$ and the same T/CH as in (b), neither the error nor

the fit is improved. The lifetime value did increase slightly. This, and the fact that the fit is so poor, indicates that either the decay curve collected with $H_2$ is more sensitive to the variations in the sample emission or a systematic error, perhaps an instability in the lamp pulse occurred, during data collection. The latter is most unlikely since the sample was highly fluorescent and took only minutes to collect 10,000 counts in the peak channel. Figure 16 shows the decay of quinine sulfate with $N_2$ and $H_2$. Notice that, with $N_2$, it is harder to tell where exactly the decay ends and the background begins.

Table 8 compares the values obtained with our FLI to the values measured and tabulated by Lambert [18]. The lifetimes for quinine sulfate and anthracene are listed; both have been used as single exponential standards. Figure 17 shows the decay for Anthracene, with $N_2$. Notice how close the decay is to the IRF. If a laser were used for the excitation source, the decay for Anthracene would look more like figure 16 (b).

Table 7

FLA comparsion number4
Quinine Sulfate
Single exp., 3 protocols, various ROI's

| Protocol | $\tau_1$ (ns) | ± (ns) | Chi-sqr | DW | Sgr (Runs) | ROI number | chann. | (ns) |
|---|---|---|---|---|---|---|---|---|
| (a) | 19.52 | .048 | 1.24 | 1.76 | -1.16 | 512 | 370 | |
| | 19.51 | .049 | 1.24 | 1.74 | -1.28 | 450 | 330 | |
| | 19.51 | .048 | 1.17 | 1.76 | -1.05 | 350 | 255 | |
| | 19.50 | .048 | 1.21 | 1.77 | -0.52 | 250 | 180 | |
| | 19.47 | .050 | 1.26 | 1.84 | -0.10 | 200 | 145 | |
| | 19.42 | .055 | 1.24 | 1.78 | 0.09 | 150 | 110 | |
| (b) | 19.48 | .032 | 1.06 | 2.01 | 0.03 | 512 | 185 | |
| | 19.44 | .036 | 1.13 | 2.03 | 0.78 | 300 | 110 | |
| (c) | 19.81 | .030 | 1.20 | 1.71 | -1.13 | 512 | 185 | |
| | 19.80 | .031 | 1.24 | 1.61 | -1.22 | 400 | 145 | |
| | 19.59 | .045 | 1.24 | 1.55 | -1.27 | 200 | 75 | |

(a) $N_2$ gas, T/CH .729

(b) $N_2$ gas, T/CH .365

(c) $H_2$ gas, T/CH .365

Table 8

Fluorescence lifetime comparison
Standard single exp. compounds

| Compound | Solvent | Conc. (M) | $\lambda_{ex}$ (nm) | $\lambda_{em}$ (nm) | $\tau_F$* (ns) Published | Measured |
|---|---|---|---|---|---|---|
| Anthracene | Cyclo-hexane (undegassed) | $5x10^{-6}$ | 308 | 410 | $4.10^1$<br>$4.1^2$ | 4.15 ±.03<br>4.17 ±.02<br>4.19 ±.03 |
| Quinine Sulfate | .1N $H_2SO_4$ | $10^{-4}$ | 365 | 470 | $18.8, 19.4^2$ | 19.5 ±.03 |

[1] - Measured by Lampert et al. [18].

[2] - Tabulated in [18], previously published.

* - all values are at room temperature.

FIGURE 16

The fluorescence decay of quinine sulfate
16a: with $N_2$
16b: with $H_2$

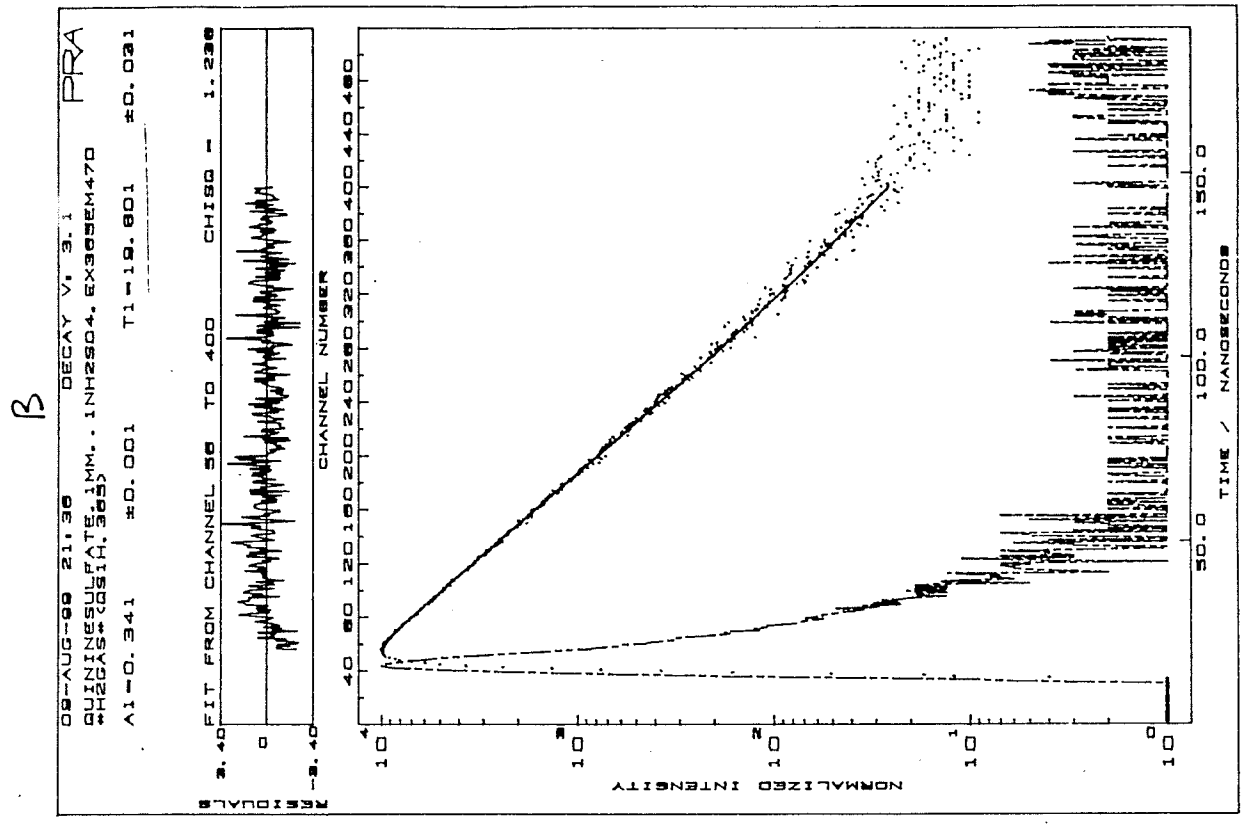
B
09-AUG-00 21:36
DECAY V. 3.1
PRA
QUININESULFATE.1MM..1NH2SO4.EX365EM470
#H2OAS*COSIN.365)
A1=0.341 ±0.001 T1=19.801 ±0.031
FIT FROM CHANNEL 56 TO 400 CHISQ = 1.230
RESIDUALS
CHANNEL NUMBER
NORMALIZED INTENSITY
TIME / NANOSECONDS

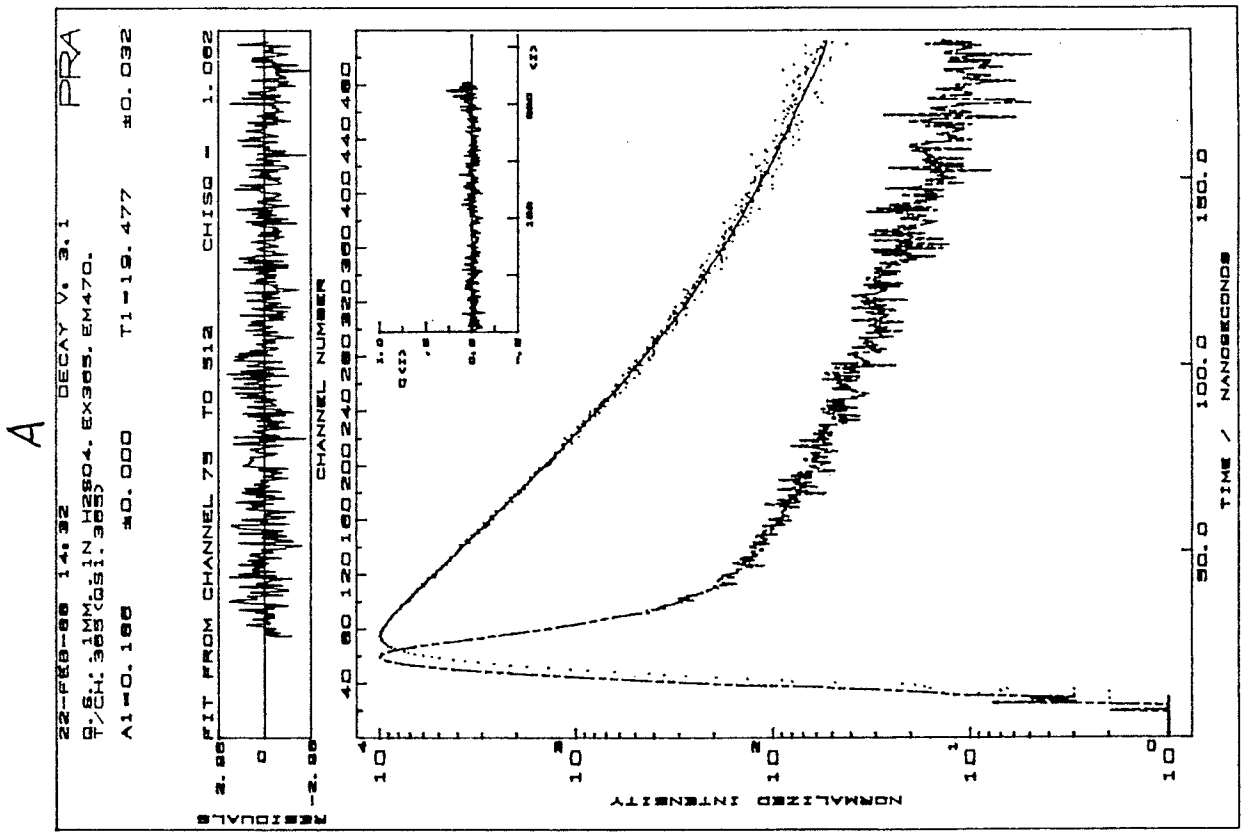
A
22-FEB-00 14:32
DECAY V. 3.1
PRA
Q.S.:.1MM..1N H2SO4. EX365. EM470.
#/CH.:365*COSIN.365)
A1=0.166 ±0.000 T1=19.477 ±0.032
FIT FROM CHANNEL 75 TO 512 CHISQ = 1.062
RESIDUALS
CHANNEL NUMBER
NORMALIZED INTENSITY
TIME / NANOSECONDS

FIGURE 17

The fluorescence decay of anthracene

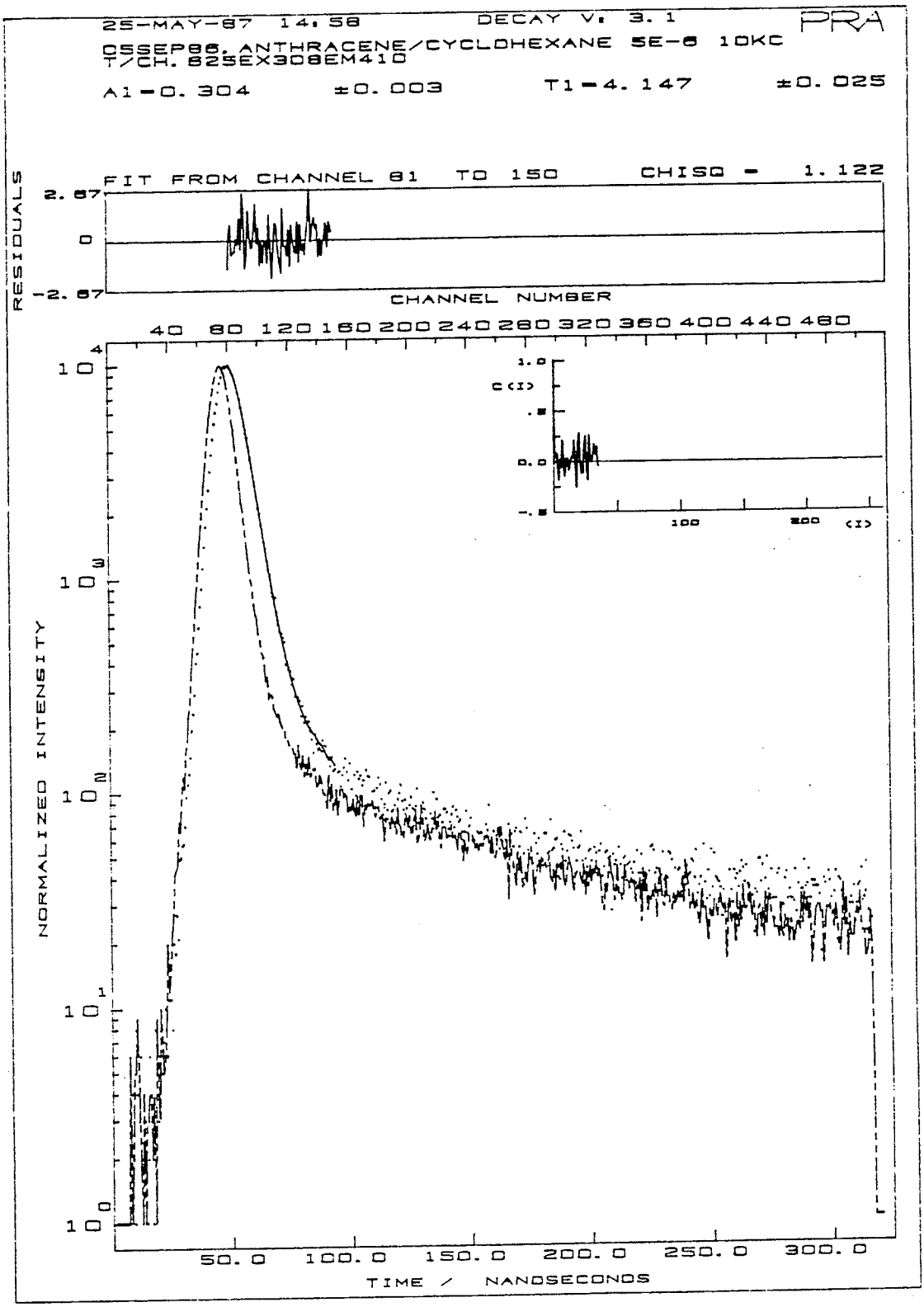
25-MAY-87 14:58
DECAY V: 3.1
PRA
OSSEP86, ANTHRACENE/CYCLOHEXANE 5E-6 10KC
T/CH. 825EX308EM410
A1 = 0.304 ±0.003
T1 = 4.147 ±0.025
FIT FROM CHANNEL 81 TO 150
CHISQ = 1.122
RESIDUALS
2.67
0
-2.67
CHANNEL NUMBER
40 80 120 160 200 240 280 320 360 400 440 480
C(I)
1.0
0.0
100
200
(I)
NORMALIZED INTENSITY
10^4
10^3
10^2
10^1
10^0
50.0 100.0 150.0 200.0 250.0 300.0
TIME / NANOSECONDS

## 10.0 Background Subtraction

A single photon counting system has associated with its PMT's, a certain amount of noise. This noise translates into an extra finite number of counts to be recorded in every channel of the MCA. The actual number of counts recorded depends upon the intensity of the background noise and the sample collection time.

A good SPC instrument has a very low noise level from leaked room light and thermionic emission in the PMT's. The PMT's chosen for SPC have very good dark current noise characteristics. In our FLI, the emission PMT is cooled by circulating water. With the PMT cooled to -10° C, the emission monochromator wrapped in a dark cloth, and the fluorescent room lights dimmed, the dark count rate was reduced to 2-3 counts/sec, on average. It is interesting to note that if an incandescent light bulb is turned on in the vicinity of the FLI, the dark count rate increases to approximately 10-15 counts/sec.

The number of dark counts added to the sample decay curve is greater than the number added to the IRF since the sample curve usually takes between 2 to 5 times longer to acquire. How does this affect the FLA results? Table 9 lists the data of table 5, protocol (d), with the corresponding background subtracted values. The level of background subtraction in each case varied

slightly to maximize the fit statistics. In all cases, the $\tau$ values dropped with background subtraction. Notice that the error on the lifetime values did not change significantly. The % difference in $\tau$ is related to the %int of the components; as the %int decreases, the %diff. increases.

One would expect that the values of $\tau_1$, the fast decaying component, would not be affected by background subtraction. The decay information contributing to this component comes from the MCA channels that contain approx. $10^3$ - $10^4$ counts if $10^4$ counts are collected in the peak channel, and the few counts due to noise are only a small percentage of the total. The decay of $\tau_2$, however, extends down to the background level, and the number of counts due to noise is a significant percentage of the total. Thus one would expect a large change in these values.

As mentioned in chapter 8, the components of a multi-exponential fit are strongly correlated. This means that a change in the lifetime of one component affects the lifetime of the other component. The effect of a large change in the lower portion of a decay curve with background subtraction on $\tau_2$ could be reduced somewhat, if there is a corresponding compensation in $\tau_1$. The fact that we see a small change in both components supports this hypothesis.

Table 9

Effect of Background Subtraction
on the components of a second order FLA

| $\tau_i$ | Mixture | Background Included | | | Background Subtracted | | | % diff. |
|---|---|---|---|---|---|---|---|---|
| | | $\tau_i$ | ± | %int | $\tau_i$ | ± | %int | |
| 1 | 1 | 1.69 | .02 | 63.6 | 1.64 | .02 | 63.4 | -2.96 |
| | 2 | 1.70 | .02 | 45.5 | 1.65 | .02 | 45.2 | -2.94 |
| | 3 | 1.76 | .04 | 28.9 | 1.70 | .04 | 28.7 | -3.41 |
| | 4 | 1.77 | .10 | 13.2 | 1.56 | .10 | 13.0 | -11.86 |
| | 5 | 1.49 | .24 | 4.8 | 1.25 | .24 | 4.8 | -16.11 |
| 2 | 1 | 17.36 | .13 | 36.4 | 16.23 | .15 | 36.7 | -6.51 |
| | 2 | 18.91 | .09 | 54.5 | 18.10 | .10 | 54.8 | -4.28 |
| | 3 | 19.96 | .07 | 71.1 | 19.50 | .08 | 71.3 | -2.31 |
| | 4 | 21.04 | .06 | 86.8 | 20.56 | .05 | 87.0 | -2.28 |
| | 5 | 21.70 | .05 | 95.2 | 21.51 | .05 | 95.2 | -0.88 |

$H_2$ gas, T/CH .293
2nd order fit to data edge

Figure 18 (a) shows effects of background noise on the fit of a decay curve. A discrepancy is detectable in the residuals plot and the auto-correlation plot even though the other fit statistics are reasonable. In figure 18 (b), the background level has been subtracted, and the auto-correlation and residuals plots have been improved.

### 10.1 Comparison 5

For a single exponential decay, the number of counts subtracted to account for background was varied. It was found that by changing the subtraction values for the IRF and the sample curve by only a few counts , the fit of the data could be made better or worse, with a corresponding change in the lifetime value.

The background level in the IRF for $H_2$ is usually only 2 or 3 counts, and is easily determined, as seen in figure 18 (a). If the sample curve has not decayed to a definite constant background level prior to the end of the 512 channels, then deciding on a value to use for the background subtraction becomes more difficult. In the case of $N_2$, it is even more difficult: the sample curve never quite reaches a constant level, but decreases parallel to the IRF.

Table 10 lists the results of the FLA with varying levels of background subtraction. The background level for the IRF was set at 3, with the level for the sample curve varying from 6 to 25 counts. The residuals and auto-correlation plots are shown in figure 19. With no background subtraction, all the fit indicators are quite acceptable except the auto-correlation function plot. Choosing the wrong number of background counts for the sample curve (6 or 25) had a very obvious effect on the fit indicators, and a good fit was not obtained. With the appropriate value (12), the fit statistics are better than those with no subtraction.

The lifetime had a maximum variation of 5% over the four experiments, but changed by only 0.6% from no background subtraction to the correct background subtraction level.

It is recommended that the background counts be subtracted at all times such that results from experiments collected for different periods of time, may be compared more accurately.

Table 10

FLA comparison number5
Various background subtraction levels
Single exponential decay

| number counts plots subtracted IRF,sample | $\tau_1$ | ± | $\chi_r^2$ | DW | SGR | Randomness of Residual | Auto-corr |
|---|---|---|---|---|---|---|---|
| 0,0 | 22.36 | .042 | 1.11 | 1.99 | -0.42 | yes | no |
| 3,6 | 22.53 | .045 | 1.31 | 1.66 | -1.46 | no | no |
| 3,12 | 22.22 | .041 | 1.08 | 2.05 | 0.62 | yes | yes |
| 3,25 | 21.59 | .053 | 1.81 | 1.31 | -4.65 | no | no |

FIGURE 18

A second order fit with and without
background subtraction
18a: no background subtraction
18b: with background subtraction

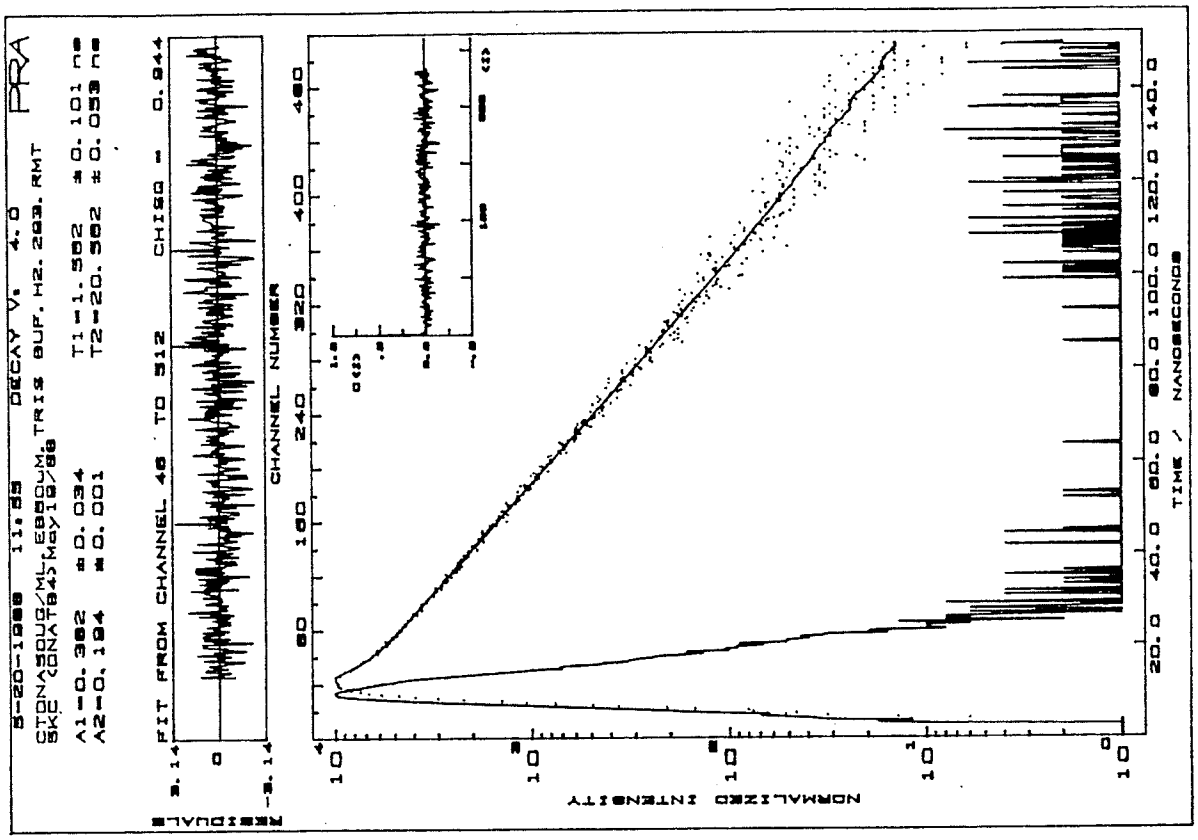
B
5-20-1988 11:55 DECAY Vs 4.0 PRA
CTDNASOUG/ML.EB80UM.TRIS BUF. H2.293. RMT
SKE CONAT843 May19/88
A1=0.382 ±0.034 T1=1.562 ±0.101 ns
A2=0.194 ±0.001 T2=20.362 ±0.053 ns
FIT FROM CHANNEL 46 TO 512 CHISQ = 0.944
RESIDUALS
CHANNEL NUMBER
NORMALIZED INTENSITY
TIME / NANOSECONDS

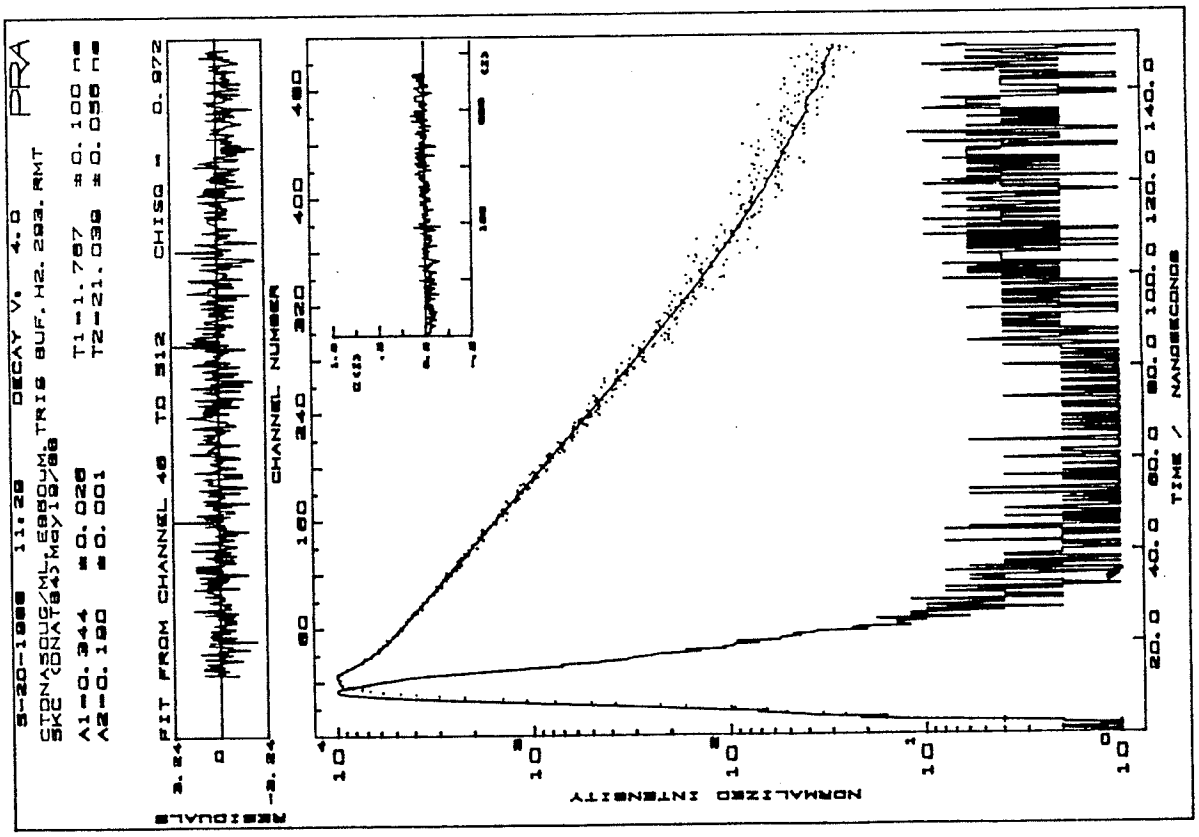
A
5-20-1988 11:28 DECAY Vs 4.0 PRA
CTDNASOUG/ML.EB80UM.TRIS BUF. H2.293. RMT
SKE CONAT843 May19/88
A1=0.344 ±0.026 T1=1.767 ±0.100 ns
A2=0.190 ±0.001 T2=21.038 ±0.056 ns
FIT FROM CHANNEL 46 TO 512 CHISQ = 0.972
RESIDUALS
CHANNEL NUMBER
NORMALIZED INTENSITY
TIME / NANOSECONDS

**FIGURE 19**

The residuals and auto-correlation plots
with variuos levels of background subtraction
(IRF,sample)

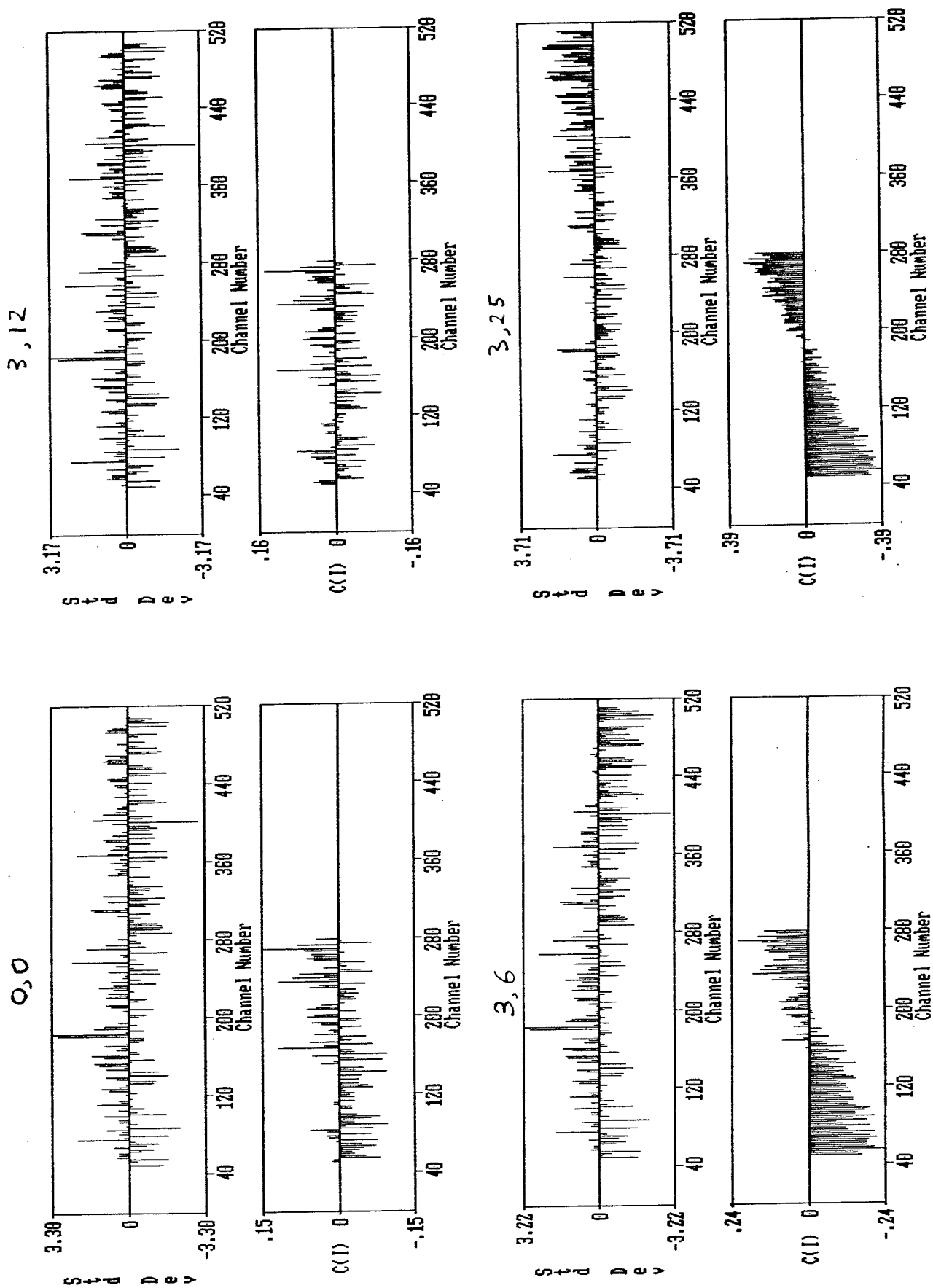
0,0
3,12
3,6
3,25
Std Dev
C(1)
Channel Number
3.30
-3.30
3.17
-3.17
3.22
-3.22
3.71
-3.71
.15
-.15
.16
-.16
.24
-.24
.39
-.39
0
40
120
200
280
360
440
520

# PART C

## DNA CONFORMATIONAL STUDIES WITH ETHIDIUM BROMIDE

## 11.0 FLA of Ethidium bromide bound to DNA

The FLA of ethidium bromide bound to DNA has been incorporated in previous chapters as examples of curve fitting optimization. In this chapter, the FLA experiments are described in detail and the results discussed in terms of the binding equilibria of Eb to DNA. In later chapters, the fluorescence lifetime of bound ethidium bromide is analyzed in terms of the conformational changes in DNA, and the possible fluorescence quenching mechanisms taking place.

### 11.1 Materials and methods

#### Samples

Calf Thymus DNA (~42% G-C content) was obtained from Sigma (type V - sodium salt, highly polymerized, #D-1751). Stock solutions were prepared at a concentration of 1 mg/ml with two levels of NaCl, 50mM and 1M. These solutions were stored at 5°C.

Ethidium bromide (2,7-Diamino-10-ethyl-9-phenyl-phenanthridinium Bromide) was also obtained from Sigma (#E-8751). Stock solutions of 1mM were prepared at the two salt concentrations and were stored in the dark at 5°C.

In each experiment, the final concentration of ctDNA was 50 $\mu$g/ml, or 143 $\mu$M (assuming the molecular weight of one nucleotide is 350). The final ethidium bromide concentration varied from 3$\mu$M to 400$\mu$M. This gave a range in the DNA/Eb ratio from .36 to 47.7.

In several experiments, the DNA and Eb solutions were prepared in 0.1M Tris buffer at a pH of 7.5 with 50mM NaCl.

Absorption measurements

To accurately determine the bound and free ethidium bromide concentrations at the various DNA/EB ratios and salt concentrations, the spectrophotometric method used by Waring [9] and Angerer [4] was employed. This involves measuring the absorbance of DNA-Eb solutions at several key wavelengths and establishing a calibration curve relating the concentration of free dye to the DNA/EB ratio. The method is described thoroughly by Waring [9].

The ethidium bromide concentration was kept constant at 100 $\mu$M and DNA was added in $\mu$g/ml increments. Absorbance measurements were made with an Hewlett Packard 8451A Diode Array Spectrophotometer. As more and more ethidium bromide binds to the DNA the absorption maximum shifts from 480 nm (free dye) to 520 nm (maximum binding). See Figure 20. Figure 21 shows the

absorbance at 460 nm verses the amount of DNA added for low salt (50mM NaCl). The plateau level defines the absorbance range from 100% free to 0% free. These data were then used to produce a calibration curve relating the amount of free Eb, expressed as a percentage of the total Eb concentration, to the DNA/Eb molar ratio. The graph at the top of figure 22 shows the calibration curve for ctDNA, under low salt conditions. The same procedure was followed at high salt conditions (1 M NaCl) and a similar calibration curve was generated. However, unlike low salt, the plateau of the absorbance curve for high salt does not correspond to 0% free Eb As seen later, the Fluorescence Lifetime Analysis shows that there is always some free Eb present. Therefore, the absorbance range for low salt was used to define the 0% free limit for high salt. The resulting calibration curve for high salt is shown at the bottom of figure 22, with the plateau level corresponding to 19.6% free Eb.

Fluorescence intensity measurements

Since a spectrofluorimeter was not available to accurately determine the fluorescence intensity at the various DNA/Eb ratios, the Fluorescence Lifetime Instrument (FLI) was utilized to obtain relative fluorescence intensity estimates.

This was done by monitoring the fluorescence emission from the constant fraction timing discriminator. The counts were recorded for 5 second intervals to average out the minor variations in the counts/sec. values. The counts/sec. from the Ludox scattering solution were also recorded each time. These values which are a function of the excitation intensity were normalized and the corresponding fluorescence intensity values appropriately adjusted. This was necessary because of the instabilities in the arc lamp which were discussed in chapter 6.0. Figure 23 shows a fluorescence intensity calibration curve for free ethidium bromide. Notice that free Eb undergoes a concentration related self-quenching after aprrox. 100$\mu$M.

Fluorescence Lifetime measurements

All Fluorescence Lifetime Analyses were obtained with $H_2$ in the flashlamp, a T/CH of .293, 5,000 counts recorded in the peak channel, a second order fit to the data edge, and with background subtraction.

Note throughout this paper, 'low salt' refers to 50mM NaCl, and 'high salt' refers to 1M NaCl. Also, unless otherwise stated, all experiments were performed at room temperature, (~ 21°C).

FIGURE 20

Absorption shift of ethidium bromide
upon binding to DNA
Curve A: unbound Eb
Curve E: maximum Eb binding

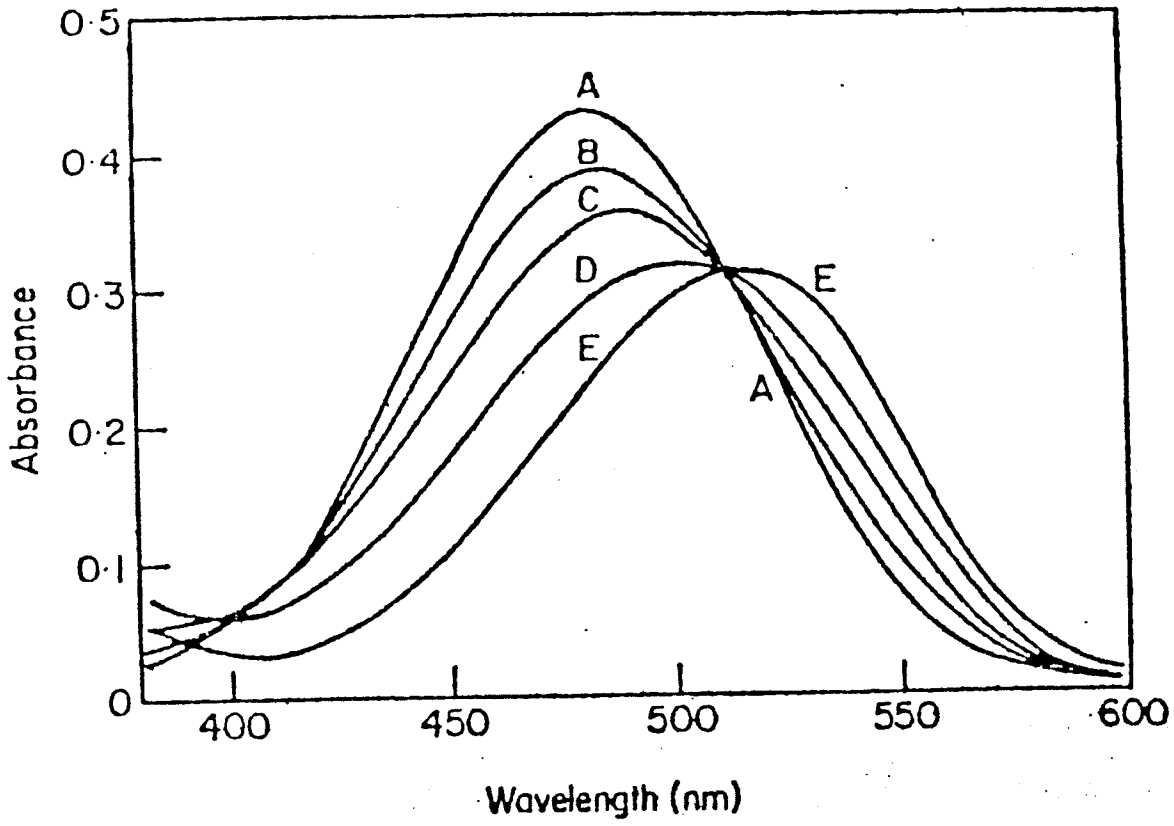
0·5
0·4
0·3
0·2
0·1
0
Absorbance
A
B
C
D
E
E
A
400
450
500
550
600
Wavelength (nm)

FIGURE 21

The absorbance of 100$\mu$M Eb at 460 nm
as a function of the amount of DNA added

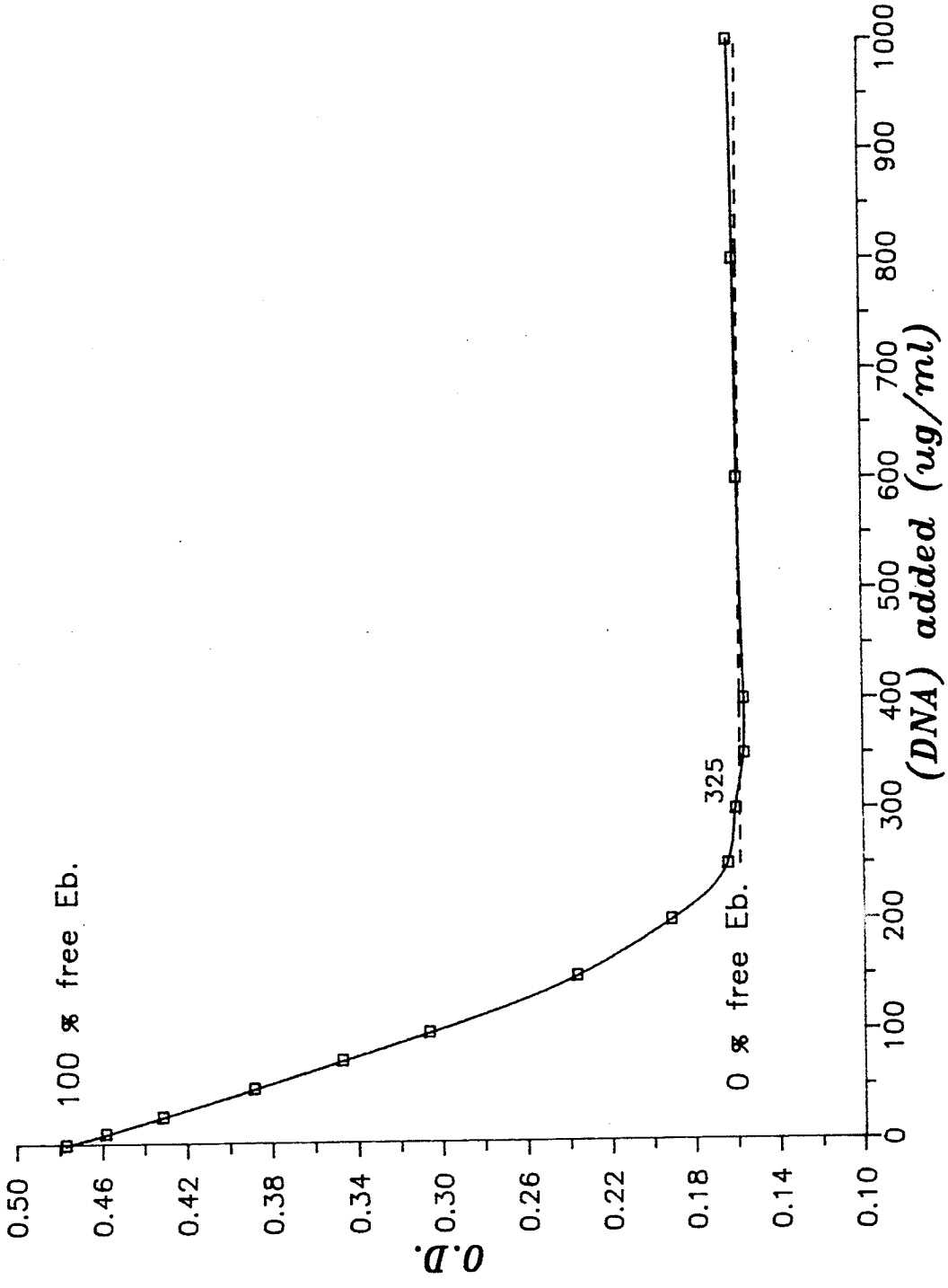
0.50
0.46
0.42
0.38
0.34
0.30
0.26
0.22
0.18
0.14
0.10
O.D.
0
100
200
300
400
500
600
700
800
900
1000
(DNA) added (ug/ml)
100 % free Eb.
0 % free Eb.
325

FIGURE 22

A calibration of the % unbound Eb as a function of the DNA/Eb ratio

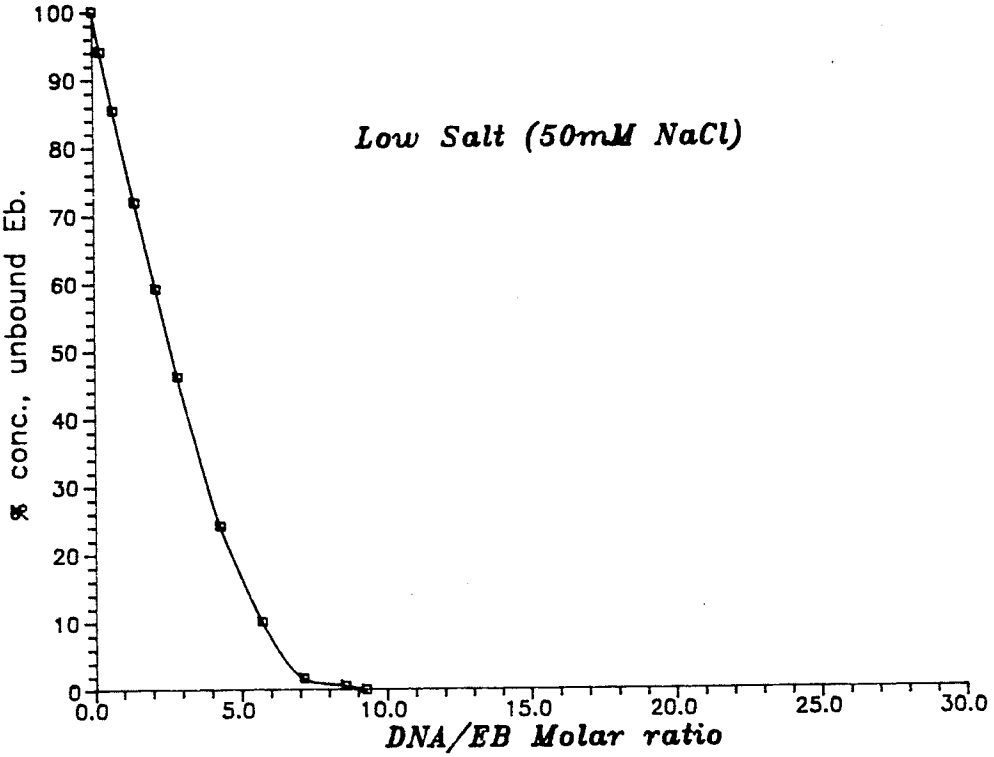
Low Salt (50mM NaCl)
% conc., unbound Eb.
100
90
80
70
60
50
40
30
20
10
0
0.0
5.0
10.0
15.0
20.0
25.0
30.0
DNA/EB Molar ratio

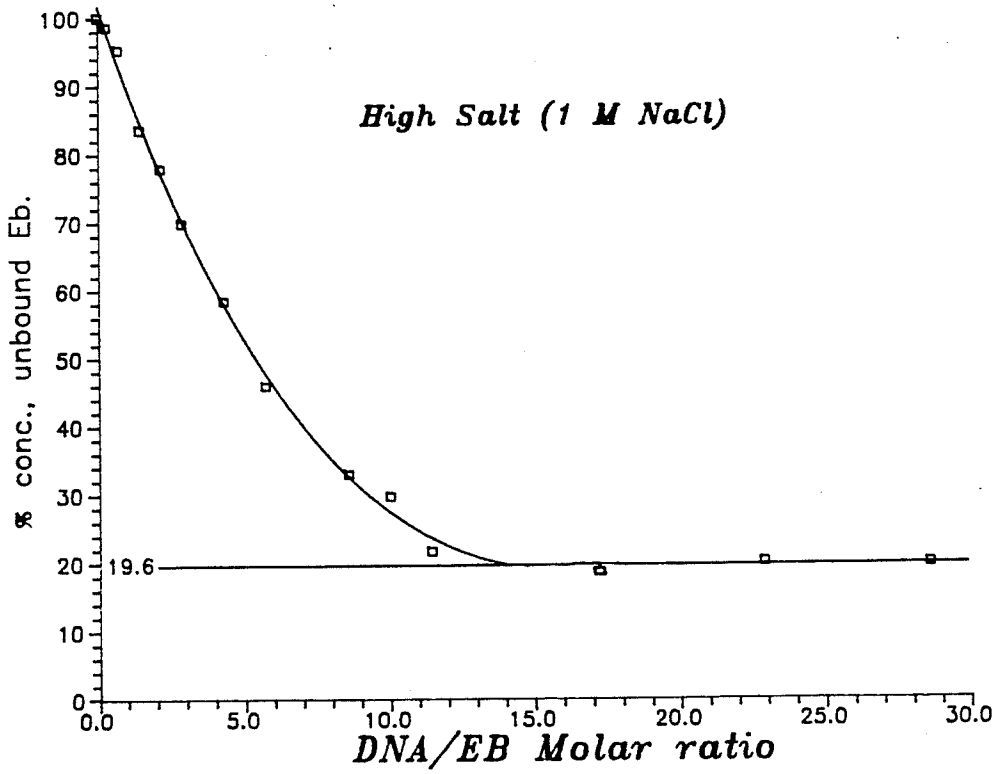
High Salt (1 M NaCl)
% conc., unbound Eb.
100
90
80
70
60
50
40
30
20
19.6
10
0
0.0
5.0
10.0
15.0
20.0
25.0
30.0
DNA/EB Molar ratio

**FIGURE 23**

Fluorescence intensity profile of Eb
Ex. λ 485 nm, Em λ 610 nm
50 mM NaCl, room temp.

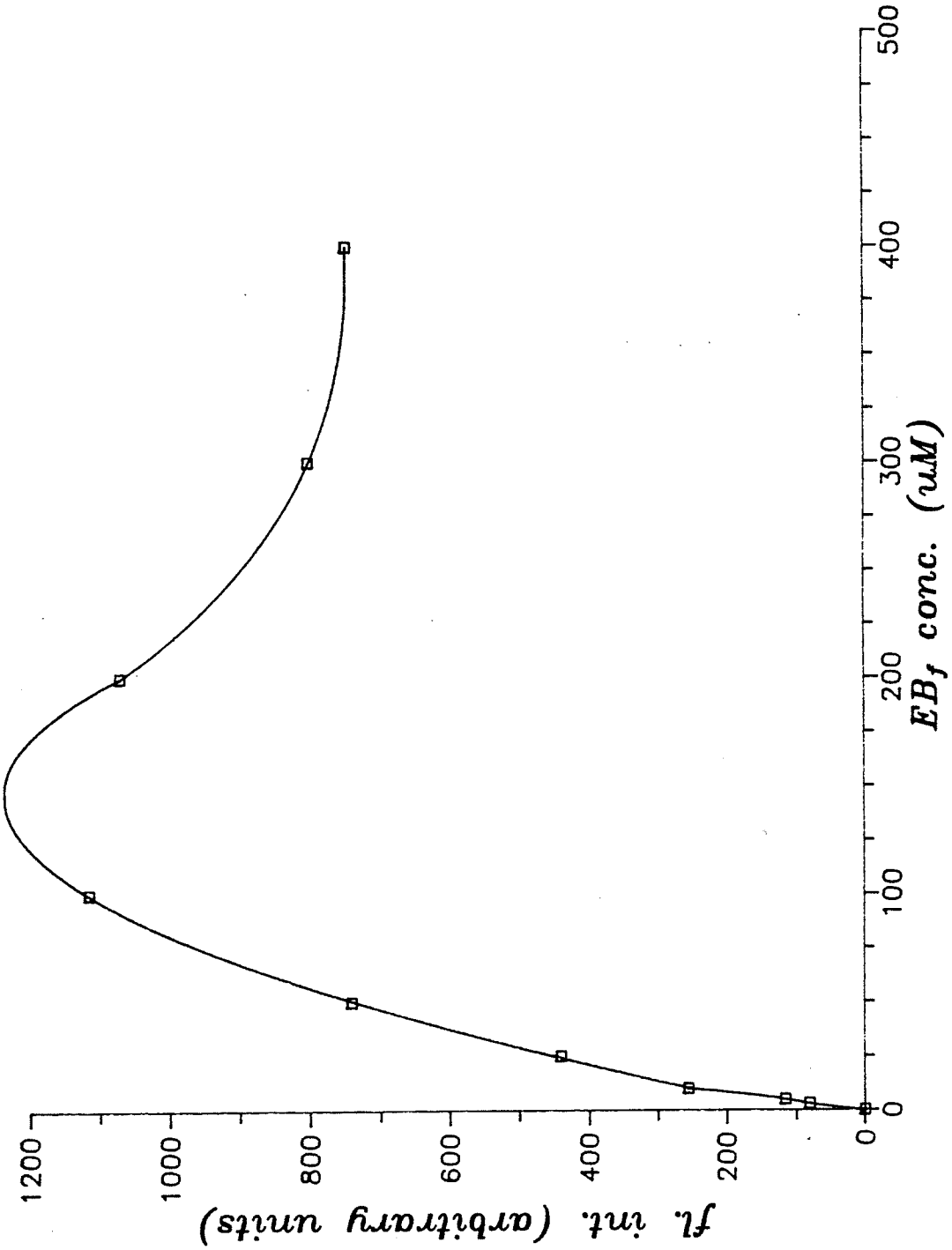
fl. int. (arbitrary units)
1200
1000
800
600
400
200
0
0
100
200
300
400
500
$EB_f$ conc. (uM)

## 11.2 Fluorescence lifetime results

The Fluorescence Lifetime Analysis (FLA) for ethidium bromide at various DNA/EB ratio's is shown is table 11. The analyses for low and high salt concentrations are listed.

As the amount of Eb added decreases, the %int of $\tau_1$ decreases, while the %int of $\tau_2$ increases. At both salt concentrations, the value of $\tau_2$ plateaus at 23.1 nsec. The lifetime of ethidium bromide bound to DNA has been measured several times, with reported values of 23 nsec [10] and 24 nsec [1]. From the above information, one would hypothesize that $\tau_2$ is from Eb bound to DNA, and $\tau_1$ is from unbound, or 'free' Eb

The fluorescence lifetime of free ethidium bromide in the absence of DNA was measured under the conditions of low salt, high salt, and .1M Tris, pH 7.5, low salt. The lifetime was found to be independent of salt concentration and had an average value of $1.67\pm.02$ nsec. The effect of varying the pH was also examined. Measurements were obtained in a low salt, 0.1M buffer solution with a pH that varied from 5.0 to 10.5. Hepes buffer was used for the pH range of 5.0 to 8.5, and glycine was used for the pH range of 8.5 to 10.5. The average value for ten different pH levels was $1.70\pm.05$, with an average individual error of 0.03 as calculated by the FLA.

Table 11

FLA of Eb at various DNA/EB ratios

| DNA/EB (Molar ratio) | $\tau_i$ | Low Salt | | | High Salt | | |
|---|---|---|---|---|---|---|---|
| | | $\tau_i$ | ± | %int | $\tau_i$ | ± | %int |
| .36 | 1 | 1.59 | .02 | 67.4 | 1.61 | .14 | 58.8 |
| .71 | | 1.58 | .04 | 43.4 | 1.70 | .03 | 44.3 |
| 1.4 | | 1.64 | .03 | 25.2 | 1.70 | .03 | 30.2 |
| 2.8 | | 1.68 | .15 | 9.4 | 1.58 | .06 | 18.7 |
| 5.7 | | 1.12 | .93 | 2.3 | 1.60 | .08 | 11.4 |
| 14.3 | | | -- | | 1.54 | .14 | 7.7 |
| 47.7 | | | -- | | 2.06 | .20 | 6.2 |
| .36 | 2 | 14.35 | .13 | 32.6 | 18.36 | .14 | 41.2 |
| .71 | | 16.54 | .10 | 56.6 | 19.21 | .12 | 55.7 |
| 1.4 | | 18.52 | .05 | 74.8 | 20.37 | .08 | 69.8 |
| 2.8 | | 20.04 | .05 | 90.6 | 21.50 | .06 | 81.3 |
| 5.7 | | 21.20 | .05 | 97.7 | 22.23 | .06 | 88.6 |
| 14.3 | | 22.45 | .04 | 100. | 22.91 | .06 | 92.3 |
| 47.7 | | 23.10 | .04 | 100. | 23.10 | .05 | 93.8 |

$H_2$ gas, T/CH .293, 5,000 counts-peak
2nd order fit to data edge
Background subtracted

The average values of $\tau_1$ in low salt, high salt, and .1M Tris, at the various DNA/Eb ratio's are: 1.62±.05, 1.62±.07, and 1.64±.06 respectively. These lifetimes are slightly lower than the free Eb lifetime in the absence of DNA. This is probably due to the presence of $\tau_2$, and the fact that the $\tau_1$ and $\tau 2$ components are correlated. The correlation of multi-exponential components was discussed in the previous section.

Figure 24 shows the bound Eb lifetime for high and low salt as a function of the DNA/Eb ratio. The reasons for the decrease in the lifetime as a function of the DNA/Eb ratio are discussed in the next two chapters. Similar results are reported by Burns [10] except in his results, the lifetime at a DNA/Eb ratio of 1.0 is 14 nsec at 0.5M NaCl and 10 nsec at 100mM NaCl. These values are somewhat lower than those shown in figure 24. The difference is due to the resolution of $\tau_1$. Burns could not resolve this component above a DNA/Eb ratio of 1.0, and below this level, the lifetime for free Eb was given an approximate value of 1 nsec. With the free Eb component not resolved accurately, the values of $\tau_b$ were underestimated. As seen in table 11, $\tau_f$ has been resolved up to a DNA/Eb ratio of 5.7 for low salt, and at all DNA/Eb ratio's for high salt, and hence the values of $\tau_b$ are higher.

Burns also reported that the bound lifetime has no

temperature dependence above room temp. We investigated the effect of lowering the temperature to 2°C, a temperature used with cells. The results are shown in figure 25. The lifetime profile is consistently higher at 2°C. This was anticipated since the fluorescence lifetime should increase as the viscosity increases. The sensitivity of the lifetime to temperature makes it crucial to maintain a constant temperature during the data collection.

**FIGURE 24**

The fluorescence lifetime of Eb bound to DNA as a function of the DNA/Eb ratio

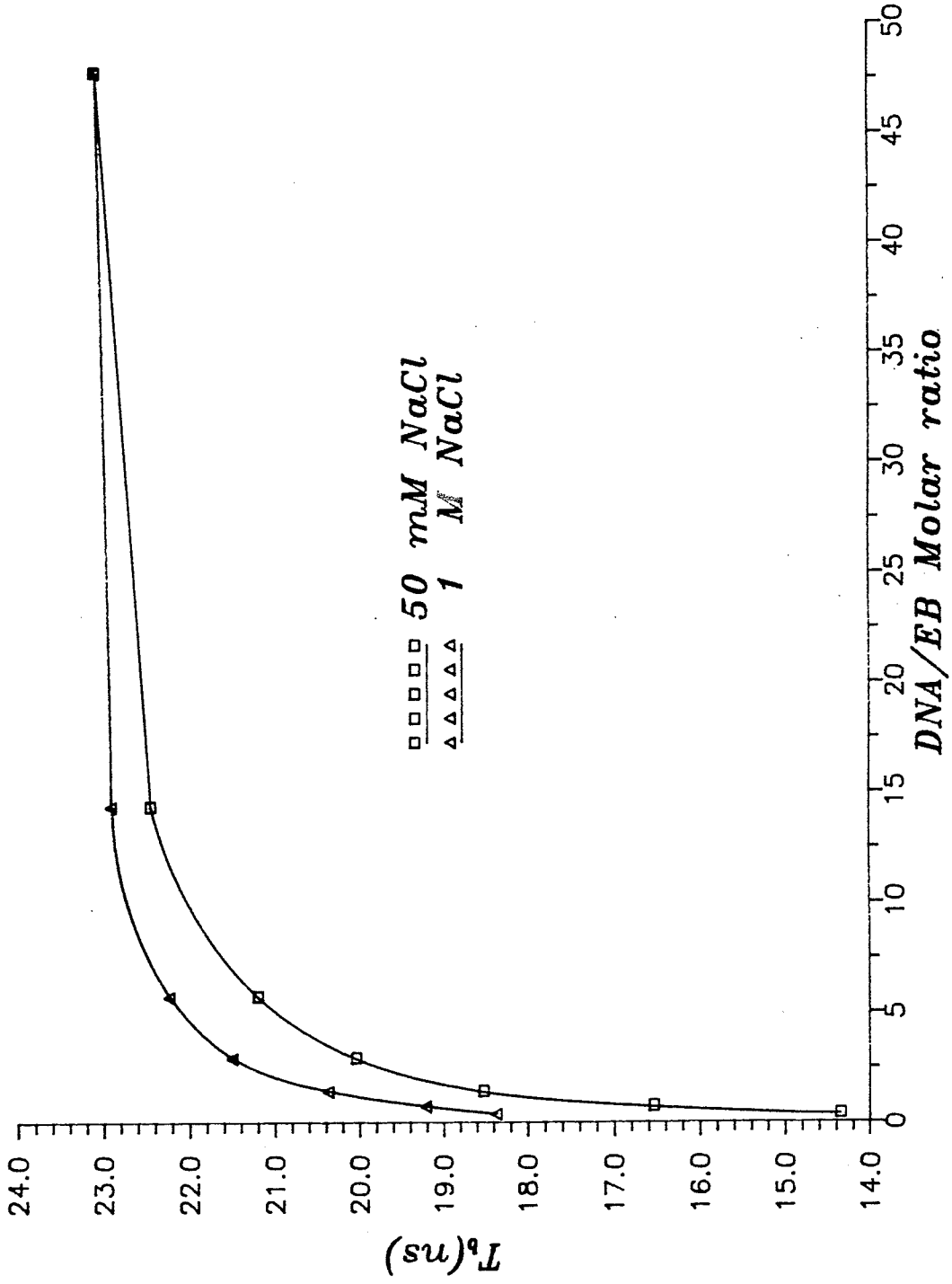
24.0
23.0
22.0
21.0
20.0
19.0
18.0
17.0
16.0
15.0
14.0
$T_b$(ns)
0
5
10
15
20
25
30
35
40
45
50
DNA/EB Molar ratio
50 mM NaCl
1 M NaCl

FIGURE 25

The bound fluorescence lifetime at 2°C
and at room temperature

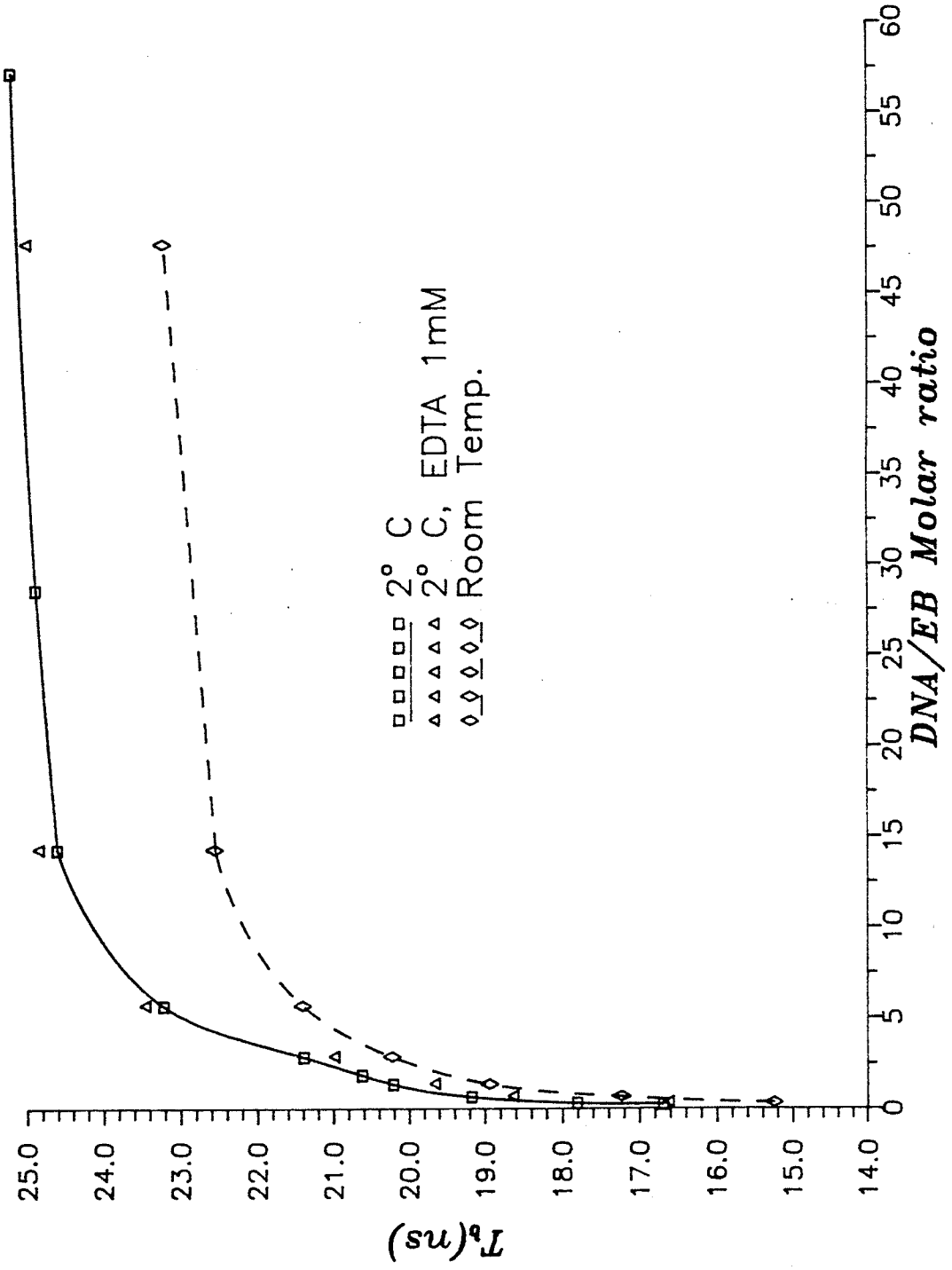
25.0
24.0
23.0
22.0
21.0
20.0
19.0
18.0
17.0
16.0
15.0
14.0
$T_b(ns)$
0
5
10
15
20
25
30
35
40
45
50
55
60
DNA/EB Molar ratio
2° C
2° C, EDTA 1mM
Room Temp.

## 11.3 Analyses of the binding equilibria

The molar concentrations of the bound and free ethidium bromide cannot be obtained directly from the %int values of the lifetime components. The respective concentrations were determined by the spectrophotometric method outlined in section 11.1. The results for high and low salt are shown in figure 26. The y-axis was plotted as a log scale to allow both the free and bound concentration curves to be seen clearly on the same graph.

When small molecules bind independently to a set of equivalent sites on a polymer, the equilibrium between free and bound molecules is given by the Scatchard equation:

$$\frac{r}{c} = Kn - Kr \qquad (25)$$

where, in the present case, r is the ratio of bound Eb per nucleic acid phosphate, n is the number of binding sites per nucleic acid phosphate, K is the intrinsic association constant to a site, and c is the free Eb concentration [2]. If r/c is plotted against r, a straight line through the data intercepts the x-axis at r = n, and indicates that the assumptions underlying equation 25 are satisfied.

The value of r was calculated from the data used to create the %free calibration curves shown in figure 22. Figure 27 shows the value of r, for low and high salt, as a function of the

DNA/EB ratio. In equation 25, if the concentration of free Eb increases to infinity, then in the limit, r = n. In figure 27, this corresponds to a DNA/EB ratio approaching zero. Thus from the data in figure 27, n = 0.21±.005 for low salt, and n = 0.11±.005 for high salt.

Waring [9] reported an n value for DNA of ~ 0.2, which was independent of G-C content. He also reported that, as the salt concentration increases, the value of n decreases. Le Pecq and Paoletti [2] also calculated a value of .2 for n. They found that the intrinsic association constant (K) decreased 100 fold as the salt concentration was lowered from 1M to 40mM., with the total number of sites remaining constant. This result agrees with our data which shows less binding at high salt.

Angerer and Moudrianakis [4] suggest a competitive binding model between $Na^+$ and $Eb^+$ for the intercalation site. They found that the average number of available binding sites is reduced by 1/3 as the salt concentration increases 100 fold.

Our data is consistent with the above findings, namely, that as the salt concentration increases the value of n decreases. At 50mM NaCl, maximum Eb binding is reached when 1 Eb molecule is bound for every 5 base pairs (r = 0.2). At 1M NaCl, 1 Eb

molecule binds approx. every 10 base pairs (r = 0.1). As the salt concentration is increased by a factor of 20, the number of available binding sites is reduced by 1/2.

The above mentioned references also obtained r values which were greater than .2, when saturating quantities of free Eb were present. The straight line extrapolation of their Scatchard plots to the x-intercept (n = 0.2), indicated binding by intercalation, to the so called primary site. It was postulated that r values that deviated from this straight line were due to Eb binding at a second site. They concluded that binding to this 2nd site does not occur at high salt, only at low salt, and only after saturation of the primary site. It was also concluded that the 2nd site is located on the exterior of the DNA helix, with the Eb molecules held by electrostatic interactions.

In our studies, r values above .2 were not found. Since r was calculated by measuring the shift in the absorption spectra upon the intercalation of Eb within DNA, only primary site binding was being monitored, and therefore values for $r > .2$ would not be expected if .2 is the limit for primary site binding. If any secondary site binding is occurring, it should not affect the value of r as measured by the above technique.

In the next chapter, it is postulated that 2nd site binding does occur before r reaches a value of .2, and that it occurs to a greater extent under low salt conditions. It will be argued that the electrostatic binding of Eb to the exterior of the DNA helix facilitates a collisional energy transfer mechanism which quenches the fluorescence lifetime and the fluorescence intensity of the ethidium bromide intercalated at the primary site.

FIGURE 26

The concentration of bound and unbound
Eb as a function of the DNA/Eb ratio

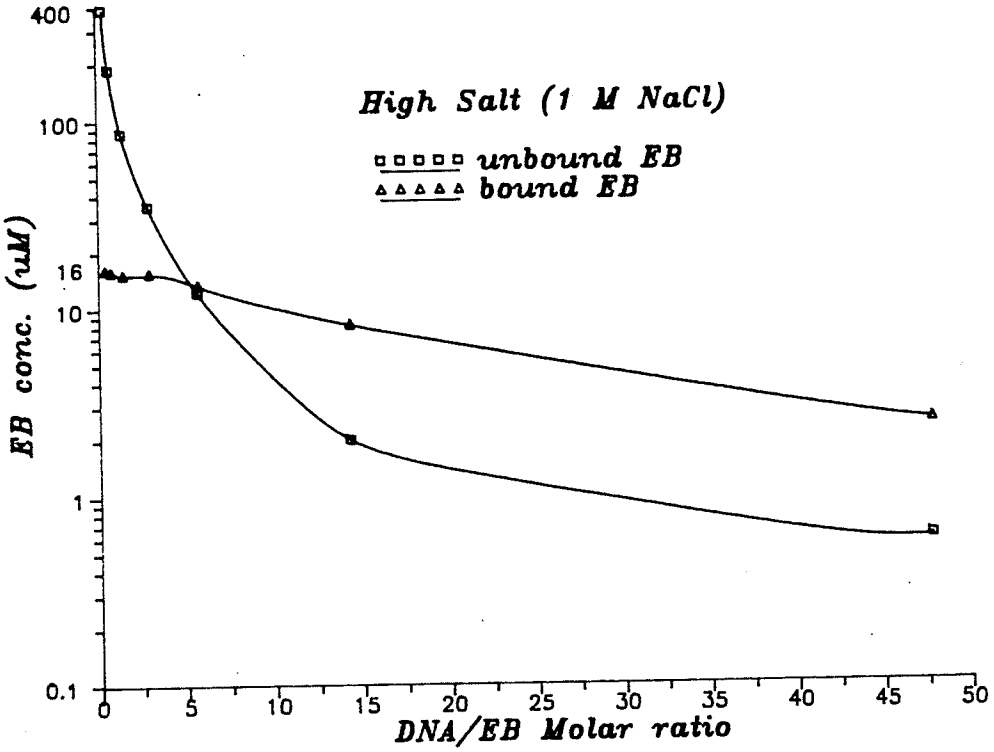
High Salt (1 M NaCl)
unbound EB
bound EB
EB conc. (uM)
400
100
16
10
1
0.1
0
5
10
15
20
25
30
35
40
45
50
DNA/EB Molar ratio

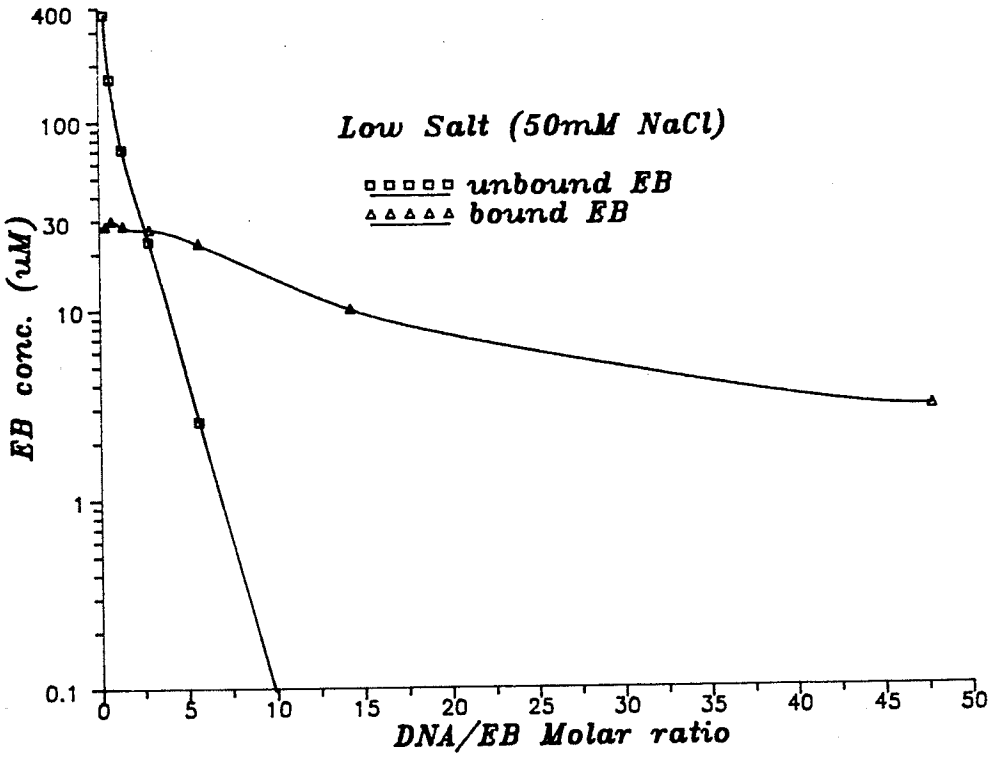
Low Salt (50mM NaCl)
unbound EB
bound EB
EB conc. (uM)
400
100
30
10
1
0.1
0
5
10
15
20
25
30
35
40
45
50
DNA/EB Molar ratio

FIGURE 27

The binding parameter 'r' as a function
of the DNA/Eb ratio

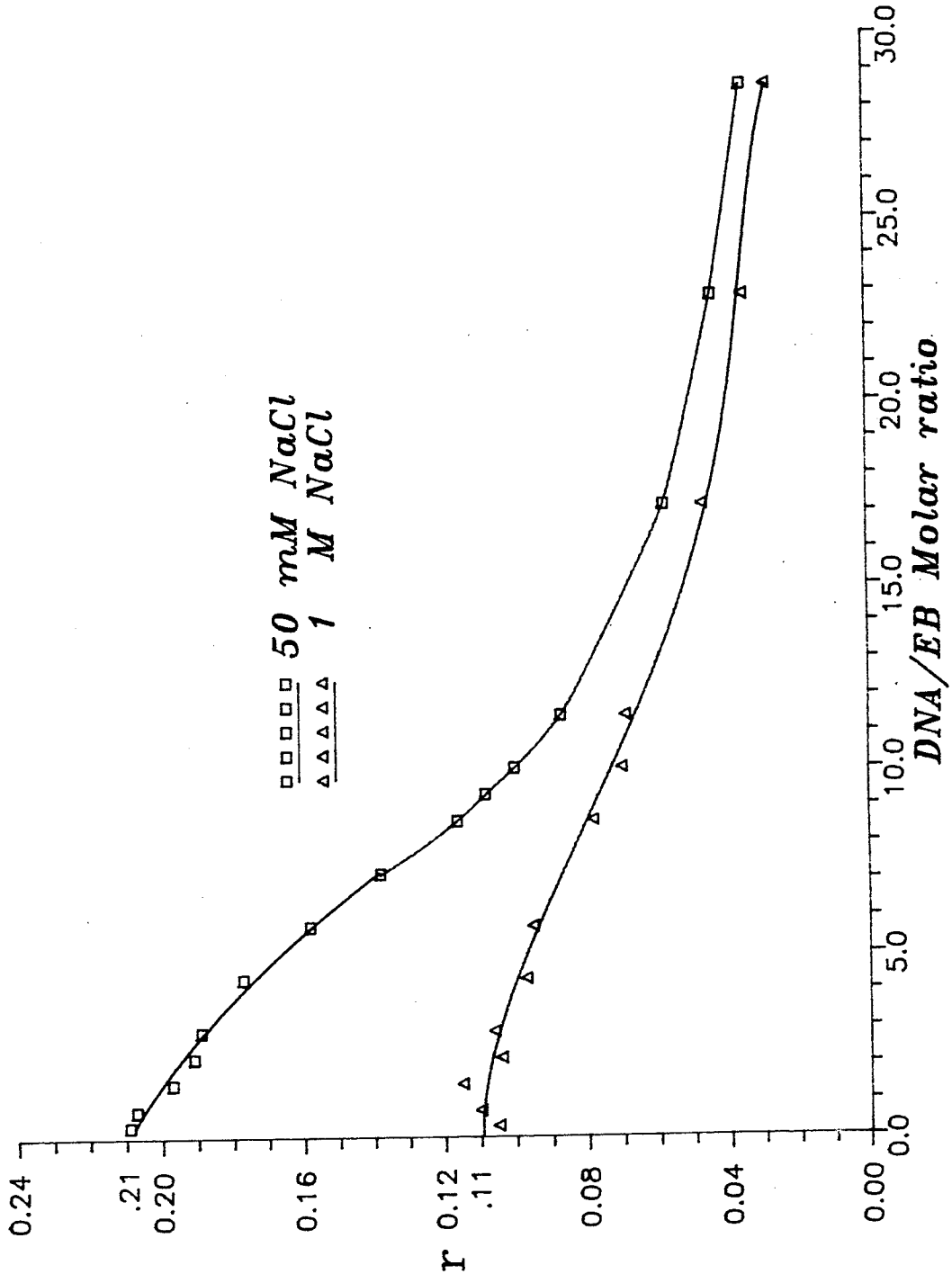
50 mM NaCl
1 M NaCl
r
DNA/EB Molar ratio
0.24
.21
0.20
0.16
0.12
.11
0.08
0.04
0.00
0.0
5.0
10.0
15.0
20.0
25.0
30.0

## 12.0 Bimolecular quenching

A variety of processes can result in the quenching of fluorescence. These include excited state reactions, energy transfer, complex formation, and collisional quenching [8].

Collisional quenching requires physical contact between the quenching molecule and the fluorophore. There are two types of collisional quenching, dynamic and static. For dynamic collisional quenching, the quencher diffuses to the fluorophore during the lifetime of the excited state. Upon contact, the fluorophore returns to its ground state, without the emission of a fluorescent photon, and hence the fluorescence intensity is decreased. For static collisional quenching, a complex is formed between the quencher and the fluorophore prior to fluorophore excitation. This complex is non-fluorescent. With fewer fluorophores available for excitation, the fluorescence intensity will decrease.

If bimolecular collisional quenching occurs, it competes with the other processes that depopulate the excited state

$$M^*(S_1) + Q \xrightarrow{k_q} M(S_o) + Q \qquad (26)$$

If the concentration of $M^*$ remains constant, collisional quenching is described by the Stern-Volmer equation

$$\frac{F_1}{F_{1q}} = 1 + k_q \tau [Q] \tag{27}$$

$F_1$ and $\tau$ being the fluorescence intensity and fluorescence lifetime in the absence of the quencher.
$k_q$ is the bimolecular quenching constant

The derivation of the Stern-Volmer equation can be found in Lakowicz [8], from which the following important relationship is derived

$$\frac{F_1}{F_{1q}} = \frac{\tau}{\tau_q} \tag{28}$$

$F_{1q}$ and $\tau_q$, being the fluorescence intensity and fluorescence lifetime in the presence of the quencher.

Recall that the fluorescence lifetime is the reciprocal of the sum of all of the emission rate constants (eq. 8). If quenching occurs, then equation 8 becomes

$$\tau_q = \frac{1}{k_f + k_{nr} + k_q[Q]} \tag{29}$$

and the fluorescence lifetime decreases appropriately.

In static collisional quenching, the fluorescence lifetime is unaffected because the complex formed is non-fluorescent, therefore

$$\frac{F_1}{F_{1q}} = \frac{\tau}{\tau_q} = 1 \tag{30}$$

The Stern-Volmer equation, expressed in terms of fluorescence lifetimes, becomes

$$\frac{\tau}{\tau_q} = 1 + k_q \tau [Q] \qquad (31)$$

or

$$\frac{1}{\tau_q} = \frac{1}{\tau} + k_q [Q] \qquad (32)$$

Provided the concentration of the fluorophore remains constant, a plot of $1/\tau_q$ v. [Q] is expected to be linear with $k_q$ equalling the slope. If this is not the case, all the fluorophores are not accessible to the quencher, and the non-linear curve will dip towards the x-axis.

## 12.1 Collisional quenching of primary DNA-Eb fluorescence by secondary Eb binding

As seen earlier, the lifetime of ethidium bromide bound to DNA decreases as the amount of ethidium bromide added increases. This occurs at both low and high salt levels. The bound lifetime and the bound fluorescence intensity drop dramatically as the concentration of free ethidium bromide increases. This is shown for low and high salt in figure 28. Angerer and Moudrianakis [4] postulate that the decrease in fluorescence enchancement can be explained by a radiative or non-radiative energy transfer from intercalated dye molecules to those bound in the non-fluorescent, or weakly fluorescent sites, which may be equivalent to the secondary sites mentioned by Le Pecq and Paoletti [2]. The drop in $\tau_b$ is also shown in figure 29. Here the concentration of free ethidium bromide is plotted against the difference between the

maximum lifetime $\tau_m$ and the quenched lifetime. If free ethidium bromide, once present at a high enough concentration, is quenching the bound ethidium bromide by an electrostatic association with the outside of the DNA helix, then

$$Eb_b^* + Eb_f \xrightarrow{k_q} Eb_b + Eb_f \qquad (33)$$

and

$$\frac{1}{\tau_{bq}} = \frac{1}{\tau_b} + k_q [Eb_f] \qquad (34)$$

It is known that ethidium bromide intercalated within the base pairs of DNA, forms a highly planar complex, and that the susceptibility to concentration-dependent quenching increases with the planarity of the molecule [8].

Figure 30 is a plot of $1/\tau_{bq}$ v. $[Eb_f]$ normalized for a constant $Eb_b$ concentration, which is a condition of this equation. Above a threshold concentration of ~ 3.5$\mu$M, a Stern-Volmer relationship is seen for both salt levels. Note that in both curves, the initial slope values ($k_q$) are the same. The curves slowly deviate toward the x-axis, with the high salt curve approaching a plateau level faster. This is also seen in figure 29, where the drop in the lifetime for high salt soon becomes independent of the free Eb conc. In the Stern-Volmer plot this deviation toward the x-axis is to be expected, since the concentration of free ethidium bromide soon overwhelms the concentration of the bound Eb, and there are not enough fluorophores accessible to the quencher. Under high salt conditions, there are

less ethidium bromide molecules bound to the DNA, therefore the curves plateau faster.

An initial drop occurs in the fluorescence lifetime of bound Eb, prior to the threshold free Eb concentration. This initial drop will be discussed in the next chapter. As shown in figure 29, at low salt, the drop in $\tau_b$ is quite substantial, around 2 nsec, and is responsible for the separation between the two curves.

FIGURE 28

The fluorescence intensity and fluorescence lifetime of bound Eb and the %int of unbound Eb, as a function of the DNA/Eb ratio

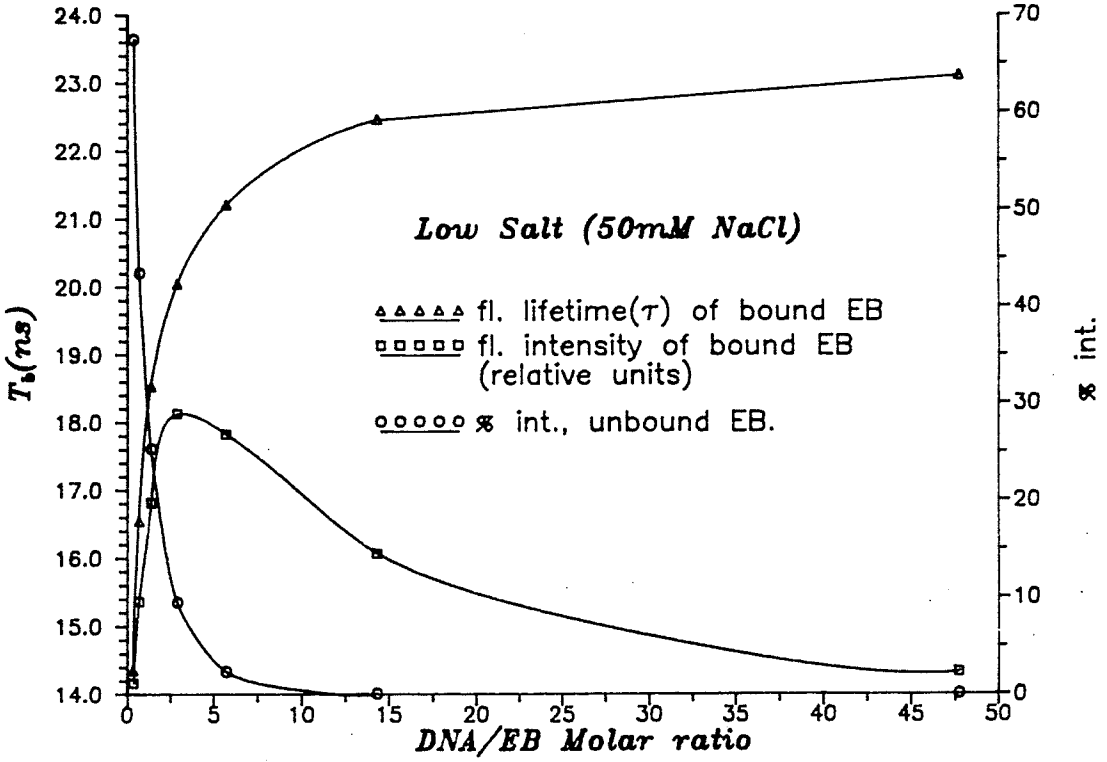
Low Salt (50mM NaCl)
fl. lifetime(τ) of bound EB
fl. intensity of bound EB (relative units)
% int., unbound EB.
$T_b$(ns)
% int.
DNA/EB Molar ratio

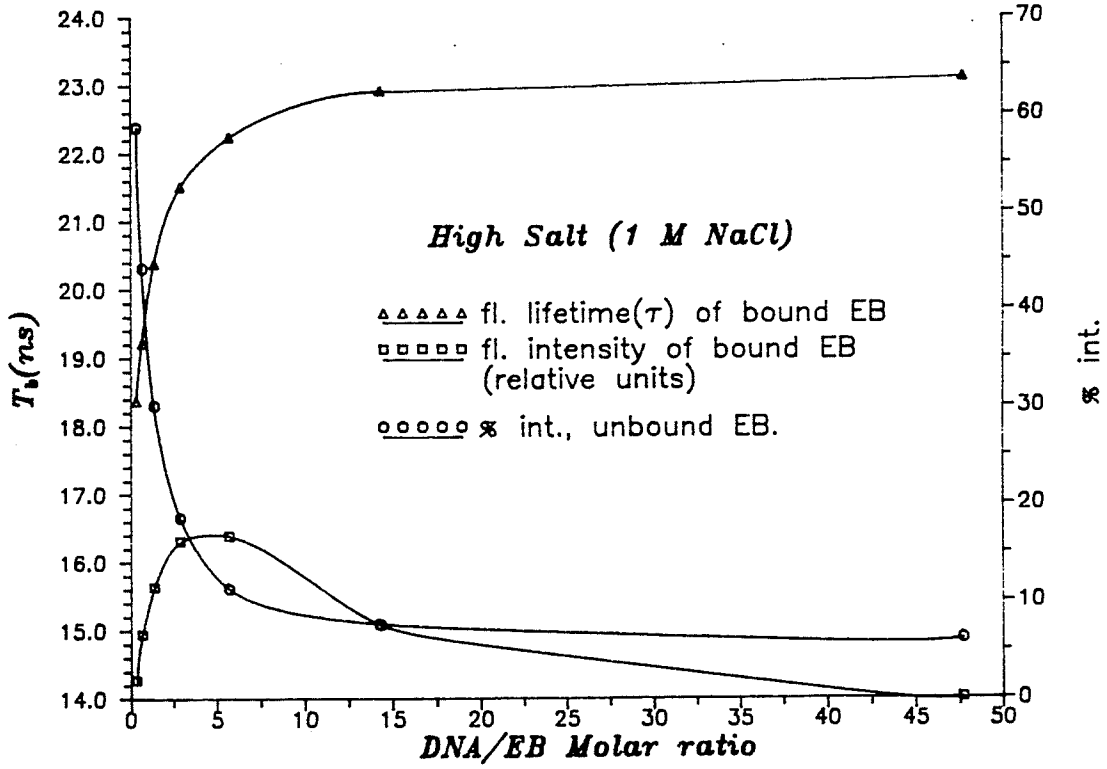
High Salt (1 M NaCl)
fl. lifetime(τ) of bound EB
fl. intensity of bound EB (relative units)
% int., unbound EB.
$T_b$(ns)
% int.
DNA/EB Molar ratio

**FIGURE 29**

The unbound Eb concentration
as a function of the drop in the
bound Eb lifetime

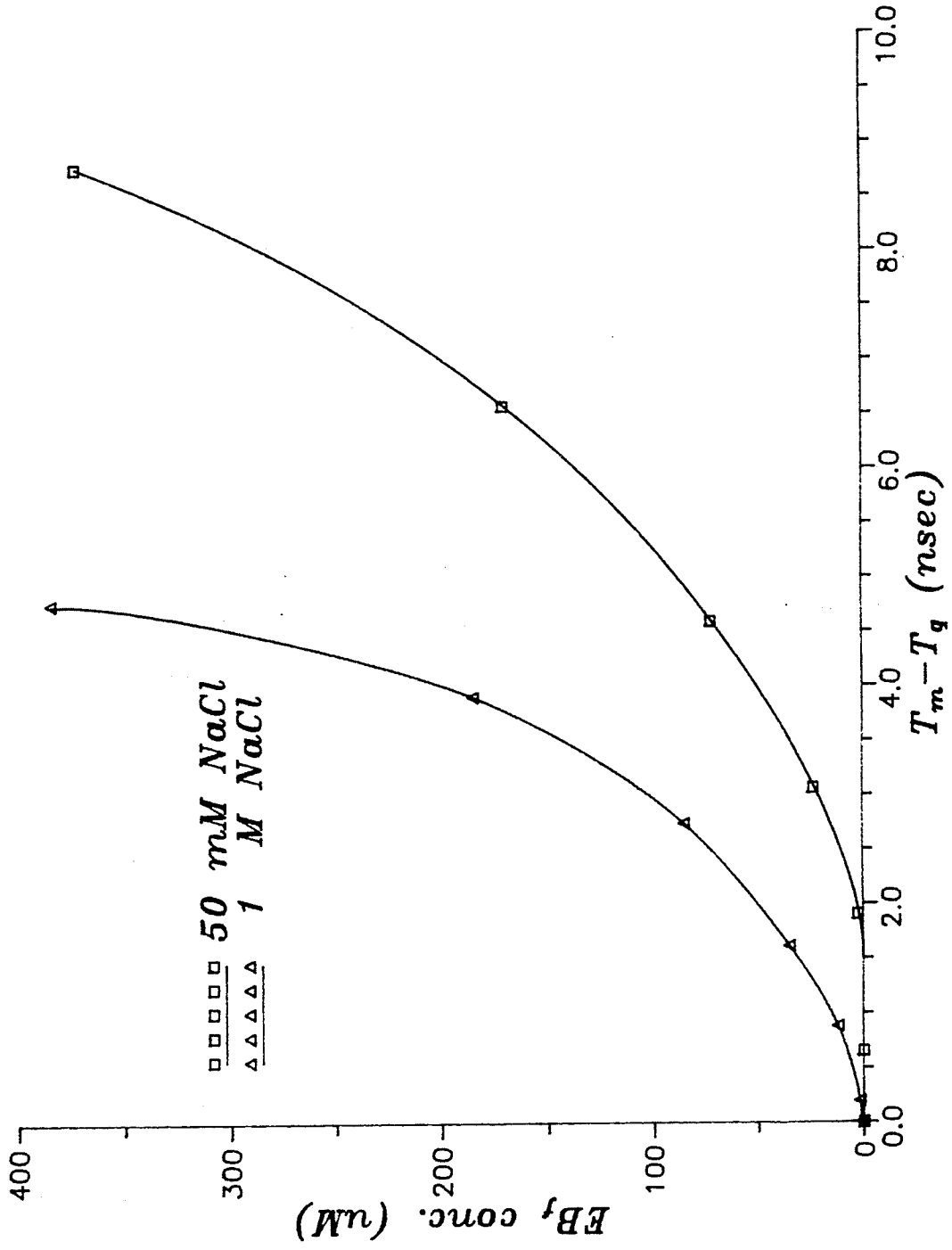
400
300
200
100
0
0.0
2.0
4.0
6.0
8.0
10.0
$EB_f$ conc. ($\mu M$)
$T_m - T_q$ (nsec)
50 mM NaCl
1 M NaCl

FIGURE 30

A Stern-Volmer plot for unbound Eb
as a quenching molecule

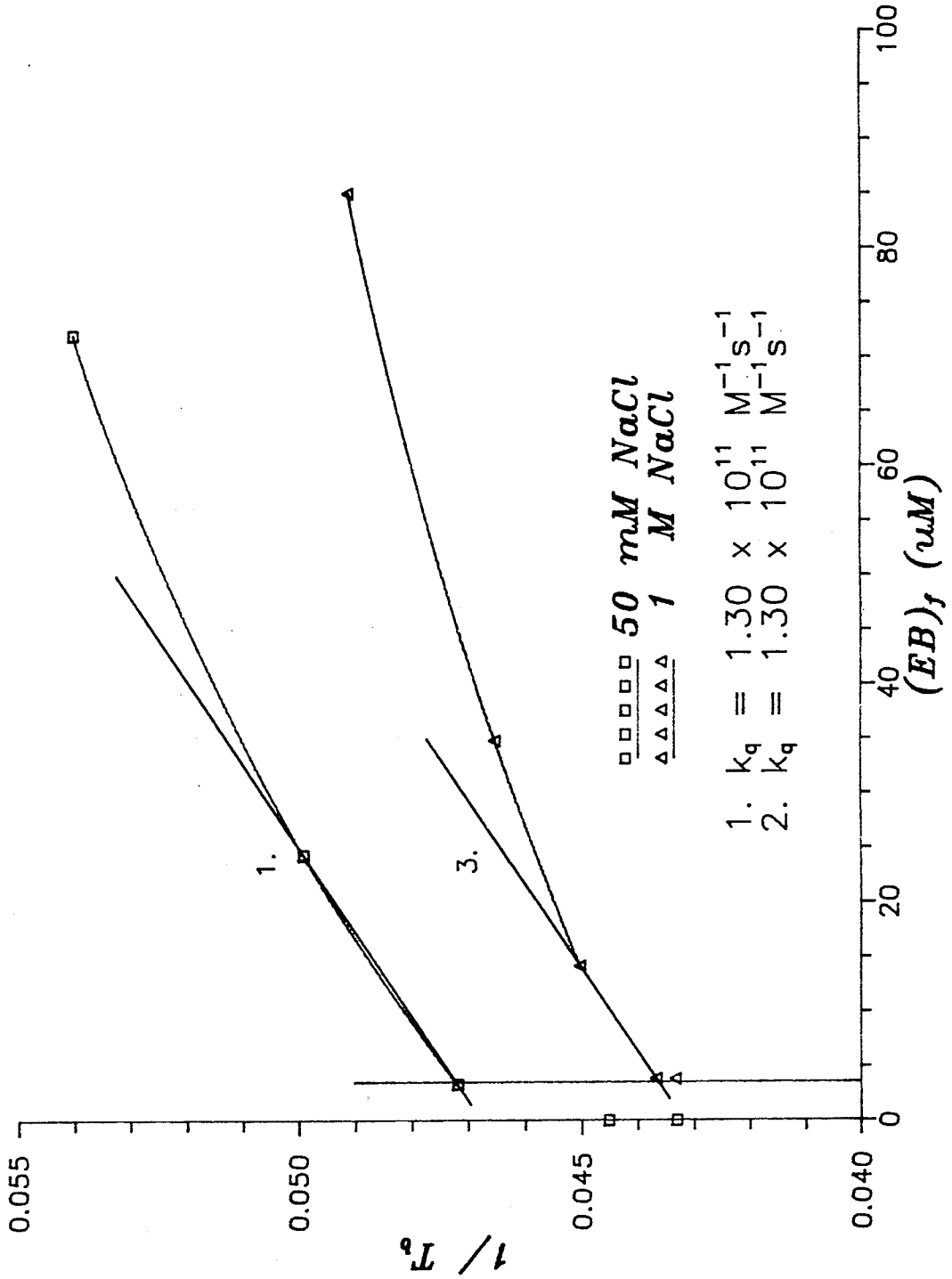
0.055
0.050
0.045
0.040
1/ $T_b$
0
20
40
60
80
100
$(EB)_f$ (uM)
50 mM NaCl
1 M NaCl
1. $k_q$ = 1.30 x $10^{11}$ $M^{-1}s^{-1}$
2. $k_q$ = 1.30 x $10^{11}$ $M^{-1}s^{-1}$
1.
3.

## 12.2 Quenching by oxygen

The dramatic decrease in $\tau_b$ has been attributed to collisional quenching by ethidium bromide bound at a secondary site on the outside of the DNA helix. In the DNA/EB ratio range where the free Eb concentration is below the threshold level for Eb collisional quenching, the bound lifetime has a subtle decrease, with no apparent loss in fluorescence intensity. This occurs to a greater degree under low salt conditions (see figures 28, and 29).

As mentioned earlier, under low salt conditions, as more Eb molecules intercalate, the DNA helix takes on a more open configuration . As each Eb molecule binds, the base pair separation increases by 3.4 Angstroms (A), and the helical structure unwinds slightly [6]. Under high salt conditions, it has been suggested [20] that the DNA helix takes on a rigid, collapsed state, due to cations, in this case Sodium, clustering around the negatively charged phosphates, reducing the phosphate-phosphate repulsive interactions. If this is so, we would expect less unwinding at high salt, than at low salt.

Recall from chapter 5, ethidium bromide, intercalated between the base pairs of DNA, is protected from $O_2$ quenching and hence its fluorescence intensity increases. If, under low salt

conditions, the helix opens up its configuration as more and more Eb molecules bind, then the bound Eb molecules will not have the same level of protection. Consequently, the rate of fluorescence quenching by $O_2$ molecules should increase slightly. This would translate into a decrease in the fluorescence intensity and the fluorescence lifetime. The results at high salt show less of a decrease in $\tau_b$. This is consistent with the hypothesis that the helix is more rigid at high salt, and therefore does not open as much to allow $O_2$ quenching.

Since our measurements of fluorescence intensity were not very precise, the drop in fluorescence intensity may not have been noticed, especially when it was occurring at the same time as more and more Eb molecules were intercalating thus producing an overall increase in fluorescence intensity , as shown in figure 28.

## 12.3 Quenching by energy transfer

The drop in $\tau_b$ described in the previous chapter, can also be explained in terms of quenching by energy transfer between bound ethidium bromide molecules.

The process of a radiationless energy transfer from a donor (D) molecule to an acceptor molecule (A), has been summarized by LePecq [5]. The donor absorbs energy ($h\nu$) and forms an excited state $D^*$. The energy from the donor is transferred by resonance in a radiationless process to an acceptor forming an excited state $A^*$, as the donor returns to its ground state.

$$D + h\nu \dashrightarrow D^* \tag{35}$$

$$D^* + A \dashrightarrow D + A^* \tag{36}$$

The excited state $A^*$ returns to its ground state A either by emitting a photon ($h\nu'$) by fluorescence, or is deactivated by a radiationless process.

$$A^* \dashrightarrow A + h\nu' \text{ (fluorescence)} \tag{37}$$

or

$$A^* \dashrightarrow A + \text{thermal energy} \tag{38}$$

In an ideal energy transfer experiment, the donor and acceptor molecules are different, with emission spectra well separated. Techniques for measuring energy transfer under these conditions are described by Schiller [21]. The quenching of the

donor can be monitored with steady state techniques or by monitoring the drop in the fluorescence lifetime. The fluorescence intensity and fluorescence lifetime of the acceptor can also be monitored.

In the present experiments, the donor and acceptor are the same molecule, and hence the above mentioned techniques cannot be used. The only way to measure the energy transfer is by measuring the fluorescence depolarization. Energy transferred between like molecules causes a depolarization of the emitted light since the transition moments of the molecules are not parallel. Also, the lifetime of the donor excited state is shortened by the presence of the acceptor [7]. The conditions for energy transfer are the following:

1. The excited donor must luminesce.
2. The energy spectrum of the donor must overlap the absorption spectrum of the acceptor.
3. The distance between the molecules is $\leq$ 50 A.
4. The orientation of the donor and acceptor must be correct.

Conditions 1. and 2. are met by DNA-bound ethidium bromide. If the base pairs are separated by 3.4 A. and each Eb molecule increases the separation by 3.4 A. [6], then for energy transfer to take place, there must be at least 1 Eb molecule bound every 15 base pairs, or an r value of .07. As seen in figure 27, the

value of r is .07 at a DNA/EB ratio of 15 for low salt and 11 for high salt. If the local environment of one donor is not identical to that of another, some will have acceptors close to them, and some will not, causing the fluorescence decay to deviate markedly from a monoexponential [7]. Our FLA results in the DNA/EB range where no free Eb is present, show a good fit to the mono-exponential decay of bound Eb

ethidium bromide has been used in energy transfer experiments to study the modification of the torsion of the DNA helix induced by intercalation [1,6]. In these studies the fluorescence emission anisotropy decay of the bound ethidium bromide was measured. Wahl, Paoletti and Le Pecq [1], show results supporting the hypothesis that, "the observed depolarization of the ethidium bromide fluorescence is the result of a motion of the DNA molecule itself". Genest and Wahl [6] demonstrate that the rate of fluorescence depolarization due to energy transfer between bound ethidium bromide molecules increases as the average distance between bound ethidium bromide molecules decreases in the DNA/EB range of 1000 to 7.4 where the excitation energy transfer (quenching by free ethidium bromide) is negligible.

The difference in our FLA results at high salt is also consistent with the energy transfer hypothesis. With less binding at high salt, the bound Eb molecules are spaced further apart.

This results in less energy transfer, and consequently, the lifetime does not drop as much. At the point where free Eb appears (DNA/EB ratio of 3.5), the r value for low salt is .18, whereas for high salt it is only .10.

If quenching is by energy transfer between bound Eb molecules, there would not be a decrease in the fluorescence intensity since both the donor and acceptor are fluorescent. This was the result obtained with our measurements of fluorescence intensity.

The PRA FLI is capable of measuring the decay of fluorescence emission anisotropy, although we have not yet attempted such experiments. With depolarization experiments, this energy transfer mechanism in the DNA-Eb system may be verified.

## 12.4 Quenching by excited state reactions

The possibility of quenching by an energy transfer, or inter-system crossing mechanism, between the excited states of free and bound Eb, was investigated.

As seen in figure 20, free Eb has an absorption peak at ~ 480 nm, while bound Eb has an absorption maximum at ~ 520 nm. Normally, in the FLA, the excitation wavelength was set to 485 nm. The emission monochromator was set to 610 nm. Free Eb has a fluorescence maximum at ~ 645 nm, while bound Eb has maximum fluorescence at ~ 615 nm [4]. By shifting the excitation wavelength to 550 nm, away from the absorption peak for free Eb, the majority of molecules being excited would be bound Eb molecules. By selectively exciting just bound Eb with very little free Eb excitation, there would be less energy transfer taking place, and thus less quenching of the fluorescence lifetime would occur.

Figure 31 shows the fluorescence lifetime of bound Eb at 485 nm and 550 nm. Also shown is the %int of the free component. At 550 nm, less free Eb was excited, as can be seen by the drop in the %int curve, but the bound fluorescence lifetime profile did not change significantly. These findings demonstrate that quenching by excited state energy transfer is not taking place at a significant level.

FIGURE 31

The fluorescence lifetime of bound Eb
at two excitation wavelengths

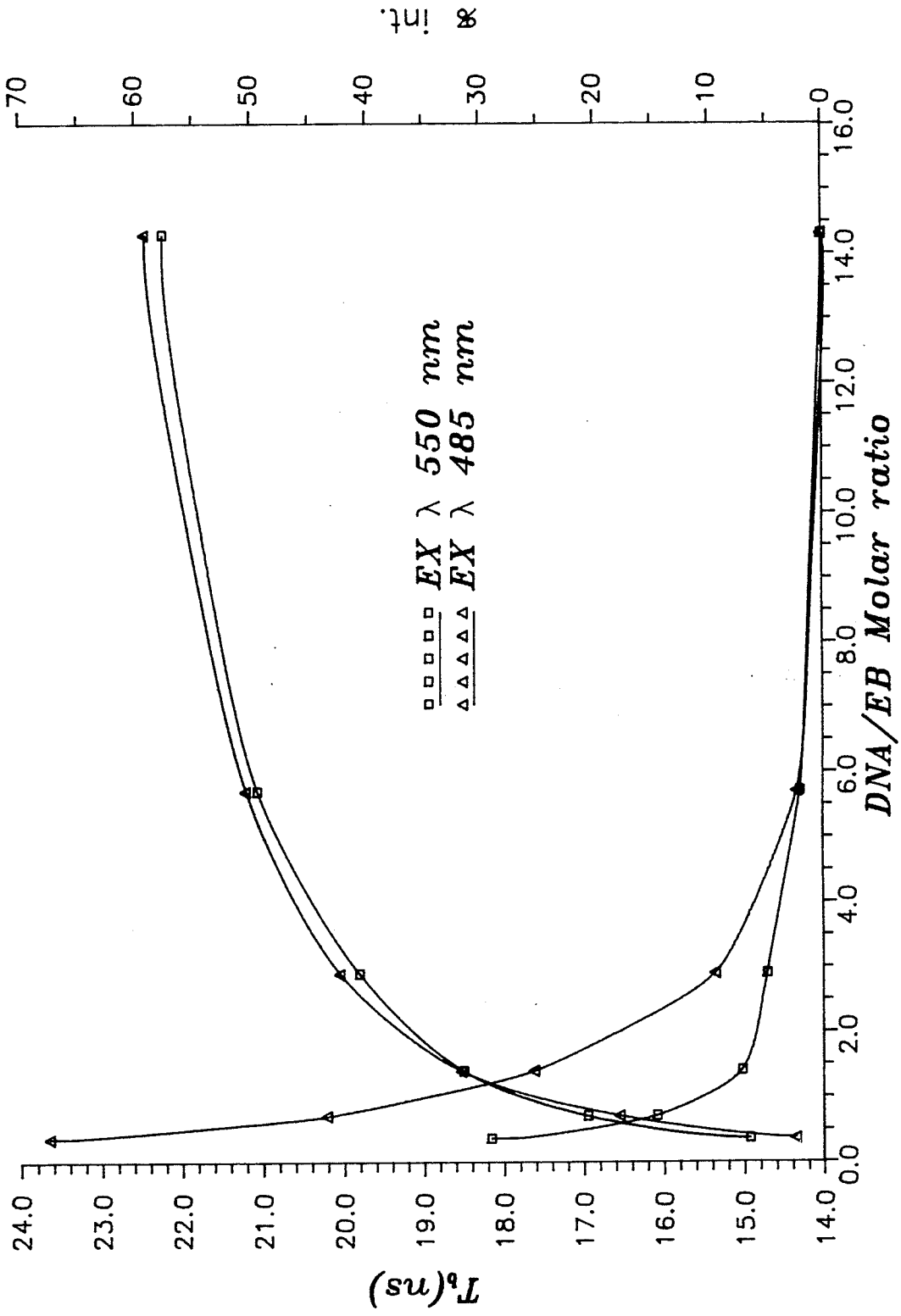
$T_b(ns)$
24.0
23.0
22.0
21.0
20.0
19.0
18.0
17.0
16.0
15.0
14.0
0.0
2.0
4.0
6.0
8.0
10.0
12.0
14.0
16.0
DNA/EB Molar ratio
EX λ 550 nm
EX λ 485 nm
% int.
70
60
50
40
30
20
10
0

## 13.0 Quantum fluorescence increase

As has been stated in equation 8, the fluorescence lifetime $\tau$ is equal to the reciprocal of the sum of all of the rate processes that depopulate an excited state.

$$\tau = \frac{1}{k_f + k_{nr}} \tag{39}$$

The fluorescence quantum yield $\Phi$ is the ratio of the number of photons emitted to the number absorbed. The rate constants $k_f$ and $k_{nr}$ both depopulate the excited state. The fraction of excited states which decay through emission, and hence the quantum yield, is given by

$$\Phi = \frac{k_f}{k_f + k_{nr}} \tag{40}$$

The fluorescence lifetime in the absence of any non-radiative (nr) processes is called the intrinsic lifetime $\tau_o$. Hence the relationship between $\tau$ and $\Phi$ becomes

$$\Phi = \frac{\tau}{\tau_o} \tag{41}$$

We will define QI, the quantum increase in fluorescence occurring when a given concentration of free ethidium bromide becomes bound, as follows:

$$QI = \frac{\Phi_b}{\Phi_f} \tag{42}$$

or from equation (41)

$$QI = \frac{\tau_b}{\tau_f} \tag{43}$$

This quantum fluorescence increase can also be defined in terms of the fluorescence intensity and molecular extinction coefficient of bound and free ethidium bromide.

The absorption of light by a sample is related to the concentration of the absorber by the Beer-Lambert law

$$\frac{I_o}{I_1} = e^{-\epsilon cl} \tag{44}$$

where $I_1$ = intensity of transmitted light
$I_o$ = intensity of incident light
$\epsilon$ = molecular extinction coefficient
$c$ = molar concentration of absorber
$l$ = path length (usually 1 cm)

Absorbance or optical density is expressed as

$$\log_{10} \frac{I_o}{I_1} = \epsilon cl \tag{45}$$

The fluorescence intensity $F_1$ is related to the transmitted intensity $I_1$ by

$$\begin{aligned} F_1 &= I_1 \cdot \Phi \\ &= I_o e^{\epsilon cl} \cdot \Phi \\ &= I_o (2.303) \epsilon cl \cdot \Phi \end{aligned} \tag{46}$$

Using this equation, the quantum fluorescence increase QI can be expressed as

$$\begin{aligned} QI &= \frac{\Phi_b}{\Phi_f} \\ &= \frac{F_{1b} \cdot I_o (2.303) cl \cdot \epsilon_f}{F_{1f} \cdot I_o (2.303) cl \cdot \epsilon_b} \\ &= \frac{F_{1b} \cdot \epsilon_f}{F_{1f} \cdot \epsilon_b} \end{aligned} \tag{47}$$

Using the relative fluorescence intensity numbers obtained with the FLI, an estimate for QI was calculated at each DNA/EB ratio. The data used for these calculations for low salt are shown in table 12. $F_{1b}$ was calculated assuming that

$$F_{1T} = F_{1f} + F_{1b} \quad \text{and} \tag{48}$$

$$F_{1f} = F_{1T} \times \%int_f \tag{49}$$

with the $\%int_f$ values coming from the FLA. The fluorescence intensity of free Eb at the bound concentration (column 7) was obtained from the calibration curve shown in figure 23. The worst error in QI, estimated at 10%, occurred when the fluorescence intensity was the lowest. The values for QI obtained for low and high salt are shown in figure 32. Angerer and Moudrianakis [4] reported a QI of 13.7 at a DNA/EB ratio of 50.

The QI calculated using equation 43, is shown in figure 33, plotted against the QI's calculated in table 12. In equation 43, the value used for $\tau_f$ was set at 1.67 nsec. This plot has three significant features. Firstly, it shows that the salt concentration has no effect on the QI at high DNA/EB ratios. This was also found by Angerer and Moudrianakis [4]. Secondly, the initial drop in $\tau_b$ at high DNA/EB ratios does not correspond to a drop in fluorescence intensity of bound Eb This supports the hypothesis that the initial drop is due to an energy transfer between bound Eb molecules, as discussed in chapter 12.3. The energy transferred from the donor molecule would be re-emitted by the accep-

tor molecule, with no net loss in fluorescence. Thirdly, this plot shows that a 1:1 relationship does not exist between the two methods of calculating QI at low DNA/EB ratios, where free Eb is present. This arises from the calculation of QI using equations 48 and 49. As seen in the previous section, the %int values are dependent on the excitation and emission wavelengths. If an emission wavelength of 645 nm was used instead of 610 nm, the %int of the bound Eb would decrease, and the %int of the free Eb would increase, and this would alter the value of QI. Therefore the value of QI as calculated in table 12 is dependent on the excitation and emission wavelengths, when free Eb is present.

Table 12

Calculation of Quantum Fluorescence Increase

| (1) $[Eb]_t$ $\mu M$ | (2) DNA/Eb | (3) $F_1$ | (4) $F_{1f}$ % | (5) $F_{1b}$ | (6) $[Eb]_b$ $\mu M$ | (7) $F_{f@b}$ | (8) $\epsilon_f/\epsilon_b$ | (9) QI |
|---|---|---|---|---|---|---|---|---|
| 400 | .36 | 1460 | 67.42 | 476 | 28.0 | 490 | 1.038 | 1.010 |
| 200 | .71 | 2455 | 43.35 | 1391 | 30.0 | 495 | 1.075 | 3.020 |
| 100 | 1.4 | 3345 | 25.22 | 2501 | 28.0 | 490 | 1.165 | 5.090 |
| 50 | 2.9 | 3870 | 9.38 | 3507 | 26.8 | 480 | 1.265 | 9.240 |
| 25 | 5.7 | 3345 | 2.26 | 3270 | 22.4 | 420 | 1.587 | 12.36 |
| 10 | 14.3 | 1930 | 0.0 | 1930 | 10.0 | 240 | 1.576 | 12.67 |
| 3 | 47.7 | 600 | 0.0 | 600 | 3.0 | 70 | 1.525 | 13.07 |

(3) Fluorescence intensity at (2), as measured with the FLI.

(4) % int. of the free Eb decay component, from the FLA.

(5) [100-(4)] x (3)

(6) Calculated Spectrophotometrically.

(7) fl. int. of unbound Eb at the bound concentration, from figure 23.

(8) From absorption measurements.

(9) [(3)/(8) x (9)]

FIGURE 32

Quantum fluorescence increase as a function
of the DNA/Eb ratio

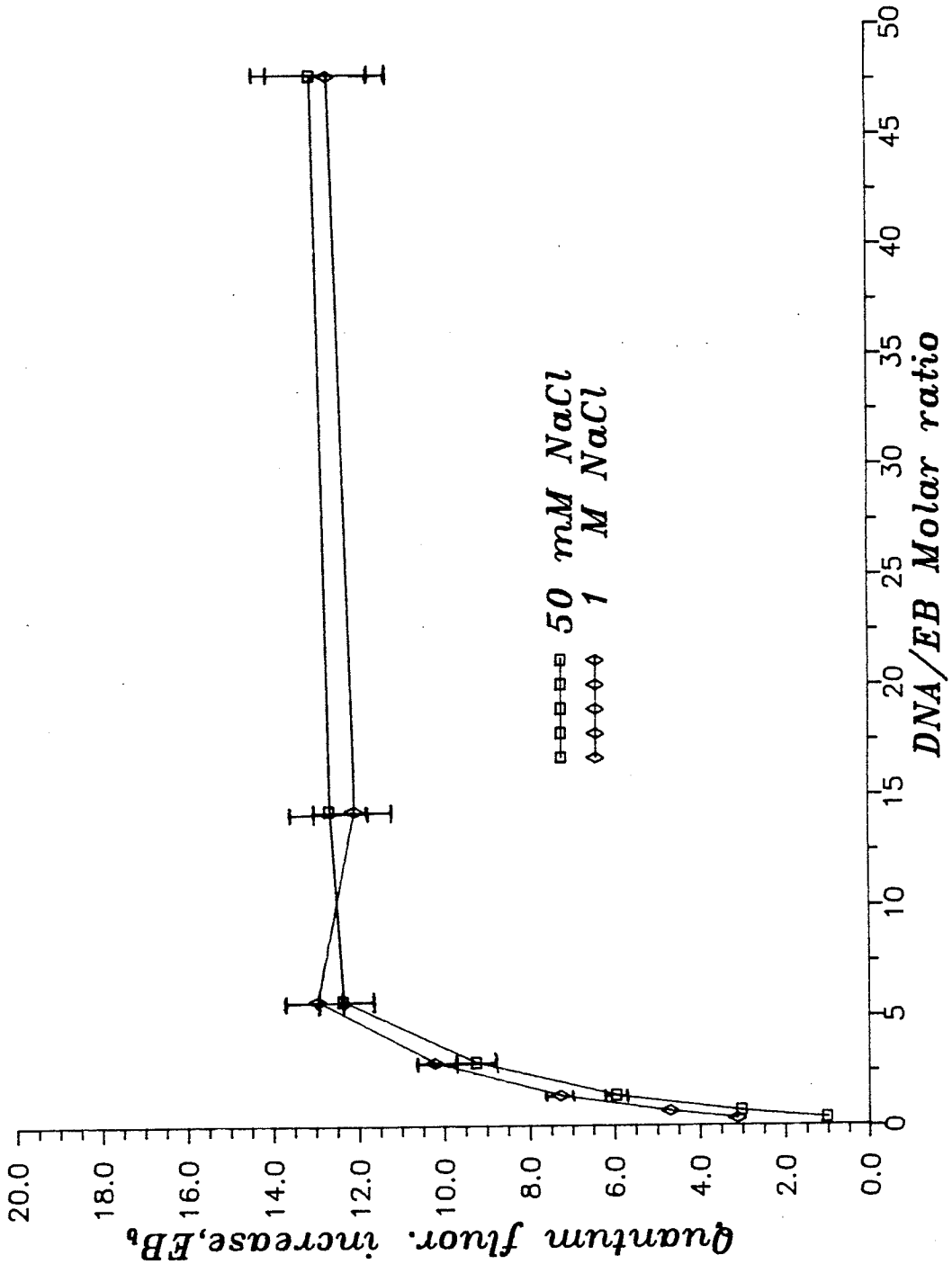
Quantum fluor. increase, EB_b
20.0
18.0
16.0
14.0
12.0
10.0
8.0
6.0
4.0
2.0
0.0
0
5
10
15
20
25
30
35
40
45
50
DNA/EB Molar ratio
50 mM NaCl
1 M NaCl

**FIGURE 33**

A comparison between two methods
used to calculate QI

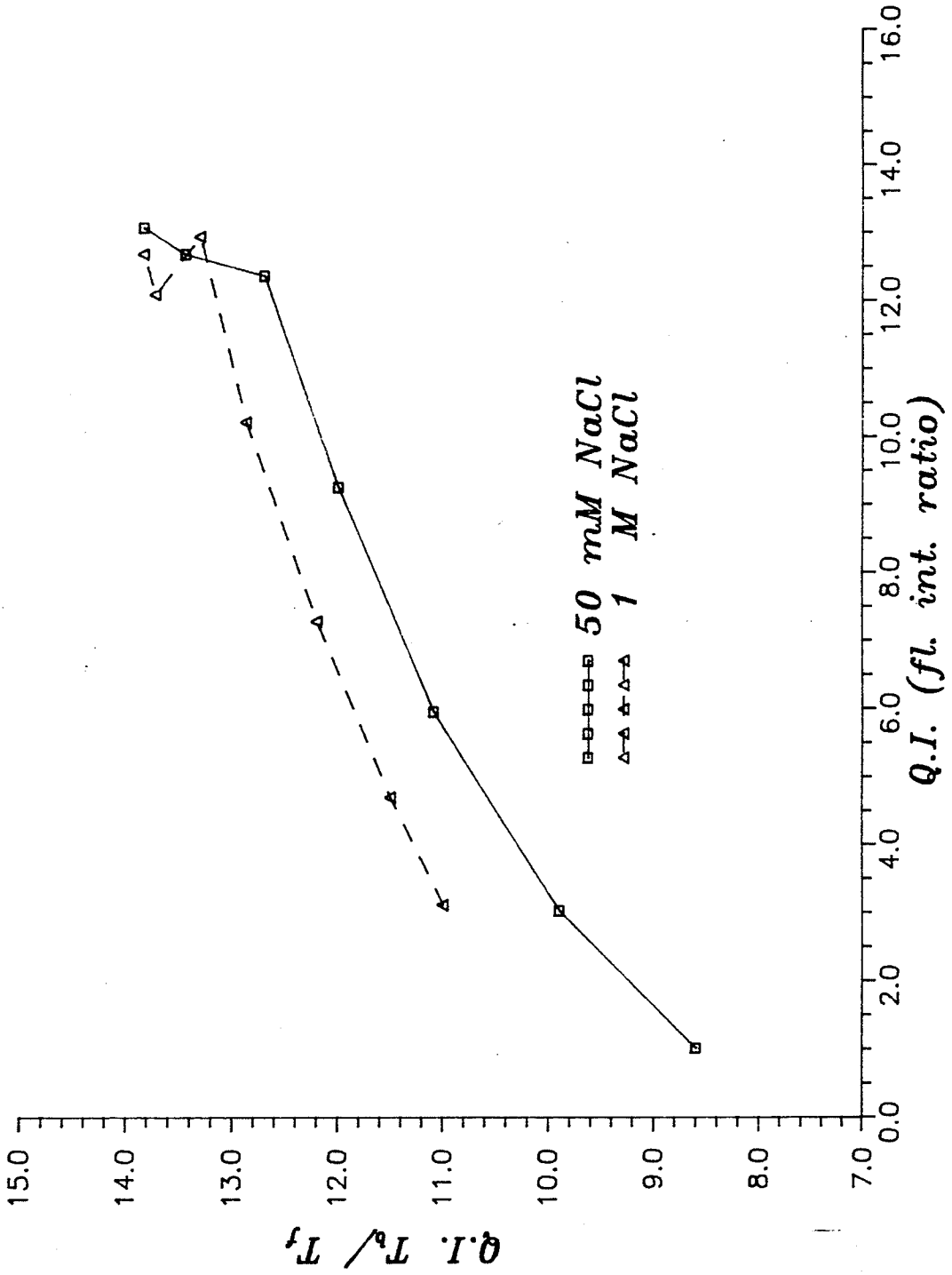
Q.I. $T_b/T_f$
15.0
14.0
13.0
12.0
11.0
10.0
9.0
8.0
7.0
0.0
2.0
4.0
6.0
8.0
10.0
12.0
14.0
16.0
Q.I. (fl. int. ratio)
50 mM NaCl
1 M NaCl

# PART D

## FLUORESCENCE LIFETIME STUDIES IN VITRO

## 14.0 FLA of P388leukemic mouse cells

Three cell lines cloned from P388 leukemia cells were used for initial FLA experiments in vitro. The P388 cells were derived from DBA/2 mice and were originally established by R.K. Johnson of the National Cancer Institute in Bethesda, Maryland. The cloned cell lines were obtained from the Manitoba Institute of Cell Biology. The first 'parental' clone is the $P_4$ cell line. The $P_4$'s serve as the drug sensitive control cells. The second and third cell lines are the $P/A_3$'s and the $P/A_7$'s. The $P/A_3$'s and $P/A_7$'s are 3 and 7 times as resistant to Adriamycin as the $P_4$'s.

### 14.1 Materials and methods

Tissue culture

Cells were set up in suspension in 75 $cm^2$ Lux flasks at 5x $10^4$ cells/ml, and maintained in exponential growth phase in humidified incubators with a 95% air and 5% $CO_2$ atmosphere.

For the $P/A_3$ and $P/A_7$ cells, the culture medium was RPMI supplemented with 8% heat-inactivated Fetal Bovine Serum (FBS), 4% horse serum, and 10$\mu$M Dithiothreitol (DTT). The RPMI (#1640), the FBS (lot 84F-0702), the horse serum (lot 96F-0073), and the

DTT (D-0632) were all purchased from Sigma Chemical Company.

For the $P_4$ cells the medium was RPMI (24$\mu$M sodium bicarbonate) supplemented with 15% heat-inactivated FBS. In this case, the FBS and RPMI were purchased from Gibco chemical Co.

The cells were harvested in log phase, spun down, and re-suspended in .1M Tris buffer, pH 7.6, 100mM NaCl., at a cell density of 5 x $10^7$ cells/ml.

A stock solution of adriamycin (Doxorubicin hydrochloride) (Aldrich # 86,036-0) was prepared at 50 $\mu$g/ml in Earle's balanced salts. Adriamycin was added to the culture flask's 24 hrs post suspension with a final adriamycin concentration of .5 $\mu$g/ml. The first treatment consisted of a 5 minute exposure to the adriamycin, followed by a 24 hour incubation in fresh medium, prior to the FLA. The second treatment consisted of a 24 hour exposure to the adriamycin, with no incubation.

Ethidium bromide staining

A simple 'one-step' ethidium bromide DNA/Cell staining protocol was implemented to prepare the cells for the FLA. This staining procedure has been traditionally used for DNA analysis by flow cytometry. Appendix 2 is a copy of the original

procedure as published by Ortho Diagnostics. This protocol yields intact cell nuclei, containing only DNA stained with ethidium bromide. If possible each .2ml cell sample contained $10^7$ cells. The original protocol used $2x10^6$ cells per .2ml sample. The number of cells per sample was increased to obtain a higher fluorescence intensity from bound ethidium bromide. The final Eb concentration was 11.3$\mu$M such that the ratio of cell number to Eb concentration was .89 million per $\mu$M. If $10^7$ cells were not available, the Eb concentration was adjusted accordingly, to maintain the same ratio.

Fluorescence Lifetime Analysis

The FLA protocol included $H_2$ in the flashlamp, a T/CH of .293, 5000 counts-peak channel, a 3 component fit to 512 channels, and no background subtraction. The cells were maintained at 2°C during the data collection, and the average collection time for each sample was ~ 1 hour.

## 14.2 Results

A typical fluorescence decay curve is shown in figure 15 (b). Initially, the source of the second decay time (~ 6-7 nsec) was investigated, as it did not occur with DNA in solution. It was found that this component was due to ethidium bromide

associating with Triton-X 100, a detergent contained in Solution A of the staining protocol (see Appendix 2).

Solution A was prepared at two different Triton-X 100 concentrations, and ethidium bromide added at 11.3 $\mu$M. The FLA yielded a 2 component model with a $\tau_1$ of ~ 1.8-2.0 nsec and a $\tau_2$ of ~ 6.6-7.0 nsec. With solution A at .1% Triton-X, the %int of $\tau_2$ was 61.7%. With solution A at .2% Triton-X, the %int of $\tau_2$ increased to 74.8%. Figure 34 shows a decay curve obtained. Triton-X 100 is actually a generic name for Polyethylene Glycol p-Isooctylphenyl Ether (Octyl-phenoxy polyethoxyethanol), a non-toxic detergent or emulsifier. Since the p-Isooctylphenyl group is hydrophilic and the polyethylene glycol ether group is hydrophobic, this compound may be forming micelle structures, within which the ethidium bromide may bind (see figure 35). If this is occurring, the ethidium bromide would be partially protected from $O_2$ quenching. This would explain the slightly higher lifetime over free Eb

The effect of a variation in the amount of ethidium bromide added, on the bound ethidium bromide lifetime, at a constant cell number, was investigated with the $P_4$ cells. The results are shown in figure 36. The lifetime profile obtained, is similar to those obtained with DNA in solution. Surprisingly, the data is fitted nicely by a logarithmic function. If the # cells/$\mu$M Eb is plotted on a log scale, a straight line fit results (fig. 36,

bottom). From this plot it is easily seen that if the cell # varies by a factor of 10, the bound lifetime will vary by 5 nsec. If the uncertainty in a count of $10^7$ cells were $\pm$ $10^6$, then with 11.3 $\mu$M Eb, the lifetime would have an uncertainty of $\pm$ .2 nsec ($10^7$ cells and 11.3 $\mu$M Eb are the standard values as per the protocol).

The results of the two adriamycin treatments are shown in table 13. In each case, control samples in the absence of adriamycin were analyzed with the same cell#/[Eb] ratio as in the treatment samples. For the 5 minute exposure to adriamycin, $10^7$ cells were available per sample, and thus the standard Eb concentration was used. Due to the toxic affects of adriamycin during the 24 hour treatment, such a large number of cells was not available, and therefore the Eb concentration was lowered to keep the cell#/[Eb] ratio constant.

Since the quantum yield of fluorescence is different for each lifetime component, a change in the number of cells, will affect the relative intensity of each component differently. This can be see in the control results for the 24 hour treatment. With a lower number of cells, the %int of $\tau_3$ decreased, and the %int of $\tau_2$ increased. This necessitates a control experiment at each cell number.

There is another factor which can affect the %int values. As the cells tend to settle to the bottom of the cuvette, the relative amount of free Eb in the excitation light path will increase, and hence the %int of free component will increase. However, if the rate of settling is the same for each cell sample, and the data collection time is constant, then this effect should be the same in each experiment. Given the above two influencing factors, relative %int values are not very useful as indicators of any possible change in the binding rates of a fluorophore.

The lifetimes, on the other hand, are independent of their %int value. The results for the adriamycin resistant $P/A_3$ and $P/A_7$ cells, at both adriamycin exposures, show no significant difference in the value of $\tau_3$. However for the 24 hour treatment, the adriamycin sensitive $P_4$ cells showed no bound component at all. The FLA resembled that of ethidium bromide in solution A, with no DNA present (figure 34). These results imply that there was cosiderable disruption of the double stranded DNA in the cell nuclei, after the adriamycin exposure. This $P_4$ experiment was only done once, and should be repeated several times to verify the dramatic FLA results.

Table 13

FLA summary for $P/A_3$, $P/A_7$ cell lines with two adriamycin treatments

| Treatment # | Cell Line | Treatment $\tau_i$ | ± | %int | Control $\tau_i$ | ± | %int |
|---|---|---|---|---|---|---|---|
| 5 min[1] | $P/A_3$ | 2.20 | 0.10 | 7.3 | 2.09 | 0.51 | 8.9 |
| | | 8.89 | 1.31 | 11.1 | 8.72 | 1.30 | 12.3 |
| | | 24.16 | 0.12 | 82.9 | 24.41 | 0.25 | 78.8 |
| | $P/A_7$ | 1.33 | 0.18 | 4.6 | 2.04 | 0.26 | 10.4 |
| | | 6.65 | 0.71 | 10.2 | 8.60 | 2.82 | 15.2 |
| | | 24.05 | 0.20 | 85.3 | 23.89 | 0.26 | 74.4 |
| 24 hrs[2] | $P/A_3$ | 1.05 | 0.37 | 7.6 | 1.59 | 0.28 | 12.8 |
| | | 5.46 | 0.24 | 32.8 | 6.58 | 0.30 | 35.4 |
| | | 23.75 | 0.17 | 59.6 | 24.77 | 0.22 | 51.7 |
| | $P/A_7$ | 1.64 | 0.35 | 9.5 | 2.21 | 0.28 | 14.4 |
| | | 5.94 | 0.38 | 26.7 | 6.62 | 0.40 | 33.4 |
| | | 23.76 | 0.16 | 63.8 | 24.26 | 0.23 | 52.2 |
| | $P_4$ | 1.89 | 0.35 | 19.7 | 2.02 | 0.38 | 9.2 |
| | | 6.08 | 0.20 | 80.3 | 6.87 | 0.57 | 22.3 |
| | | | --- | | 24.75 | 0.18 | 68.5 |

[1] 5 min treatment followed by 24 hrs incubation. Data shown is the mean of 5 trials.

[2] One trial only.

**FIGURE 34**

Decay of Eb in a .2% Triton-X100 solution A

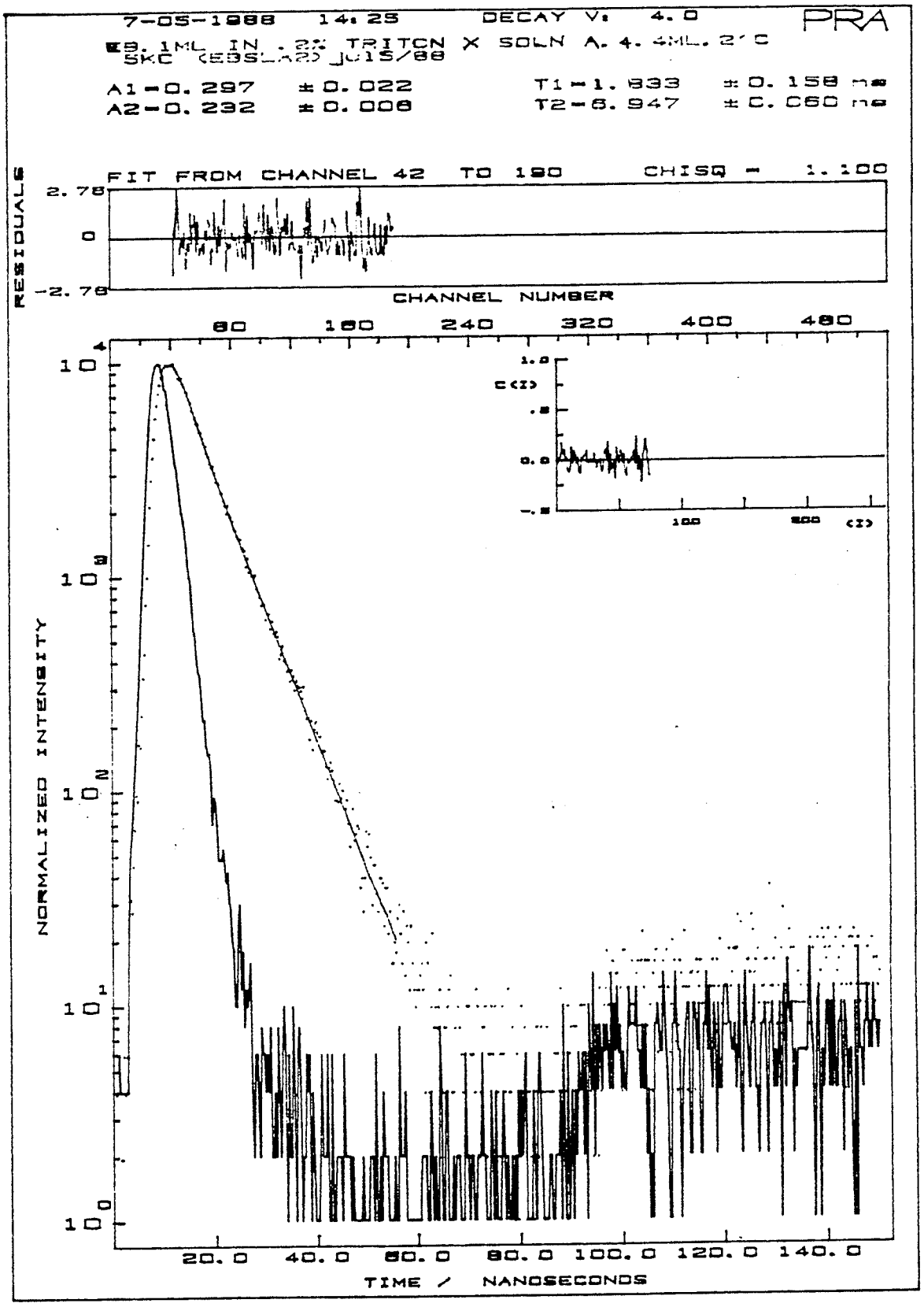
7-05-1988 14:25 DECAY V: 4.0
PRA
8.1ML IN .2% TRITON X SOLN A. 4.4ML. 2°C
SKC (EOSLA2) JUL5/88
A1=0.297 ±0.022 T1=1.833 ±0.158 ns
A2=0.232 ±0.008 T2=6.947 ±0.060 ns
FIT FROM CHANNEL 42 TO 190 CHISQ = 1.100
RESIDUALS
2.78
0
-2.78
CHANNEL NUMBER
80 160 240 320 400 480
NORMALIZED INTENSITY
10^4
10^3
10^2
10^1
10^0
20.0 40.0 60.0 80.0 100.0 120.0 140.0
TIME / NANOSECONDS

**FIGURE 35**

Chemical structure of Triton-X100
(Polyethylene Glycol)

Polyethylene Glycol (Triton -X 100)

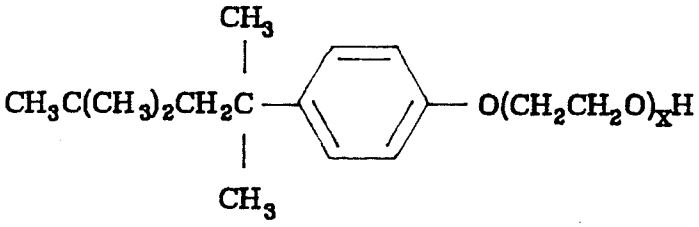


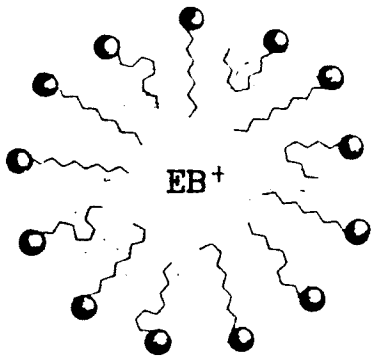


MICELLE STRUCTURE

FIGURE 36

The fluorescence lifetime of bound Eb
as a function of the #cells/$\mu$M Eb ratio

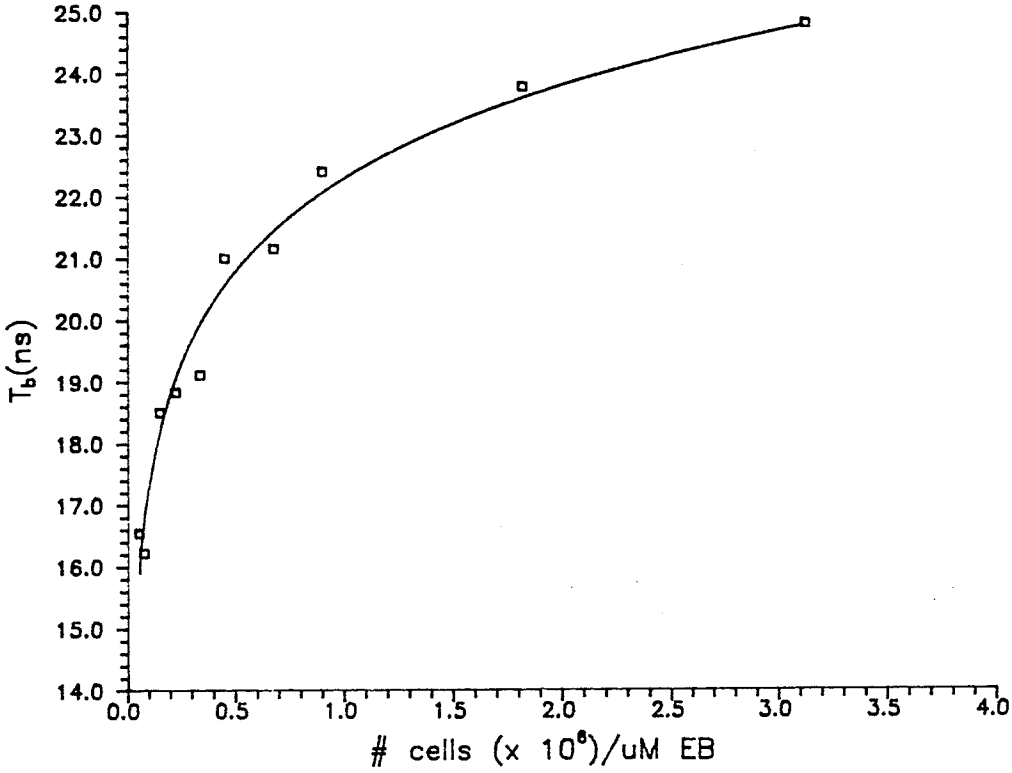
25.0
24.0
23.0
22.0
21.0
20.0
19.0
18.0
17.0
16.0
15.0
14.0
$T_b$(ns)
0.0
0.5
1.0
1.5
2.0
2.5
3.0
3.5
4.0
# cells (x $10^6$)/uM EB

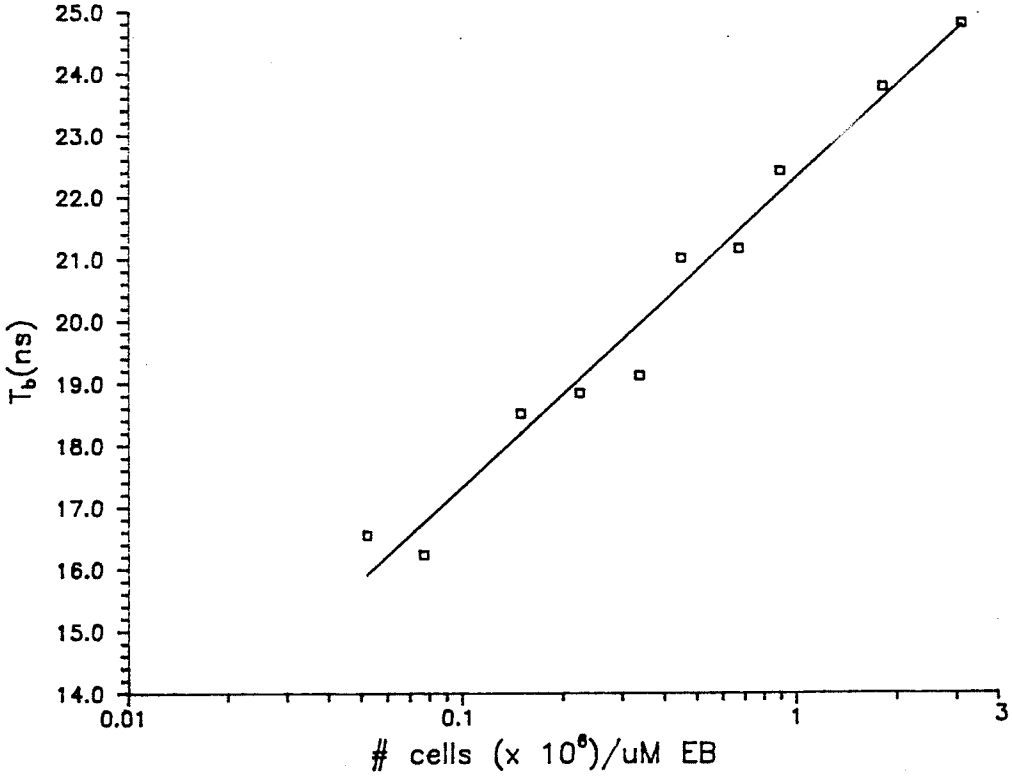
25.0
24.0
23.0
22.0
21.0
20.0
19.0
18.0
17.0
16.0
15.0
14.0
$T_b$(ns)
0.01
0.1
1
3
# cells (x $10^6$)/uM EB

## CONCLUSIONS AND RECOMMENDATIONS

The technique of time-resolved fluorescence spectroscopy has been used to study DNA conformation. The material presented in this thesis has shown that an analysis of the decay kinetics of fluorescent probes, specifically ethidium bromide, bound within macromolecules such as DNA, is highly sensitive to the local molecular environment and conformation of the macromolecule, and is a technique capable of providing additional information about the underlying processes taking place.

Part B of this thesis has shown that $H_2$ and $N_2$ provide very different instrument response functions which in turn, yield slightly different decay analyses. The advantage of using $N_2$ in the flashlamp is that it provides a steady, high intensity fluorescence signal. The disadvantage of using $N_2$ is that the resultant decay curve is highly convoluted, making the analysis more complex. A multi-exponential decay analysis may provide inaccurate lifetime values by fitting the exponential tail of the sample decay curve with a long lived lifetime component. This long component, in the case of ethidium bromide bound to DNA, was not found when $H_2$ gas was used in the flashlamp, and therefore it was ruled out as a true fluorescence decay of the sample.

In addition to the differences in the FLA associated with the excitation source, it has been demonstrated that the region of interest and the level of background, chosen for the analysis, have an effect on the resultant lifetime values, especially in the case of multi-exponential models. The statistical tests provided in the analysis software package, have proven to be highly sensitive indicators of the goodness of fit.

A nitrogen dye laser system is available for this FLI [24], which would provide a much shorter (200-300 ps), stable, high intensity excitation pulse. With a laser excitation source, the variabilities associated with the deconvolution process discussed in this thesis, would decrease considerably. Also, with a narrower IRF, the resolution of fast decay components (~ 1 nsec) would improve. With the higher excitation intensity of a laser, the collection time will be shortened. This is especially advantageous when monitoring samples which contain either a very low fluorophore concentration, or if the fluorophore has a low fluorescence quantum yield.

The FLA of Eb intercalated within calf thymus DNA has shown that bound Eb, in the absence of unbound 'free' Eb, has a maximum fluorescence lifetime of 23.1 nsec. independent of a salt concentration between 50mM and 1M, although there is considerably less binding (50% less) under high salt conditions, due to the difference in the conformation of the DNA.

Unbound Eb quenches the fluorescence intensity and the fluorescence lifetime of the bound Eb. The fluorescence lifetime decreases as a function of the amount of free Eb present in solution. A collisional quenching mechanism based on free Eb associating at a second external site has been proposed.

The lifetime values obtained for Quinine Sulfate and Anthracene, two standard single exponential compounds, are in good agreement with published values.

A rapid Eb staining procedure was adapted to FLA studies of P388 leukemic mouse cells, providing high levels of Eb bound to the nuclear DNA. A difference in the FLA of adriamycin sensitive and adriamycin resistant cells, after a 24 hour exposure to .5$\mu$g/ml of adriamycin, was observed. The sensitive cell line did not indicate an appreciable level of Eb binding.

Current experiments include the FLA of DNA which is in Z form. Eb bound within this more compact structure [20], should have a significantly different fluorescence lifetime. Initial lifetime analyses with poly dG-dC·poly dG-dC have yielded a bound fluorescence lifetime of ~ 11 nsec.

FLA shows great potential as a highly sensitive technique for monitoring subtle changes within the local molecular

environment and conformation of DNA. There are a large number of intercalating and groove binding fluorescent dyes available with which Fluorescence Lifetime Analysis may provide important information leading to a better understanding of the processes taking place within the DNA of normal, transformed, and malignant cells.

REFERENCES


1. Ph. Wahl, J. Paoletti, and J.-B. Le Pecq, Proc. Natl. Acad. Sci. U.S.A., 65, 417 (1970).

2. J.-B. Le Pecq and C. Paoletti, J. Mol. Biol., 27, 87 (1967).

3. J.-B. Le Pecq, in Fluorescence Techniques in Cell Biology, A.A.Thaer and M. Sernetz (eds), Springer Verlag, Berlin, 1973, pp. 301-309.

4. L.M. Angerer and E.N. Moudrianakis, J. Mol. Biol., 63, 505 (1972).

5. J.-B. Le Pecq, in Biochemical Fluorescence: Concepts, Vol. 2., R. Chen and H. Edelhoch (eds), Dekker, New York, 1976, pp. 711-736.

6. D. Genest and Ph. Wahl, in Time-Resolved Fluorescence Spectroscopy in Biochemistry and Biology, Nato ASI Series A, 69, R. Cundall and R. Dale (eds), Plenum Press, New York, 1983, pp. 523-539.

7. I.Z. Steinberg et al., in Time-Resolved Fluorescence Spectroscopy in Biochemistry and Biology, Nato ASI Series A, 69, R. Cundall and R. Dale (eds), Plenum Press, New York, 1983, pp. 411-450.

8. J.R. Lakowicz, Principles of Fluorescence Spectroscopy, Plenum Press, New York, 1983, pp. 275.

9. M.J. Waring, J. Mol. Biol., 13, 269 (1965).

10. V.W. Burns, Arch. of Biochemistry and Biophysics, 133, 420 (1969).

11. R.B. Cundall and R.E. Dale, Time-Resolved Fluorescence Spectroscopy in Biochemistry and Biology, Nato ASI Series A, 69, Plenum Press, New York, 1983, pp. 115-296.

12. W.R. Ware, in Time-Resolved Fluorescence Spectroscopy in Biochemistry and Biology, Nato ASI Series A, 69, R. Cundall and R. Dale (eds), Plenum Press, New York, 1983, pp. 23-55.

13. J.R. Lakowicz, in Applications of Fluorescence in the Biomedical Sciences, D. Taylor et al. (eds), Alan R. Liss Inc, New York, 1986, pp. 29-65.

14. D.P. Heller, An Introduction to Fluorescence Lifetime Measuremnts for studying DNA Conformation., unpublished report, Atomic Energy of Canada Ltd., WNRE, 1987.

15. PRA (Photochemical Research Associates Inc.), Fluorescence Lifetime instrumentation operating manual, 1984/85.

16. B.K. Selinger et al., in Time-Resolved Fluorescence Spectroscopy in Biochemistry and Biology, Nato ASI Series A, 69, R. Cundall and R. Dale (eds), Plenum Press, New York, 1983, pp. 143-153.

17. D.V. O'Connor and D. Phillips, Time-correlated Single Photon Counting, Academic Press, London, 1984.

18. R.A. Lampert, L.A.Chewter, D.V. O'Connor et al., Anal. Chem., 55, 68 (1983).

19. G. Badea and L. Brand, in Methods in Enzymology, 61, Hirs and Timasheff (eds), Academic Press, 1979, pp. 378-400.

20. A. Rich, A. Nordheim, and A.H.-J. Wang, Ann. Rev. Biochem., 53, 791-846 (1984).

21. P. W. Schiller, in Biochemical Fluorescence: Concepts, Vol. 1., R. Chen and H. Edelhoch (eds), Dekker, New York, 1975, pp. 285-303.

22. E. Soini and T. Lövgren, CRC Critical Reviews in Analytical Chemistry, 18-2, 105-154 (1987).

23. A. Grinvald and I.Z. Steinberg, Anal. Biochem., 59, 583 (1974).

24. LN120C Dye Laser System, product information sheet, PRA Laser Inc., 45 Meg Drive, London, Ont., N2E 2V2

APPENDIX I

To assist users in accepted or rejecting models for observed behaviour, PRA has incorporated six statistical tests in the DECAY "deconvolution" software. In addition to a $\chi^2$ (chi-squared) test, the program evaluates the randomness of the weighted residuals, calculates the correlation between parameters which are being adjusted to fit the model to the experimental data, calculates the runs test statistic, calculates the autocorrelation function of the weighted residuals, and evaluates the Durbin-Watson test parameter.

(i) Reduced Chi-Squared Test

$$\chi_r^2 = \frac{1}{NCHAN-p} \sum_{i=1}^{NCHAN} \frac{[D_{obs}\ (i) - D_{calc}\ (i)]^2}{D_{obs}\ (i)} ,$$

where NCHAN is the number of channels over which the fitting is to be performed, p is the number of fitting parameters in the assumed decay law, $D_{obs}$ (i) is the number of experimental events in channel i, and $D_{calc}$ (i) is the calculated number of counts in that channel.

$D_{obs}$ (i) is also the expected variance in channel i, based on Poisson statistics.

If [$D_{obs}$ (i) - $D_{calc}$ (i)] have a Poisson distribution, and $D_{obs}$ (i) is >100, the value of $\chi_r^2$ is expected to be approximately 1.0 <u>if</u> the model chosen for the calculation of $D_{calc}$ is correct.

The precision of $\chi_r^2$ depends on $\sum_{i}^{NCHAN} D_{obs}\ (i)$.

(ii) Runs Test

This test examines the randomness of the distribution of the statistically weighted differences between $D_{obs}$ and $D_{calc}$, i.e. of

$$\frac{D_{obs}\ (i) - D_{calc}\ (i)}{D_{obs}\ (i)}$$

It does this by calculating the number of times

$$\frac{D_{obs}(i) - D_{calc}}{D_{obs}(i)}$$

goes from a positive value to a negative value or from a negative value to a positive value; the program calls this the number of runs, NR.

The program then calculates the number of runs that can be expected, NRE, and the standard deviation of NRE, NRE based on the number of data points (i.e. NCHAN).

The runs test parameter is called SGR and is equal to:

$$SGR = \frac{NR-NRE}{\sigma_{NRE}}$$

When $-1 \leq SGR \leq +1$, NR is within one standard deviation of NRE.

This test is much more sensitive to small deviations from the expected kinetic behaviour than the result of $\chi^2_r$ test.

To assist the user in the interpretation of this result, the null Hypothesis $H_0$: NR=NRE is examined. If NR-NRE falls within the 95% confidence interval, i.e., if abs(SGR) $\leq$ 1.96, the null hypothesis is accepted.

(iii) Correlation Coefficient Matrix

As DECAY searches for the best fit parameters, it keeps track of the correlation between parameters as they change. These correlation coefficients are reported in matrix form once the best fit parameters have been found. A correlation coefficient greater than 0.985, indicates that the values of the indicated parameters have a significant interdependence. This often happens when:

a) there is a low intensity component and the search is only sensitive to the relative intensity of that component, $\alpha_i$ and $\tau_i$.

b) a decay phenomenon may be encountered that can be described by $a_i e^{-t/\tau_i}$ where the actual kinetic behaviour has some other functional form. In these cases some or all of the correlation coefficients will be >0.99, because the program is merely curve fitting. Examples of this behaviour have been:
- fluorescence of aromatic molecules adsorbed onto silica surfaces
- energy transfer kinetics, where $F(t) \propto e^{-a't-b't^{1/2}}$
- a system where $F(t) \propto \ln[A^*]$

(iv) Weighted Residuals Plot

This is simply a plot of: $\dfrac{D_{obs}(i) - D_{calc}(i)}{D_{obs}(i)} = W_i * r_i$, where

$$r_i = D_{obs}(i) - D_{calc}(i) \text{ and } W_i = 1/\sqrt{D_{obs}(i)}$$

The plot has been scaled to the maximum (or minimum) value. The scale factor on the side of the plot is the number of standard deviations of the maximum residual. A visual inspection of the weighted residuals plot is a very useful tool for checking for non-random fluctuations in the data.

(v) Autocorrelation Function Plot

This function examines the correlation between neighbouring values of residuals.

The correlation of the residual in channel i with the residual in channel i+j is summed over some number of channels, m, and normalized, i.e.,

$$C_j = \frac{\frac{1}{m} \sum_{i=n_1}^{n_1+m-1} (W_i * r_i) * (W_{i+j} * r_{i+j})}{\frac{1}{n_3} \sum_{i=n_1}^{n_2} (W_i * r_i)^2}$$

$n_1$ and $n_2$ are the first and last channels of the selection of the decay to be analyzed, and $n_3 = n_2 - n_1 + 1$, and $W_1 = 1/\sqrt{D_{obs}(i)}$. In practice an upper limit of $n_3/2$ is put on j so that the number of terms in the numerator, $n_3 - j$, is sufficient for proper averaging. Again, one looks for $c_j$ values randomly scattered about zero.

(vi) Durbin-Watson Parameter

A statistical test which seems to be more sensitive than $\chi^2$ to small non-random patterns in the residuals is the Durbin-Watson parameter, given by:

$$DW = \frac{\sum_{n_1+1}^{n_2} [W_i * r_i - (W_{i-1} * r_{i-1})]^2}{\sum_{n_1}^{n_2} (W_i * r_i)^2}$$

For a good single exponential fit, DW should be greater than 1.65. For acceptable double and triple exponential fits, minimum DW values are 1.75 and 1.85, respectively.

APPENDIX II

# One-Step Ethidium Bromide DNA/Cell Staining Procedure

ONE-STEP PREPARATION AND STAINING OF CELL NUCLEI FOR DNA ANALYSIS BY FLOW CYTOMETRY


## ACKNOWLEDGEMENT

This issue of Protocols kindly contributed by Prof. H. Dertinger, Institut fur Genetik und Toxikologie von Spaltstoffen, Kernforschungszentrum, Karlsruhe, West Germany.


## INTRODUCTION

This method is a modification of Vindelov's "pH 10 procedure" for rapid preparation and staining of cell nuclei (1). The original instructions have been condensed into a single-step procedure especially useful for work with tissue cultures.

## MATERIALS AND METHODS

I. Reagents

1. *Solution A*
   (a) Dissolve 0.75g glycine in 300 ml distilled $H_2O$
   (b) Adjust to pH 10 by adding 600-700 ml 0.01N NaOH.
   (c) Add 17.53g NaCl and 1ml TRITON-X-100
   (d) Q.S. to 1 liter with distilled water
2. *TRIS buffer*
   (a) Dissolve 12g TRIS and 6g NaCl in 1 liter of distilled $H_2O$.
   (b) Adjust to pH 7.6 with 84ml of 1N HCl.
3. *RNase solution (1%).*
   Dissolve 1 gram RNase in 100ml TRIS buffer
4. *Ethidium bromide staining solution*
   Dissolve 20mg ethidium bromide in 100ml distilled water.

II. Procedure

The quantities given below are adjusted to yield a 4.5ml suspension of stained nuclei.

1. Prepare a suspension of cells in TRIS buffer at a concentration of about $10^7$ cells per ml. ($5 \times 10^7$) FLA
2. To 4ml of ice-cold Solution A, add:
   (a) 0.2ml cell suspension
   (b) 0.2ml 1% RNase solution
   (c) 0.1ml ethidium bromide solution (0.2mg/ml)
3. Seal test tube and invert three times (no pipetting).
4. Incubate on ice for ten minutes.
5. Warm to room temperature in a water bath for five minutes.
6. Invert test tube three times.
7. Run sample.

*Notes:*

- The solutions can be stored at 0°C for several weeks.
- The prepared and stained samples are stable for several days if stored in the dark at 0°C.

## DISCUSSION

This simple procedure yields DNA histograms with excellent resolution. The pH prevents the formation of aggregates. The method has been used with success on a variety of cell lines including human, mammalian and insect cells. A typical result is shown in Figure 1.

## REFERENCE


1. L. Vindelov: Flow microfluorometric analysis of nuclear DNA in cells from solid tumors and cell suspensions. Virchows Arch. B. Cell. Path. 24;227-242, 1977.


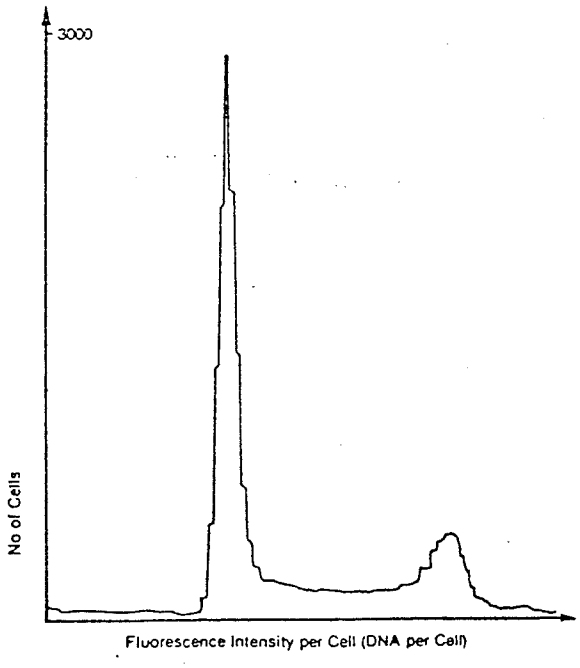


Figure 1. DNA content per cell distribution for V79 Cinese hamster spheroid cells